



Search for non-resonant Higgs boson pair production in final states with leptons, taus, and photons in pp collisions at $\sqrt{s} = 13$ TeV with the ATLAS detector

The ATLAS Collaboration

A search is presented for non-resonant Higgs boson pair production, targeting the $bbZZ$, $4V$ ($V = W$ or Z), $VV\tau\tau$, 4τ , $\gamma\gamma VV$ and $\gamma\gamma\tau\tau$ decay channels. Events are categorised based on the multiplicity of light charged leptons (electrons or muons), hadronically decaying tau leptons, and photons. The search is based on a data sample of proton–proton collisions at $\sqrt{s} = 13$ TeV recorded with the ATLAS detector during Run 2 of the Large Hadron Collider, corresponding to an integrated luminosity of 140 fb^{-1} . No evidence of the signal is found and the observed (expected) upper limit on the cross-section for non-resonant Higgs boson pair production is determined to be 17 (11) times the Standard Model predicted cross-section at 95% confidence level under the background-only hypothesis. The observed (expected) constraints on the HHH coupling modifier, κ_λ , are determined to be $-6.2 < \kappa_\lambda < 11.6$ ($-4.5 < \kappa_\lambda < 9.6$) at 95% confidence level, assuming the Standard Model for the expected limits and that new physics would only affect κ_λ .

Contents

1	Introduction	2
2	ATLAS detector	5
3	Data and simulated event samples	6
3.1	Data sample	6
3.2	Simulated event samples	6
4	Object definitions	8
5	Event categorisation and preselection	12
6	Search strategy	15
7	Background estimation	18
7.1	Prompt leptons	18
7.2	Non-prompt leptons	21
7.3	Charge misassignment	22
7.4	Misidentified hadronic taus	23
7.5	Non-resonant $\gamma\gamma$ production	24
8	Systematic uncertainties	24
8.1	Experimental uncertainties	25
8.2	Theoretical uncertainties	26
9	Statistical treatment and results	27
10	Conclusion	30
	Appendix	32

1 Introduction

Since the discovery of the Higgs boson by the ATLAS and CMS Collaborations in 2012 [1, 2], a major focus in particle physics has been understanding how the Higgs boson interacts with other particles. Tremendous progress has been made in determining the strength of the Higgs boson’s couplings to fermions and vector bosons [3, 4], but its self-interaction has yet to be established. Measurements of the Higgs self-coupling are an essential component of understanding electroweak symmetry breaking and are a sensitive probe for new physics. Many models for new physics predict the existence of additional particles, the presence of which would lead to deviations from the Standard Model (SM) prediction for the strength of the Higgs self-coupling. Moreover, the nature of the electroweak phase transition, when the electromagnetic and weak forces differentiated as the universe cooled down after the Big Bang, is still unknown. The SM predicts a smooth continuous cross-over from one phase to the other, but a first-order phase transition is needed in most models in order to accommodate phenomena like baryonic asymmetry with baryogenesis. New

particles or fields that interact with the Higgs boson are required to accommodate the needed first-order phase transition, and this in turn may lead to a large modification ($\mathcal{O}(1)$ times the SM prediction) to the Higgs self-coupling [5–7]. Some inflation models require that the Higgs boson couples to gravity, which in turn modifies the shape of the Higgs potential [8]. Measurements of the Higgs self-coupling can provide important information to constrain such models. In addition to providing information about the formation of the universe, Higgs self-coupling measurements can also proffer insight into its stability [9] and eventual fate.

The most natural way to probe the Higgs self-interaction is via searches for Higgs boson pair production, HH . At the LHC the dominant HH production mode in the SM is gluon–gluon fusion (ggF). The leading-order (LO) Feynman diagrams for this process are shown in Figure 1. The ggF cross-section, for a Higgs boson mass of $m_H = 125$ GeV, calculated at next-to-next-to-leading-order (NNLO) accuracy in the finite top-quark mass approximation, is $\sigma_{HH}(\text{ggF}) = 31.1^{+6.7\%}_{-23.2\%}$ fb [10–17]. The two ggF production modes shown in Figure 1 interfere with each other destructively in the SM. The cross-section of the $pp \rightarrow HH$ process and shape of the m_{HH} distribution both change as the strength of the Higgs self-coupling relative to the SM prediction (denoted by $\kappa_\lambda = \lambda_{HHH}/\lambda_{SM}$) is varied.

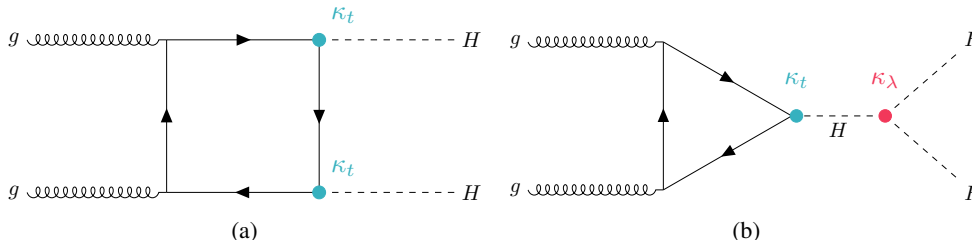


Figure 1: Leading-order diagrams for gluon–gluon fusion HH production, via (a) the top-quark box, and (b) the self-interaction ‘triangle’ modes. The $t\bar{t}H$ and HHH coupling strength modifiers are denoted as κ_t and κ_λ , respectively.

The vector-boson fusion (VBF) HH process provides a sub-leading source of HH production in the SM, and has a cross-section of $1.73 \pm 2.1\%$ fb, calculated at next-to-next-to-next-to-leading order ($N^3\text{LO}$) with $m_H = 125$ GeV [18–23]. The VBF production mode provides sensitivity to the $VVHH$ coupling (where the coupling strength with respect to the SM prediction is denoted as κ_{2V}), as well as additional sensitivity to the Higgs self-coupling, as shown in Figure 2. Both the gluon–gluon fusion and VBF production modes of Higgs boson pairs are considered as signal in this paper. Other production modes have lower cross-sections and are neglected.

Many searches for HH production have been made by both the ATLAS and CMS Collaborations. A statistical combination of ATLAS results in the $HH \rightarrow bb\gamma\gamma$ [24], $HH \rightarrow bb\tau\tau$ [25], and $HH \rightarrow 4b$ [26]¹ channels using the full Run 2 data set (up to 140 fb^{-1} of data collected during 2015–2018 with centre-of-mass energy $\sqrt{s} = 13$ TeV) sets an observed (expected) upper limit on the Higgs boson pair production cross-section at 2.4 (2.9) times the SM prediction at 95% confidence level (CL) [27]. These results are further combined with precision measurements of single Higgs boson production to constrain the self-coupling strength modifier to be within the range of $-0.4 \leq \kappa_\lambda \leq 6.3$ ($-1.9 \leq \kappa_\lambda \leq 7.6$ expected) at 95% CL. More recent results improve the performance of the individual $HH \rightarrow bb\gamma\gamma$ [28] and $HH \rightarrow bb\tau\tau$ [29] channels, and probe the HH process in final states with two b -jets, two light leptons ($\ell = e/\mu$) and missing transverse momentum (E_T^{miss}) [30], but the aforementioned combination continues to set the

¹ Where unspecified, charge conjugation is implied and the notations $\tau\tau$, WW etc. are used in place of $\tau^+\tau^-$, W^+W^- etc.

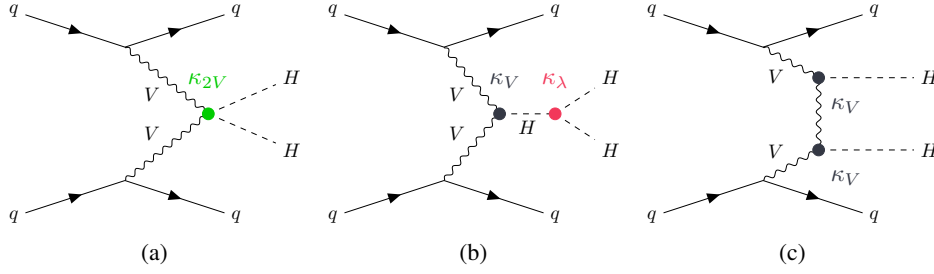


Figure 2: Leading-order diagrams for VBF HH production containing (a) the $HHVV$ vertex, (b) the trilinear HHH vertex, and (c) via the $VVHH$ production mode. The $HHVV$ and HVV coupling strength modifiers are denoted by κ_{2V} and κ_V , respectively.

overall strongest limits on the HH cross-section and self-coupling strength. An analysis exploring the VBF $HH \rightarrow 4b$ channel in boosted topologies [31] improves upon the κ_{2V} coupling constraints of Ref. [27].

The CMS Collaboration achieves similar sensitivity to the ATLAS results in a combination of results [4] from analyses of the $HH \rightarrow bb\gamma\gamma$ [32], $HH \rightarrow bb\tau\tau$ [33], $HH \rightarrow 4b$ [34, 35] and $HH \rightarrow bbZZ (ZZ \rightarrow 4\ell)$ [36] decay channels, and a ‘multilepton’ analysis covering the $HH \rightarrow 4W$, $WW\tau\tau$, and 4τ decay modes in final states with two, three or four light leptons or hadronic taus [37]. This combination sets an observed (expected) upper limit on the HH cross-section of 3.4 (2.5) times the SM prediction and constrains the self-coupling strength to $-1.24 \leq \kappa_\lambda \leq 6.49$. The analysis probing the $HH \rightarrow bbZZ (ZZ \rightarrow 4\ell)$ decay mode sets an observed (expected) limit on the cross-section of 32 (40) times the SM prediction and constrains the Higgs boson self-coupling strength to be $-8.8 \leq \kappa_\lambda \leq 13.4$ ($-9.8 \leq \kappa_\lambda \leq 15.0$), all at 95% CL. The multilepton analysis sets an observed (expected) upper limit on the cross-section of 21.3 (19.4) times the SM prediction and constrains the Higgs boson self-coupling strength to be $-6.9 \leq \kappa_\lambda \leq 11.1$ ($-6.9 \leq \kappa_\lambda \leq 11.7$) at 95% CL.

The analysis described here provides a complementary way to probe Higgs boson pair production by targeting production of the HH process in final states with multiple light leptons and hadronic taus, and in diphoton final states with one or two additional light leptons and/or hadronic taus (τ_{had}). A visualisation of the final states covered in this analysis is shown in Figure 3. The analysis is designed to select events from HH decays where $H \rightarrow WW$, ZZ , $\tau\tau$, and $\gamma\gamma$. The $HH \rightarrow bbZZ$ decay mode, with both the Z bosons undergoing a decay to light leptons, is also analysed in a dedicated search. Channels including an $H \rightarrow \gamma\gamma$ decay are classified as the diphoton plus multilepton channels (‘ $\gamma\gamma$ +ML’) while those without photons are classified as multilepton (‘ML’) channels. This is the first time these HH decay channels are explored in a multilepton analysis in ATLAS. The event selections are orthogonal by construction with those used in the ATLAS analyses of the $bb\gamma\gamma$ [24, 28], $bb\tau\tau$ [25, 29], $4b$ [26, 31], and $bb\ell\ell + E_T^{\text{miss}}$ [30] HH decay channels. Boosted decision trees (BDTs) are used to enhance signal to background separation. Upper limits are set on the HH signal strength, μ_{HH} (defined as the ratio of the HH production cross-section, including only the ggF and VBF processes, to its SM prediction of 32.8 fb), and the coupling strength modifiers κ_λ and κ_{2V} , all at 95% CL.

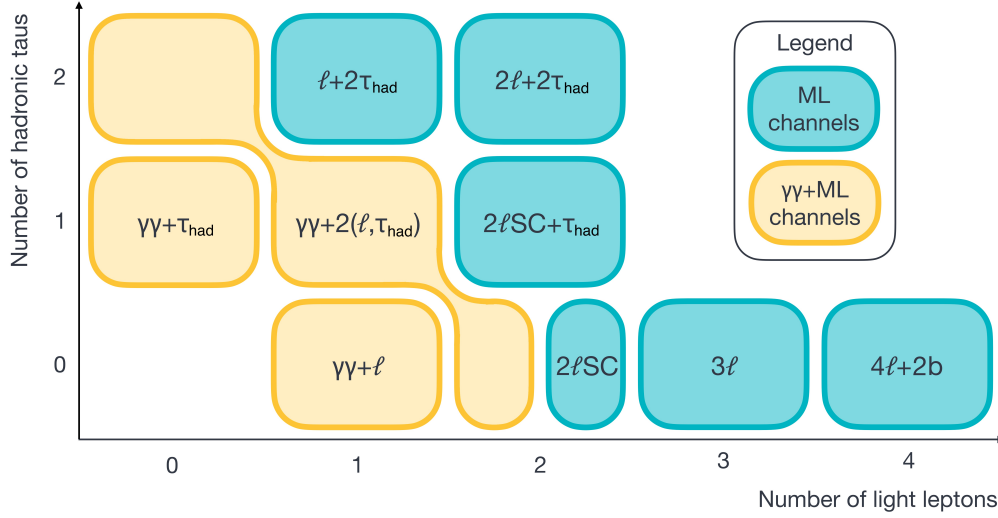


Figure 3: A visualisation of the different final states included in this analysis. The diphoton plus multilepton channels ($\gamma\gamma$ +ML channels) are shown in the lighter yellow boxes and channels with light leptons and hadronic taus ($\gamma\gamma$ +ML channels) are indicated by the darker turquoise boxes. ‘SC’ indicates that the two leptons are required to have the same charge. The two hadronic taus in the $2\ell+2\tau_{\text{had}}$ and $\ell+2\tau_{\text{had}}$ channels are required to have opposite charge (‘OC’), as are the two light leptons in the $2\ell+2\tau_{\text{had}}$ channel. The $\gamma\gamma+2(\ell, \tau_{\text{had}})$ channel requires the presence of two OC light leptons or hadronic taus in addition to the two photons, i.e. encompassing $\gamma\gamma + \ell\ell$, $\gamma\gamma + \ell\tau_{\text{had}}$, and $\gamma\gamma + \tau_{\text{had}}\tau_{\text{had}}$ signatures.

2 ATLAS detector

The ATLAS detector [38] at the LHC [39] covers nearly the entire solid angle around the collision point.² It consists of an inner tracking detector surrounded by a thin superconducting solenoid, electromagnetic and hadron calorimeters, and a muon spectrometer incorporating three large superconducting air-core toroidal magnets.

The inner-detector system is immersed in a 2 T axial magnetic field and provides charged-particle tracking in the range $|\eta| < 2.5$. The high-granularity silicon pixel detector covers the vertex region and typically provides four measurements per track, the first hit normally being in the insertable B-layer (IBL) installed before Run 2 [40, 41]. It is followed by the silicon microstrip tracker (SCT), which usually provides eight measurements per track. These silicon detectors are complemented by the transition radiation tracker (TRT), which enables radially extended track reconstruction up to $|\eta| = 2.0$. The TRT also provides electron identification information based on the fraction of hits (typically 30 in total) above a higher energy-deposit threshold corresponding to transition radiation.

² ATLAS uses a right-handed coordinate system with its origin at the nominal interaction point (IP) in the centre of the detector and the z -axis along the beam pipe. The x -axis points from the IP to the centre of the LHC ring, and the y -axis points upwards. Polar coordinates (r, ϕ) are used in the transverse plane, ϕ being the azimuthal angle around the z -axis. The pseudorapidity is defined in terms of the polar angle θ as $\eta = -\ln \tan(\theta/2)$ and is equal to the rapidity $y = \frac{1}{2} \ln \left(\frac{E+p_z c}{E-p_z c} \right)$ in the relativistic limit. Angular distance is measured in units of $\Delta R \equiv \sqrt{(\Delta y)^2 + (\Delta \phi)^2}$.

The calorimeter system covers the pseudorapidity range $|\eta| < 4.9$. Within the region $|\eta| < 3.2$, electromagnetic calorimetry is provided by barrel and endcap high-granularity lead/liquid-argon (LAr) calorimeters, with an additional thin LAr presampler covering $|\eta| < 1.8$ to correct for energy loss in material upstream of the calorimeters. Hadron calorimetry is provided by the steel/scintillator-tile calorimeter, segmented into three barrel structures within $|\eta| < 1.7$, and two copper/LAr hadron endcap calorimeters. The solid angle coverage is completed with forward copper/LAr and tungsten/LAr calorimeter modules optimised for electromagnetic and hadronic energy measurements respectively.

The muon spectrometer (MS) comprises separate trigger and high-precision tracking chambers measuring the deflection of muons in a magnetic field generated by the superconducting air-core toroidal magnets. The field integral of the toroids ranges between 2.0 and 6.0 T m across most of the detector. Three layers of precision chambers, each consisting of layers of monitored drift tubes, cover the region $|\eta| < 2.7$, complemented by cathode-strip chambers in the forward region, where the background is highest. The muon trigger system covers the range $|\eta| < 2.4$ with resistive-plate chambers in the barrel, and thin-gap chambers in the endcap regions.

Interesting events are selected by the first-level trigger system implemented in custom hardware, followed by selections made by algorithms implemented in software in the high-level trigger [42]. The first-level trigger accepts events from the 40 MHz bunch crossings at a rate below 100 kHz, which the high-level trigger further reduces in order to record events to disk at about 1 kHz.

An extensive software suite [43] is used in data simulation, in the reconstruction and analysis of real and simulated data, in detector operations, and in the trigger and data acquisition systems of the experiment.

3 Data and simulated event samples

3.1 Data sample

The analysis is performed using proton–proton (pp) collision data with $\sqrt{s} = 13$ TeV collected during the LHC Run 2. The number of pp interactions per bunch crossing (pile-up) in this data set ranges from about 8 to 70, with an average of 34. After applying data quality requirements [44] the full data set has an integrated luminosity of $140.1 \pm 1.2 \text{ fb}^{-1}$ [45, 46]. The trigger requirements are discussed in Section 5.

3.2 Simulated event samples

Monte Carlo (MC) simulation is used for the modelling of signal events and most background processes. All generated events are processed through a simulation [47] of the ATLAS detector geometry and response using GEANT4 [48], and through the same reconstruction software as the data. Corrections are applied to the simulated events so that the particle candidates' selection efficiencies, energy scales and resolutions match those determined from data control samples. The samples of simulated events are normalised to the corresponding predicted cross-sections, computed to the highest order available in perturbation theory. The mass of the top quark and Higgs boson are set to $m_t = 172.5$ GeV and $m_H = 125$ GeV, respectively.

The effect of pile-up is modelled by overlaying the simulated hard-scattering event with inelastic pp events generated with PYTHIA 8.186 [49] using the NNPDF2.3_{LO} set of parton distribution functions (PDF) [50] and the A3 set of tuned parameters [51]. The simulated events are weighted to reproduce the distribution

of the average number of interactions per bunch crossing ($\langle\mu\rangle$) observed in the data. The $\langle\mu\rangle$ value in data is rescaled by a factor of 1.03 ± 0.04 to improve agreement between data and simulation in the visible inelastic pp cross-section [52].

The ggF HH signal process is simulated using the POWHEG Box v2 generator [53, 54] at next-to-leading-order (NLO), including finite top-quark-mass effects [11], using the PDF4LHC15 [55] PDF set. Parton showers and hadronisation are simulated with PYTHIA 8.244 [56] with the A14 set of tuned parton shower parameters [57] and the NNPDF2.3LO PDF set. Signal samples for the ggF process are generated explicitly for coupling modifier values of $\kappa_\lambda = 1$ and 10. A reweighting method is used to obtain a ggF signal sample at other κ_λ values by performing a linear combination of independent generator-level samples at three different κ_λ values ($\kappa_\lambda = 0, 1$, and 20), following the method described in Ref. [58]. Scale factors are derived as a function of κ_λ in bins of the generator-level invariant mass of the HH system and applied to the simulated ggF, $\kappa_\lambda = 1$ sample. The ggF, $\kappa_\lambda = 10$ signal sample is used to validate the derived scale factors. This sample and the signal sample obtained from the reweighting method are found to agree within their statistical precision. For the reweighted ggF signal, the NNLO cross-section as a function of κ_λ is taken from Ref. [16]. To assess parton showering uncertainties, alternative ggF samples are simulated using the POWHEG Box v2 generator at NLO with the PDF4LHC15 PDF set, interfaced to HERWIG 7.1.6 [59] for parton showering and hadronisation using the HERWIG 7.1 default set of tuned parameters [60] and MMHT2014LO PDF set [61] for parton showering and hadronisation.

The VBF HH signal process is simulated using MADGRAPH5_AMC@NLO 2.7.3 [62] at LO with the NNPDF3.0NLO PDF set [63], interfaced with PYTHIA 8.244 for parton showering and hadronisation using the A14 set of tuned parameters and NNPDF2.3LO PDF set. Following the same methodology as Ref. [26], signal templates with coupling modifiers ($\kappa_\lambda \neq 1$, $\kappa_{2V} \neq 1$) are obtained by linear combination of six samples with different values for the κ_λ and κ_{2V} parameters. For the reweighted VBF signal points, the N³LO to LO cross-section ratio at the SM value is calculated, and this factor is applied to the cross-sections at each κ_λ and κ_{2V} point. To assess parton showering uncertainties, alternative LO samples are generated using MADGRAPH 2.7.3 with the NNPDF3.0NLO PDF set, interfaced to HERWIG 7.2.1 with the HERWIG 7.1 default set of tuned parameters and MMHT2014LO PDF set for parton showering and hadronisation.

The dominant background process to the ML channels is diboson (VV) production, where V refers to production of an electroweak boson (W or Z/γ^*). This background is estimated from simulation and normalised to data in control regions, as described in Section 7. Background processes involving non-prompt leptons, leptons with a wrongly assigned charge, or misidentified hadronic taus are also important backgrounds to these channels, and are estimated by using data-driven methods. The $4\ell+2b$ channel also has substantial contributions from top quark pair production ($t\bar{t}$), including in association with a Z boson ($t\bar{t}Z$), and Z boson production in association with jets (Z +jets). Non-resonant $\gamma\gamma$ production is the dominant background in the $\gamma\gamma$ +ML channels, where the components of this ‘ $\gamma\gamma$ -continuum’ background are $\gamma\gamma$ production in association with a vector boson ($V\gamma\gamma$), a top quark pair ($t\bar{t}\gamma\gamma$), or jets ($\gamma\gamma$ +jets). MC simulations of these three processes are used when training BDTs to separate signal from background (as described in Section 6), while samples with $\gamma\gamma$ production in association with one or two jets are used to derive uncertainties in the background estimate, as described in Section 7.5.

Single Higgs boson production is considered as a background to all channels, and is significant for the $4\ell+2b$ and $\gamma\gamma$ +ML channels. Higgs boson production in association with a vector boson (VH) process is the dominant source of single Higgs backgrounds in most channels and contributes between 70% and 90% of the total single Higgs background in all channels except the $\gamma\gamma+\tau_{\text{had}}$ channel where it is approximately 50%, and the $4\ell+2b$ channel where it is negligible. Gluon–gluon fusion production is negligible in all channels except in the $\gamma\gamma+\tau_{\text{had}}$ channel where it contributes approximately 40% of the total single Higgs

boson background, and in the $4\ell+2b$ channel where it is the dominant source of single Higgs boson production, contributing around 50% of the total single Higgs background. Higgs boson production in association with a top quark pair ($t\bar{t}H$) contributes between 7% and 30% of the total single Higgs background in all channels.

Simulated samples are produced for the different signal and background processes using the configurations shown in Table 1. Details of the samples used to estimate the systematic uncertainties associated with the generators are shown in parentheses. All samples include leading-logarithm photon emission, either modelled by the parton shower generator or by PHOTOS [64]. The SHERPA 2.2.4 [65] diphoton plus jets ($\gamma\gamma$ +jets) sample is simulated with NLO-accurate matrix elements for up to one parton, and LO-accurate matrix elements for up to three partons are calculated with the COMIX [66] and OPENLOOPS [67–69] libraries. Both the $\gamma\gamma$ +jets and diphoton plus vector boson ($V\gamma\gamma$) samples are matched with the SHERPA parton shower [70] using the MEPS@NLO prescription [71–74] with a dynamic merging cut [75] of 10 GeV. Photons are required to be isolated according to a smooth-cone isolation criterion [76]. These samples are generated using the NNPDF3.0_{NNLO} PDF set [63], along with the dedicated set of tuned parton-shower parameters developed by the SHERPA authors.

4 Object definitions

Vertices from pp interactions are reconstructed [85] using at least two inner detector tracks with $p_T > 500$ MeV. In the ML channel analyses, the hard scatter primary vertex is defined to be the vertex with the largest sum of squared track momenta, $\sum p_T^2$. For the $\gamma\gamma$ +ML channel analyses, the hard scatter primary vertex is chosen using a neural network that uses information about inner detector tracks and the diphoton system [86].

Electrons, muons, hadronic taus, photons, jets (including those containing b -hadrons) and missing transverse energy, E_T^{miss} , are used in this search. Their reconstruction and identification are described below. Three selection definitions are used for both electrons and muons in the ML channel analyses – ‘Baseline’, ‘Loose’, and ‘Tight’ – that are optimised for use in different channels and regions. A fourth definition is used in the $\gamma\gamma$ +ML channels. Their definitions are summarised in Table 2.

Electrons are reconstructed and identified by matching inner detector tracks to energy deposits measured in the electromagnetic calorimeter [87]. Electron candidates are required to have $p_T > 10$ GeV and $|\eta| < 2.47$, excluding the calorimeter transition region $1.37 < |\eta| < 1.52$. The minimum p_T requirement is lowered to 4.5 GeV in the $4\ell+2b$ channel, where one of the Z bosons is produced off-shell and as such its decay products are typically produced with low p_T . Electron candidates are identified using a likelihood technique and both Baseline and Loose candidates are required to satisfy a loose identification working point, which, in combination with additional track hit requirements applied to ensure that the track is high quality, provides an overall electron selection efficiency of 93% in a $Z \rightarrow ee$ sample [88]. The Tight electrons are required to satisfy a tight identification working point [88] that is 80% efficient at selecting electrons in $Z \rightarrow ee$ events. No isolation requirements are applied as part of the Baseline definition, but Loose (Tight) electrons are required to satisfy loose (tight) isolation working points of a ‘Prompt Lepton Veto’ (PLV) BDT designed to reject non-prompt electrons [89]. Several signal regions are defined based on the relative charge of two leptons, so a charge (Q) mis-ID BDT is used to reject electron candidates where the charge is likely to have been wrongly attributed. The chosen working point of the charge mis-ID BDT [87, 89] provides an electron charge mis-ID probability of typically less than 0.2% for a 95% signal efficiency in $Z \rightarrow ee$ events. Contributions from converted photons are rejected using an ambiguity solving algorithm

Table 1: The configurations used for event generation of signal and background processes. The samples used to estimate the systematic uncertainties are indicated in grey and enclosed in parentheses. The matrix element (ME) order refers to the order in the strong coupling constant of the perturbative calculation. Tune refers to the set of tuned parameters used by the parton shower generator. MG5_aMC refers to MADGRAPH5_aMC@NLO [62]. MePs@NLO is the method used in SHERPA to match the matrix element to the parton shower. Samples using PYTHIA 8 have heavy flavour hadron decays modelled by EVTGEN 1.2.0 [77].

Process	Generator	ME order	Parton shower	PDF	Tune
Signal					
ggF HH	POWHEG Box v2 (POWHEG Box v2)	NLO (NLO)	PYTHIA 8 (HERWIG 7)	PDF4LHC15NLO (MMHT2014LO)	A14 (HERWIG 7 default)
VBF HH	MG5_aMC (MG5_aMC)	LO (LO)	PYTHIA 8 (HERWIG 7)	NNPDF3.0NLO (MMHT2014LO)	A14 (HERWIG 7 default)
Top quark					
$t\bar{t}$	POWHEG Box v2 [78–80] (POWHEG Box v2)	NLO (NLO)	PYTHIA 8 (HERWIG 7)	NNPDF3.0NLO (NNPDF3.0NLO)	A14 (HERWIG 7 default)
$t\bar{t}t$	MG5_aMC	LO	PYTHIA 8	NNPDF2.3LO	A14
$t\bar{t}\bar{t}$	MG5_aMC (SHERPA 2.2.10)	NLO (NLO)	PYTHIA 8 (SHERPA)	NNPDF3.1NLO (NNPDF3.0NNLO)	A14 (SHERPA default)
Single top (t -, Wt -, s -channel)	POWHEG Box v2 [81, 82]	NLO	PYTHIA 8	NNPDF3.0NLO	A14
$t\bar{t}WW$	MG5_aMC	LO	PYTHIA 8	NNPDF2.3LO	A14
$t\bar{t}W$	SHERPA 2.2.10 (MG5_aMC)	NLO (NLO)	SHERPA (PYTHIA 8)	NNPDF3.0NNLO (NNPDF3.0NLO)	SHERPA default (A14)
$tW, tZ/\gamma^*$	MG5_aMC	NLO	PYTHIA 8	NNPDF2.3LO	A14
$t\bar{t}Z/\gamma^* (Z \rightarrow \ell\ell\gamma)$	MG5_aMC	NLO	PYTHIA 8	NNPDF3.0NLO	A14
Vector boson					
W +jets, Z +jets	SHERPA 2.2.1	NLO	SHERPA	NNPDF3.0NLO	SHERPA default
$Z \rightarrow \ell\ell\gamma$	SHERPA 2.2.1	NLO	SHERPA	NNPDF3.0NLO	SHERPA default
$VV, qqVV, VVV$	SHERPA 2.2.2	NLO	SHERPA	NNPDF3.0NNLO	SHERPA default
Photon					
$\gamma\gamma$ +jets	SHERPA 2.2.4	NLO	MePs@NLO	NNPDF3.0NNLO	SHERPA dedicated
$V\gamma\gamma$	SHERPA 2.2.4	LO	MePs@NLO	NNPDF3.0NNLO	SHERPA dedicated
$t\bar{t}\gamma\gamma$	MG5_aMC	LO	PYTHIA 8	NNPDF2.3LO	A14
Single Higgs boson					
ggF H	POWHEG	NLO	PYTHIA 8	PDF4LHC15 NNLO	AZNLO [83]
VBF H	POWHEG	NLO	PYTHIA 8	PDF4LHC15 NNLO	AZNLO
VH (inclusive)	POWHEG Box v2	NLO	PYTHIA 8	NNPDF3.0NLO	A14
$VH (H \rightarrow \gamma\gamma)$	POWHEG	NLO	PYTHIA 8	PDF4LHC15 NNLO	AZNLO
$t\bar{t}H$	POWHEG Box v2 (POWHEG Box v2)	NLO (NLO)	PYTHIA 8 (HERWIG 7)	NNPDF3.0NLO (NNPDF3.0NLO)	A14 (H7UE-MMHT [84])
bbH	POWHEG Box v2	NLO	PYTHIA 8	NNPDF3.0NLO	A14
tHb +jet(s)	MG5_aMC	NLO	PYTHIA 8	NNPDF3.0NLO	A14
tHW	MG5_aMC	NLO	PYTHIA 8	NNPDF3.0NLO	A14

Table 2: Electron and muon candidate definitions used in the analysis. A ‘-’ indicates that a cut is not applied, and ‘N/A’ indicates that a requirement is not applicable.

	Electrons				Muons			
	Baseline (B)	Loose (L)	Tight (T)	$\gamma\gamma$ +ML (P)	Baseline (B)	Loose (L)	Tight (T)	$\gamma\gamma$ +ML (P)
Minimum p_T	10 GeV ($4\ell+2b$ channel: 4.5 GeV)				10 GeV ($4\ell+2b$ channel: 3 GeV)			
η	$ \eta < 1.37$ or $1.52 < \eta < 2.47$				$ \eta < 2.5$			
Identification		Loose	Tight	Medium		Loose	Medium	
Isolation	-	PLV loose	PLV tight	Loose	-	PLV loose	PLV tight	Loose
Q mis-ID BDT	-		✓	-	-		N/A	
e/γ ambiguity	-		✓	-	-		N/A	
$ d_0 /\sigma_{d_0}$			< 5				< 3	
$ z_0 \sin \theta $			< 0.5 mm				< 0.5 mm	

based on track information [87, 89]. A fourth electron definition working point is used in the $\gamma\gamma$ +ML channels, where the electron candidates are required to have $p_T > 10$ GeV, and satisfy the medium working point of the likelihood based identification [88] that is 88% efficient at selecting electrons in $Z \rightarrow ee$ events. Isolation requirements are applied, based on the presence of tracks in a cone of p_T -dependent size around the electron and of calorimetric energy deposits in a fixed-size cone [88]. The isolation requirements are approximately 85% efficient for electrons with E_T of 10 GeV, and fully efficient for electrons with $E_T > 40$ GeV.

Muon candidates are reconstructed from tracks in the MS, which are matched to inner detector tracks where available. Baseline muon candidates are required to have $p_T > 10$ GeV and $|\eta| < 2.5$. The minimum p_T requirement is lowered to 3 GeV in the $4\ell+2b$ channel to increase acceptance of muons from the decay of an off-shell Z boson. Baseline and Loose muons are required to satisfy a loose identification working point that is typically 98% efficient at selecting prompt muons. The identification is tightened to a medium working point that is around 97% efficient for the Tight muon definition [90]. Similarly to electrons, Loose and Tight muons are required to satisfy correspondingly strict working points of the PLV [90]. The loose (tight) PLV working points are 81% (57%) efficient at selecting the lowest p_T prompt muons, rising to 93% (87%) for muons with $p_T > 20$ GeV. Muons used in the $\gamma\gamma$ +ML channels are required to have $p_T > 10$ GeV, satisfy the same medium identification working point as is used in the ML channels, and loose isolation requirements that are based on the presence of particle-flow objects [91] in a cone of p_T -dependent size around the muon. The isolation requirements are 95–99% efficient at selecting prompt muons in the p_T regions used in the analysis.

To further reduce contributions from non-prompt electrons and muons, cuts on the transverse and longitudinal impact parameters with respect to the primary vertex, $|d_0|$ and $|z_0|$ respectively, are applied to all candidates. Electrons (muons) are required to have $|d_0|/\sigma_{d_0} < 5(3)$ and $|z_0 \sin \theta| < 0.5$ mm (where σ_{d_0} is the uncertainty on the reconstructed d_0 , and θ is the polar angle of the track).

The visible hadronic tau decay ($\tau_{\text{had-vis}}$) reconstruction algorithm [92] is seeded from jets formed using the anti- κ_t algorithm [93, 94] with a radius parameter $R = 0.4$, and clusters of calorimeter cells calibrated using a local hadronic calibration (LC) [95] as inputs. The $\tau_{\text{had-vis}}$ candidates are required to have $p_T > 20$ GeV and $|\eta| < 2.5$. The calorimeter transition region ($1.37 < |\eta| < 1.52$) is vetoed. A set of BDTs are used to determine whether tracks in a cone with radius $R = 0.4$ around the $\tau_{\text{had-vis}}$ axis are consistent with

coming from a hadronic decay of a tau. Selected $\tau_{\text{had-vis}}$ candidates are required to have either one or three associated tracks (or ‘prongs’), with a total charge of ± 1 . Recurrent neural networks (RNNs) are used to identify $\tau_{\text{had-vis}}$ candidates and reject backgrounds [96]. A loose identification working point is used in the $\gamma\gamma$ +ML channels, providing an efficiency of 85% (75%) for one-prong (three-prong) $\tau_{\text{had-vis}}$. In the ML channels, the medium working point is used that has an efficiency of 75% (60%) for one-prong (three-prong) $\tau_{\text{had-vis}}$. A separate BDT is used to reject electrons that are misidentified as one-prong $\tau_{\text{had-vis}}$ candidates, with an efficiency of about 95% for real hadronic taus [97].

Anti-ID $\tau_{\text{had-vis}}$ objects, defined as a $\tau_{\text{had-vis}}$ with modified identification requirements, are used to estimate the backgrounds from jets misidentified as $\tau_{\text{had-vis}}$ in the $2\ell+2\tau_{\text{had}}$ and $\ell+2\tau_{\text{had}}$ channels, as described in Section 7.4. Anti-ID $\tau_{\text{had-vis}}$ objects are reconstructed, and their energy is calibrated in the same way as $\tau_{\text{had-vis}}$ candidates, and they must satisfy the nominal $\tau_{\text{had-vis}}$ kinematic and track selection criteria. They are required to satisfy a very loose RNN identification requirement, corresponding to an efficiency of approximately 99% for $\tau_{\text{had-vis}}$ [96], but fail to satisfy the nominal RNN requirement applied to the $\tau_{\text{had-vis}}$ candidates.

Photon candidates are required to have $E_T > 25$ GeV and $|\eta| < 2.37$. Photons inside the transition region of the calorimeter ($1.37 < |\eta| < 1.52$) are rejected. Photon identification is based on the lateral shower profile of the energy deposits in the first and second electromagnetic calorimeter layers and on the energy leakage fraction in the hadronic calorimeter. The photon candidates are also required to satisfy a tight working point of this identification algorithm, which is tuned for converted and unconverted photons separately [87]. Loose isolation requirements, based on calorimeter energy clusters and tracks in a cone with radius $R = 0.2$ around the photon are also applied [87]. For isolated photons with p_T between 30 GeV and 250 GeV, the identification efficiency for unconverted and converted photons ranges from 84% to 98%, when evaluated on a sample of $Z \rightarrow \ell\ell\gamma$ events [87].

Reconstructed jets are based on particle-flow objects built from noise-suppressed positive-energy topological clusters in the calorimeter and reconstructed tracks [91]. The anti- κ_t algorithm with a radius parameter of $R = 0.4$ is used. Jets are required to have $|\eta| < 2.5$ (extended to $|\eta| < 4.4$ for channels with photons) and $p_T > 25$ GeV. To further suppress jets produced in concurrent pp interactions, each jet within the tracking acceptance of $|\eta| < 2.4$, and with $p_T < 60$ GeV, is required to satisfy the tight jet-vertex tagger [98] criteria used to identify the jet as originating from the selected primary vertex of the event.

Jets containing b -hadrons, b -jets, are identified using a deep-learning neural network, DL1r [99] that combines information about the impact parameters of inner detector tracks, the presence of displaced secondary vertices, and reconstructed flight-paths of b - and c -hadrons inside the jet. Jets with $|\eta| < 2.5$ are considered for b -tagging. A working point that gives 77% efficiency to identify jets associated with a b -hadron in simulated $t\bar{t}$ events is used to select, or veto, b -jets. At this working point, the light-jet (charm-jet) rejection measured in $t\bar{t}$ simulation is about a factor of 130 (4.9) [100]. The DL1r algorithm is calibrated using a likelihood-based method for each jet type [100], and correction factors are applied to the simulated event samples to compensate for differences between data and simulation in the b -tagging efficiency for b -, c - and light-flavour jets. The energy of b -tagged jets containing a muon is corrected to account for the fact that a muon typically only deposits a small fraction of its energy in the calorimeters. In addition, the undetected energy of the neutrinos and out-of-cone effects are corrected for with scale factors derived as a function of the b -jet p_T from a $t\bar{t}$ MC sample. The two corrections together improve the resolution of the invariant mass of the two jets with the highest b -tagging score (m_{bb}) by about 18% for SM HH signal events that include a $H \rightarrow b\bar{b}$ decay. The procedure closely follows the one used in Ref. [101].

An overlap-removal procedure is applied to resolve ambiguities between independently reconstructed electrons, muons, (anti-ID) $\tau_{\text{had-vis}}$, photons and jets. Any electron found to share a track with a muon is removed, as is any (anti-ID) $\tau_{\text{had-vis}}$ within $\Delta R = 0.2$ of an electron or muon. Jets found within $\Delta R = 0.2$ of an electron or (anti-ID) $\tau_{\text{had-vis}}$ are removed, and any jet with less than three tracks associated with it is removed if it is found to be within $\Delta R = 0.2$ of a muon. Any electron or muon found within $\Delta R = 0.4$ of surviving jets is removed. Photons are removed if they are found within $\Delta R = 0.4$ of an electron or muon. Jets found within $\Delta R = 0.4$ of a photon are removed. All requirements are applied sequentially. A similar procedure is applied for the $\gamma\gamma$ +ML channels, but prioritising photons. All electrons and muons that satisfy the ‘Baseline’ definition are considered as inputs to the overlap-removal procedure in the ML channels while the $\gamma\gamma$ +ML channels use the definitions described in the text and referred to as type ‘P’ in Table 2. The differences between the overlap-removal procedures means that the ML and $\gamma\gamma$ +ML channels are not strictly orthogonal, but no signal or data events are found to satisfy the selection requirements of more than one channel.

The missing transverse energy $E_{\text{T}}^{\text{miss}}$ in an event is calculated as the magnitude of the negative vectorial sum of the transverse momenta of all selected and calibrated physics objects that can be matched to the primary vertex, after the overlap removal procedure is applied. A component called the ‘soft term’ is calculated from the residual tracks that originate from the primary vertex but are not associated with any other object and is included in the calculation [102].

5 Event categorisation and preselection

Events in the ML channels that have final states containing two or more light leptons are selected by requiring that they satisfy single lepton or dilepton triggers [103, 104]. Events in the $\ell+2\tau_{\text{had}}$ channel are selected using only the single lepton triggers. The single electron (muon) triggers have p_{T} thresholds of 24–26 GeV (20–26 GeV), depending on the data-taking conditions. The dilepton triggers require either two electrons, two muons, or one electron and one muon, and have p_{T} thresholds as low as 12 GeV (8 GeV) for the leading (subleading) lepton. Diphoton triggers [103] where the leading (subleading) photon is required to have $E_{\text{T}} > 35$ GeV (25 GeV) are used in the $\gamma\gamma$ +ML channels. The diphoton triggers used in 2015 and 2016 required that both the photons satisfy the loose photon identification criteria, and this was tightened to a medium identification working point during 2017–2018 data taking in response to the increased $p\bar{p}$ interaction rate. In all channels, the electrons, muons and photons that fired the trigger are required to be geometrically matched to corresponding offline objects. Electrons and muons that are geometrically matched to the trigger objects are required to have an offline p_{T} 1 GeV higher than the threshold of the corresponding trigger.

Events are categorised into sub-channels according to the number of photons, $\tau_{\text{had-vis}}$, and light leptons satisfying the definitions in Table 2, after applying the overlap removal procedure. The requirements for the different sub-channels are summarised for the ML channels in Table 3 and for the $\gamma\gamma$ +ML channels in Table 4. These sets of requirements define the signal preselection regions that are used for further multivariate analysis selections used to refine the extraction of signal as described in Section 6. The requirements also form the basis from which control and validation regions are defined in order to estimate background contributions, as described in Section 7. The contributions of the different decay modes of the Higgs boson pair to different signal regions after applying the preselection requirements is shown for the ML channels in Figure 4 and for the $\gamma\gamma$ +ML channels in Figure 5.

Table 3: Selection criteria applied to each ML channel to form the signal preselection regions. The notation ‘ $N\ell(X)$ ’ refers to the multiplicity, N , of the different types of lepton ($X = B, L, T$) as defined in Table 2. The multiplicity of $\tau_{\text{had-vis}}$, jets, and b -jets are denoted N_τ , N_{jet} , and $N_{b\text{-jet}}$, respectively. When no p_T (or E_T) threshold is specified, the default requirements for each object are used, as described in Section 4. Objects are ordered by decreasing p_T and their index denoted by a subscript. In the $4\ell+2b$ channel, the same-flavour, opposite charge (SFOC) lepton pair with an invariant mass closest to the Z boson mass is defined as the lepton pair coming from the on-shell Z boson decay (on-shell- $\ell\ell$) while the remaining SFOC lepton pair is defined as coming from the off-shell Z decay (off-shell- $\ell\ell$). In the 3ℓ channel, the lepton with opposite charge relative to the other two is denoted by ℓ_{OC} . The same-charge lepton that is nearest to ℓ_{OC} in ΔR is denoted ℓ_{SC1} and the other is ℓ_{SC2} . The ‘ Z -veto’ requires that the invariant mass of two SFOC leptons must satisfy $|m_{\ell\ell} - m_Z| > 10 \text{ GeV}$. An analogous Z -veto requirement is considered for the three-lepton system in the 3ℓ channel to remove background processes with $Z \rightarrow \ell\ell\gamma^* (\gamma^* \rightarrow \ell'\ell')$ where one lepton has very low momentum and is not reconstructed.

Channel	ℓ	$\tau_{\text{had-vis}}$	Jets	b -jets
$4\ell+2b$	$4\ell(B)$ $p_T(\ell_1) > 20 \text{ GeV}$ $p_T(\ell_2) > 15 \text{ GeV}$ $p_T(\ell_3) > 10 \text{ GeV}$ ℓ_3 or ℓ_4 pass loose PLV 2 SFOC pairs $50 < m_{\text{on-shell-}\ell\ell}^{\text{SFOC}} < 106 \text{ GeV}$ $5 < m_{\text{off-shell-}\ell\ell}^{\text{SFOC}} < 115 \text{ GeV}$ All 4 pairs $\Delta R(\ell_i, \ell_j) > 0.02$ $ m_{4\ell} - m_Z > 10 \text{ GeV}$	$N_\tau = 0$	$N_{\text{jet}} \geq 2$	$1 \leq N_{b\text{-jet}} \leq 3$
3ℓ	3ℓ , sum of charges = ± 1 $\ell_{\text{OC}}(L)$ $\ell_{\text{SC1}}(T)$, $p_T > 15 \text{ GeV}$ $\ell_{\text{SC2}}(T)$, $p_T > 15 \text{ GeV}$ All $m_{\ell\ell}^{\text{SFOC}} > 12 \text{ GeV}$ Z -veto $ m_{3\ell} - m_Z > 10 \text{ GeV}$	$N_\tau = 0$	$N_{\text{jet}} \geq 1$	$N_{b\text{-jet}} = 0$
$2\ell\text{SC}$	$2\ell(T)$, $p_T > 20 \text{ GeV}$, SC $m_{\ell\ell} > 12 \text{ GeV}$	$N_\tau = 0$	$N_{\text{jet}} \geq 2$	$N_{b\text{-jet}} = 0$
$2\ell\text{SC}+\tau_{\text{had}}$	$2\ell(T)$, $p_T > 20 \text{ GeV}$, SC $m_{\ell\ell} > 12 \text{ GeV}$	$N_\tau = 1$ $p_T > 25 \text{ GeV}$ OC to ℓ	$N_{\text{jet}} \geq 2$	$N_{b\text{-jet}} = 0$
$2\ell+2\tau_{\text{had}}$	$2\ell(L)$, OC $m_{\ell\ell} > 12 \text{ GeV}$ Z -veto	$N_\tau = 2$, OC $\Delta R(\tau_1, \tau_2) < 2$	$N_{\text{jet}} \geq 0$	$N_{b\text{-jet}} = 0$
$\ell+2\tau_{\text{had}}$	$1\ell(L)$	$N_\tau = 2$, OC $\Delta R(\tau_1, \tau_2) < 2$	$N_{\text{jet}} \geq 2$	$N_{b\text{-jet}} = 0$

Table 4: Selection criteria applied to each $\gamma\gamma$ +ML channel to form the signal preselection regions. The notation ‘ $N(\ell(P))$ ’ refers to the multiplicity, N , of P-type leptons as defined in Table 2. The multiplicity of $\tau_{\text{had-vis}}$, photons, and b -jets are denoted N_τ , N_γ , and $N_{b\text{-jet}}$, respectively. When no p_T or E_T threshold is specified, the default requirements for each object are used, as described in Section 4. Photons are ordered in decreasing E_T and their index denoted by a subscript. The invariant masses of dilepton and diphoton systems are denoted $m_{2(\ell,\tau)}$ and $m_{\gamma\gamma}$ respectively.

Channel	ℓ	$\tau_{\text{had-vis}}$	Photons	E_T^{miss}	b -jets
$\gamma\gamma+2(\ell, \tau_{\text{had}})$	$N(\ell(P)) + N_\tau = 2$, OC		$N_\gamma = 2$	$E_T^{\text{miss}} > 35 \text{ GeV}$	
$\gamma\gamma+\ell$	$N(\ell(P)) = 1$	$N_\tau = 0$	$E_T(\gamma_1) > 35 \text{ GeV}$ $105 \text{ GeV} < m_{\gamma\gamma} < 160 \text{ GeV}$ $\gamma_1 : p_T/m_{\gamma\gamma} > 0.35$ $\gamma_2 : p_T/m_{\gamma\gamma} > 0.25$	$\gamma\gamma+e: E_T^{\text{miss}} > 35 \text{ GeV}$ $\gamma\gamma+\mu: -$	$N_{b\text{-jet}} = 0$
$\gamma\gamma+\tau_{\text{had}}$	$N(\ell(P)) = 0$	$N_\tau = 1$		$E_T^{\text{miss}} > 35 \text{ GeV}$	

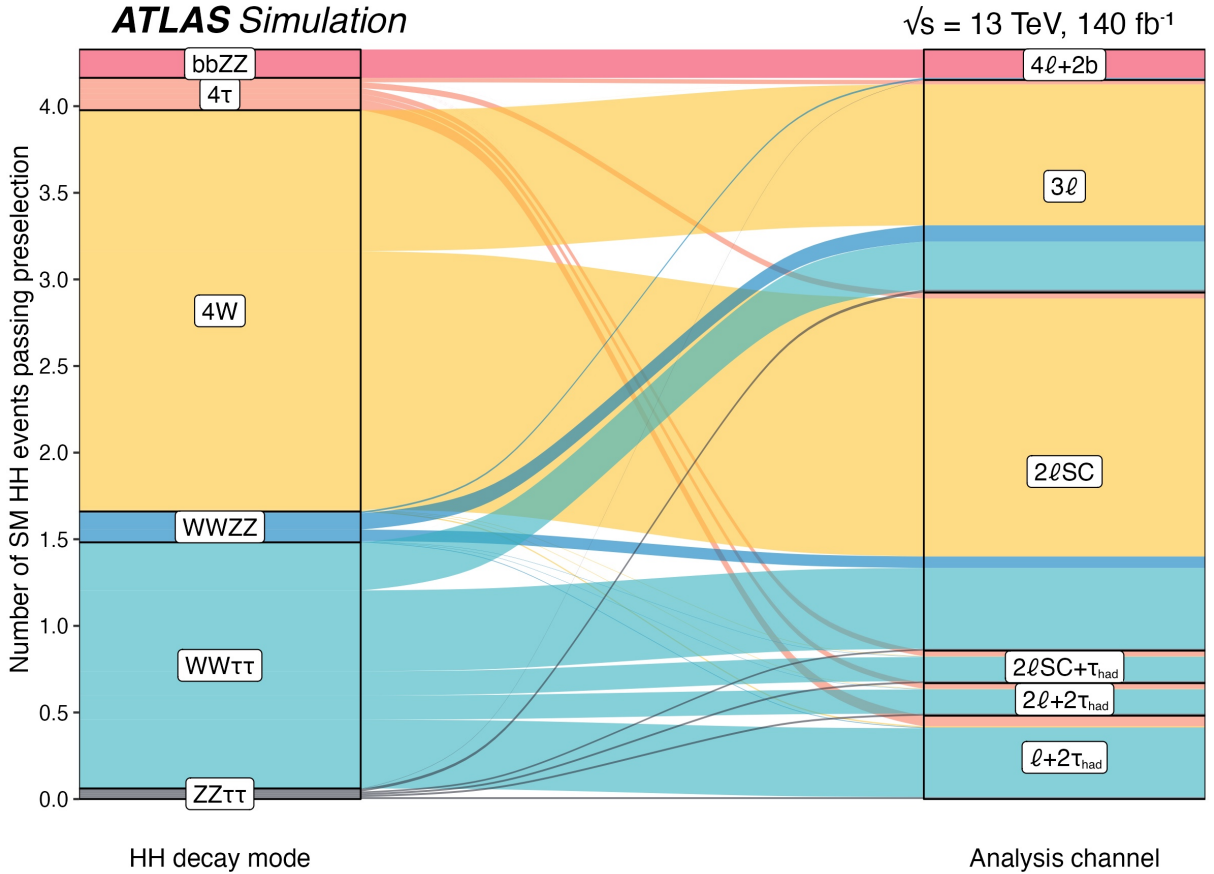


Figure 4: Number of ggF and VBF SM HH signal events satisfying the preselection requirements from the targeted HH decay modes on the left and their acceptance into the different ML search channels on the right. The $HH \rightarrow 4Z$ decay mode contributes less than 0.1% of preselected HH events and is not shown.

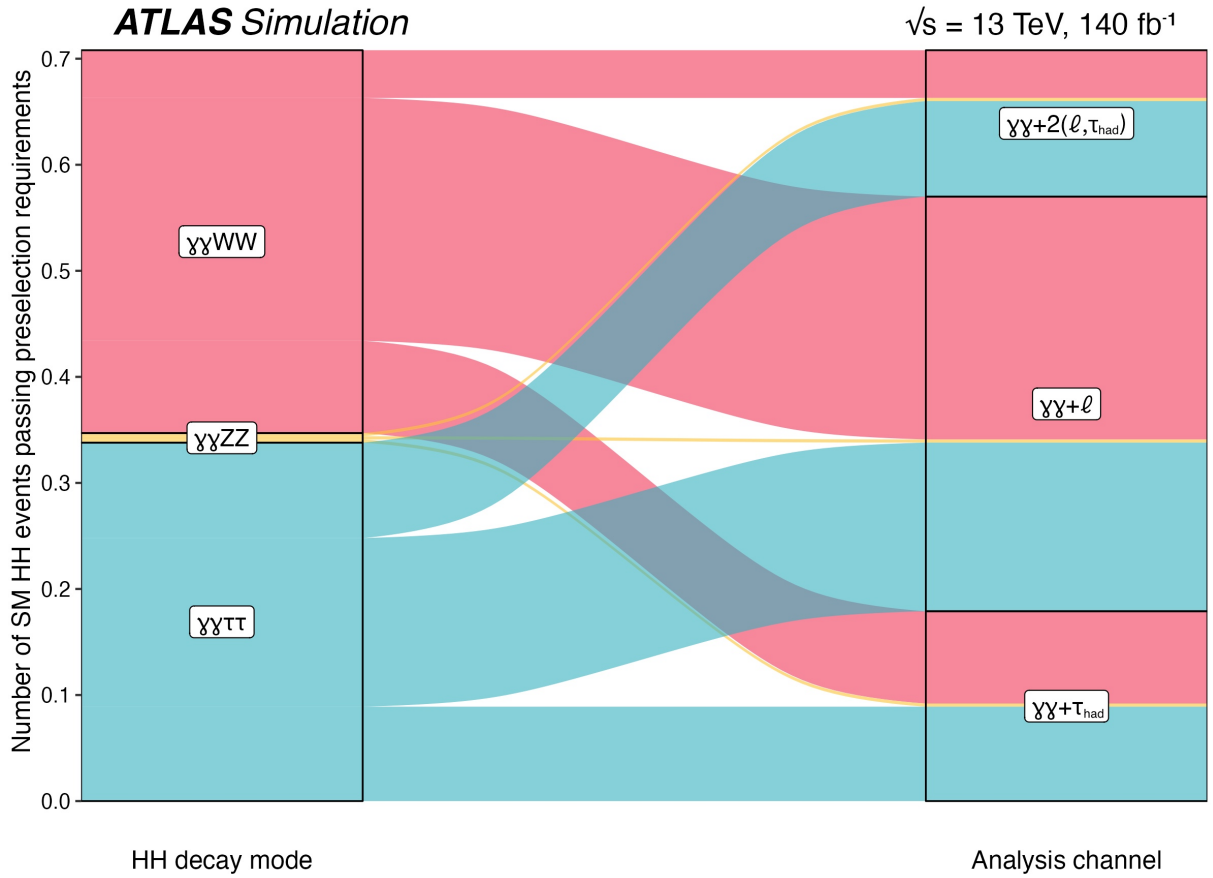


Figure 5: Number of ggF and VBF SM HH signal events satisfying the preselection requirements from the targeted HH decay modes on the left and their acceptance into the different $\gamma\gamma$ +ML search channels on the right.

6 Search strategy

All channels except the $\gamma\gamma+2(\ell, \tau_{\text{had}})$ channel use BDTs with the Gradient Boost [105] algorithm to separate signal from background processes. BDTs are optimised separately for each channel, in terms of the input variables and hyperparameters, using the area under the receiver operating characteristic (ROC) curve as the performance metric. Information about the kinematics of objects in the event are used as inputs to the BDT, as well as variables that probe the kinematic relationships between the objects, for example the angular separation or invariant mass of two or more objects. The complete list of all the variables used as inputs to the BDTs in the different channels is provided in the Appendix. No BDT or further event selection is used in the $\gamma\gamma+2(\ell, \tau_{\text{had}})$ channel analysis due to the low event yields and the signal region is therefore defined by the preselection requirements described in Section 5. Both the ggF HH and VBF HH processes are considered as signal in all channels. All background processes are included when training the BDTs used for the $4\ell+2b$, 3ℓ , and $\gamma\gamma$ +ML channel analyses, while the ML channels with hadronic taus in the final state ($2\ell\text{SC}+\tau_{\text{had}}$, $2\ell+2\tau_{\text{had}}$ and $\ell+2\tau_{\text{had}}$) are trained only against the dominant diboson (VV) background process. For the $2\ell\text{SC}$ channel, better separation of signal from background was demonstrated by training three BDTs separately to distinguish the HH signal from the main VV , $t\bar{t}$, and Z +jets background processes. The three output BDT score distributions are then used

as the input variables to a fourth BDT that is trained against all background processes and used as the final discriminating variable to separate signal from background. This strategy was found to improve the sensitivity of the $2\ell\text{SC}$ channel over the use of a single-BDT approach.

The BDT output score distribution is used as the final discriminant in each of the ML channels. The full distribution is used in the $4\ell+2b$, $2\ell+2\tau_{\text{had}}$, and $\ell+2\tau_{\text{had}}$ channels, while the 3ℓ , $2\ell\text{SC}$, and $2\ell\text{SC}+\tau_{\text{had}}$ channels use the high-BDT-score region as the signal region, and use the low-BDT-score region to validate the background model or constrain background processes, as described in Section 7. The BDT output score in the signal region is shown for each channel in Figure 6. In the $\gamma\gamma+\ell$ and $\gamma\gamma+\tau_{\text{had}}$ channels the BDT score is used to define ‘Tight’ ($0.6 < \text{BDT score} \leq 1$), ‘Medium’ ($0 < \text{BDT score} \leq 0.6$) and ‘Loose’ ($-1 \leq \text{BDT score} \leq 0$) signal regions, where the BDT score cuts are optimised to maximise the significance, and the Loose BDT score regions are used primarily as a background control region in the fit. The $m_{\gamma\gamma}$ distribution is used as the final discriminant in each $\gamma\gamma+\text{ML}$ signal region, as shown in Figure 7. The distributions in Figures 6 and 7 are shown after applying the likelihood fit to data (i.e. ‘post-fit’) under the background-only hypothesis as described in Section 9.

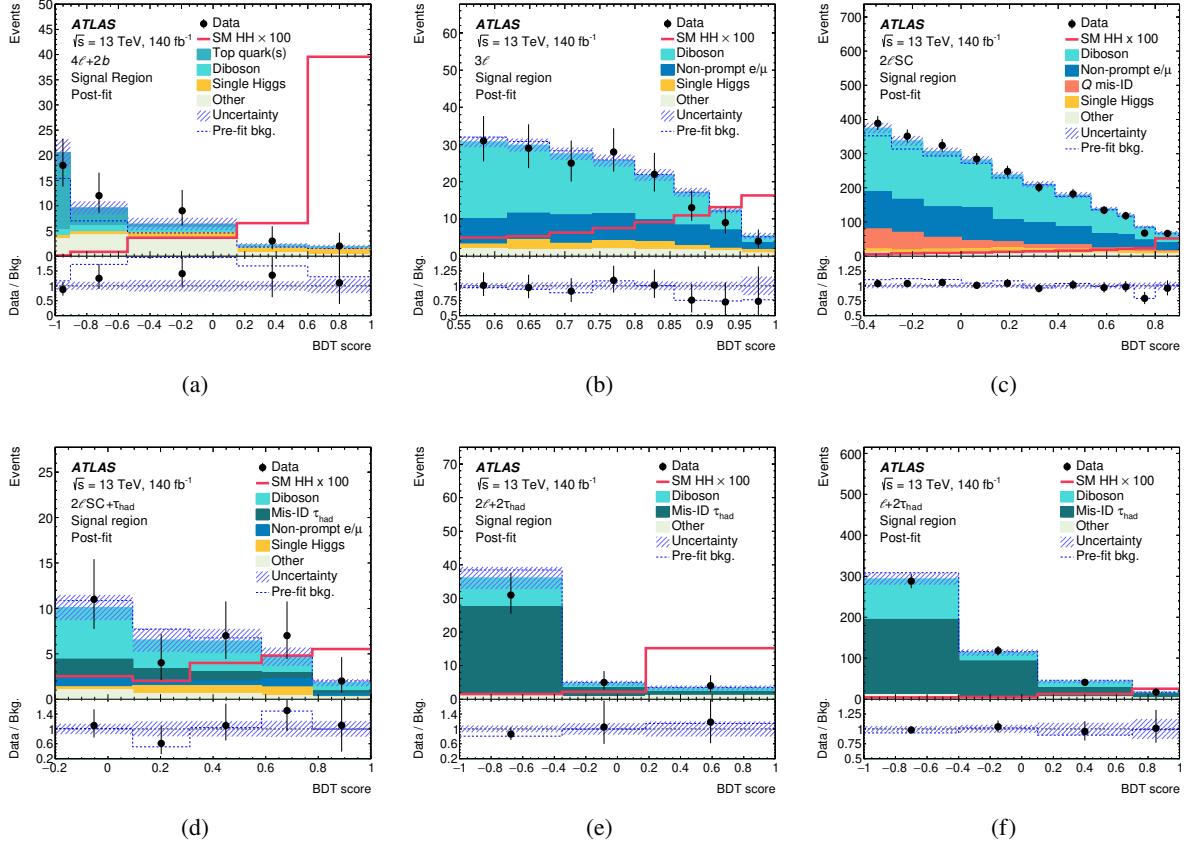


Figure 6: Distributions of the BDT output score in the signal regions of the (a) $4\ell+2b$, (b) 3ℓ , (c) $2\ell\text{SC}$, (d) $2\ell\text{SC}+\tau_{\text{had}}$, (e) $2\ell+2\tau_{\text{had}}$, and (f) $\ell+2\tau_{\text{had}}$ channels, after applying the likelihood fit to data under the background-only hypothesis as described in Section 9. The total pre-fit background (and its ratio to data) is also shown, as is the SM HH signal scaled up by a factor of 100. The uncertainty bands include all sources of statistical and systematic uncertainties in the background prediction.

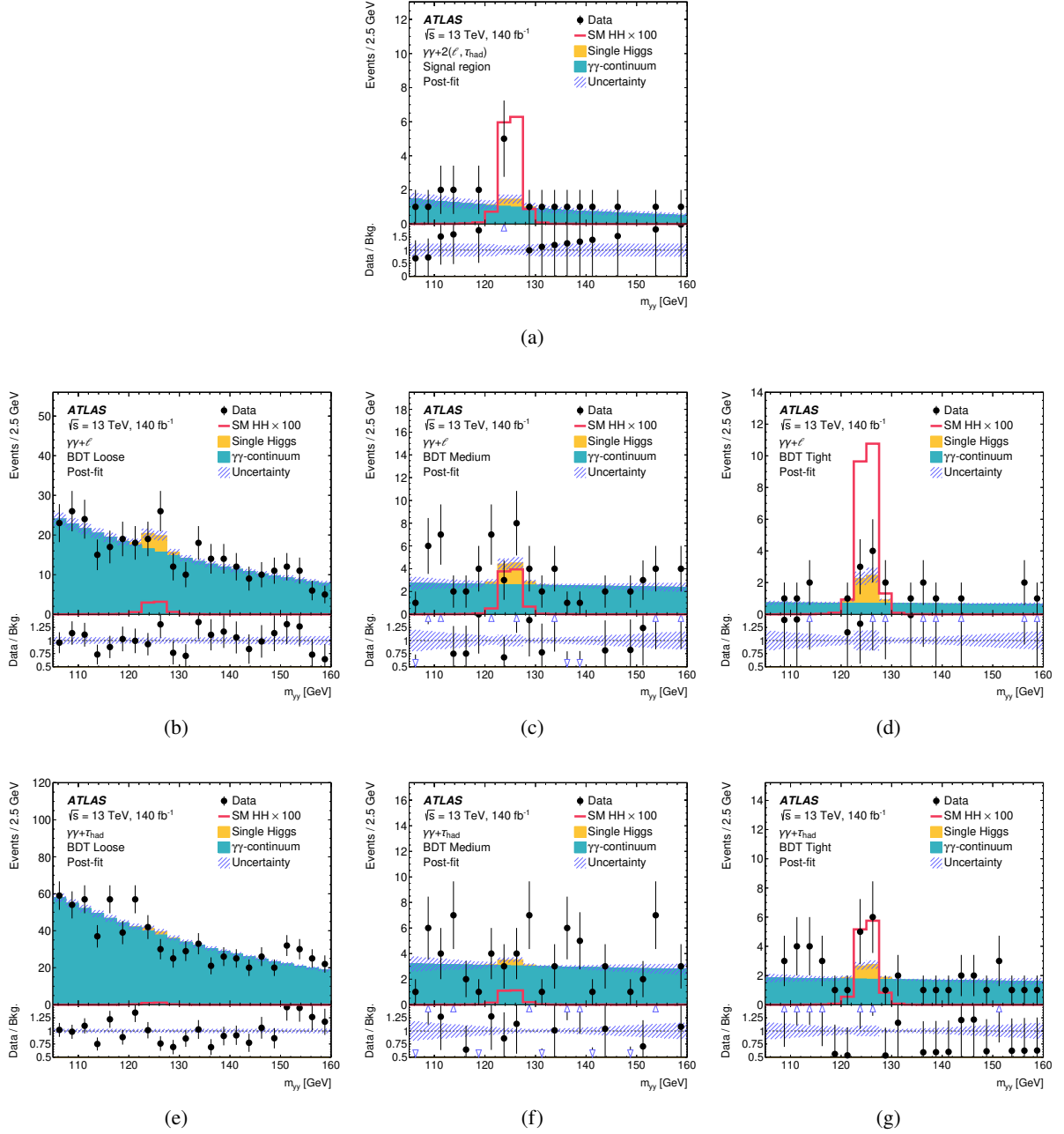


Figure 7: Distributions of the invariant mass of the diphoton system in the (a) $\gamma\gamma+2(\ell, \tau_{\text{had}})$, (b–d) $\gamma\gamma+\ell$, and (e–g) $\gamma\gamma+\tau_{\text{had}}$ channels, after applying the selection requirements described in Section 5 and the likelihood fit to data under the background-only hypothesis as described in Section 9. The $\gamma\gamma+\ell$ and $\gamma\gamma+\tau_{\text{had}}$ channel distributions are shown separately for the (b,e) Loose, (c,f) Medium, and (d,g) Tight signal regions. The SM HH signal scaled up by a factor of 100 is also shown. The uncertainty bands include all sources of statistical and systematic uncertainties in the background prediction.

7 Background estimation

The background composition varies for the different channels. Processes where the event selection requirements described in Section 5 are satisfied by prompt leptons and real hadronic taus produced in the decay chain are estimated using MC simulations (described in Section 3.2). Of these, the dominant background processes are normalised using control regions (CRs) in data that are orthogonal to the signal regions. Normalisation factors are derived by performing a simultaneous fit of all CRs and the signal region for each channel, as described in Section 9. Contributions from processes where at least one of the candidate leptons is a non-prompt lepton from b -hadron decays or photon conversions, or a lepton with misidentified charge, are estimated using template fits of simulated samples to data in CRs. Jets misidentified as $\tau_{\text{had-vis}}$ are referred to as fake- τ_{had} and are also estimated using data-informed corrections to simulations, as are the non-resonant $\gamma\gamma$ processes that constitute the dominant background in the $\gamma\gamma$ +ML channels. All ML channels use a validation region (VR) to verify the background modelling outside of the signal region and good agreement between data and the background predictions is observed throughout. The requirements that are applied to define the various control and validation regions, relative to the preselection requirements defined in Section 5, are shown in Table 5 for channels without $\tau_{\text{had-vis}}$, and Table 6 for channels with $\tau_{\text{had-vis}}$. Details about how the different types of background processes are estimated are given below. The evaluation of the systematic uncertainties associated to the (semi-)data-driven background is also described. Theoretical uncertainties in MC simulations are detailed in Section 8.2.

7.1 Prompt leptons

Diboson processes are a major background process to all of the ML channels, particularly the 3ℓ , $2\ell\text{SC}$, and $2\ell\text{SC}+\tau_{\text{had}}$ channels where these constitute approximately half the total background. A CR requiring $E_{\text{T}}^{\text{miss}} > 30$ GeV and selecting events that contain a same-flavour, opposite charge pair of leptons with an invariant mass consistent with the Z boson mass, is used in the 3ℓ channel to provide a region enriched in WZ events. Normalisation factors based on the jet multiplicity are calculated by comparing simulation to data in the CR and then applying the derived normalisation factors to simulated events in the signal region. Events with four or more jets are treated inclusively. The statistical uncertainty on the normalisation factor in each bin is taken as the systematic uncertainty associated to the method. The normalisation factors, μ , range from 0.92 ± 0.09 for events with one jet, to 0.75 ± 0.15 for events with four or more jets. Two CRs are employed in the $2\ell\text{SC}$ channel to normalise diboson processes, one enriched in WZ events (WZ CR) that follows closely the definition used for the equivalent CR in the 3ℓ channel, and the other targeting VV production in association with two or more jets ($VV\text{jj}$ CR), which controls the significant background from vector boson scattering (VBS) processes, and is dominated by the same-charge W boson pairs component (VBS $W^{\pm}W^{\pm}$). The full definitions are provided in Table 5. The WZ CR corrects for mismodellings in the MC simulations for diboson events with large jet multiplicity [106], while the $VV\text{jj}$ CR corrects for known mismodellings in the simulation of VBS processes [107]. The H_{T} (scalar sum of the p_{T} of all jets) distribution in the $VV\text{jj}$ CR is included in the final fit, as is a single bin in the WZ CR where only the overall normalisation is considered and no corrections are made to the shape of the MC simulation. Normalisation factors of 0.79 ± 0.05 and 1.61 ± 0.13 are obtained for the WZ and VBS $W^{\pm}W^{\pm}$ processes, respectively. A low-BDT-score (< -0.2) region is used to constrain the VV background in the $2\ell\text{SC}+\tau_{\text{had}}$ channel. This region is included in the final fit and a μ of 0.91 ± 0.23 is obtained.

A CR requiring that there are no b -jets in the event and that all four leptons satisfy the isolation requirements is used in the $4\ell+2b$ channel to simultaneously constrain the VV and single Higgs backgrounds in the fit.

Table 5: Selection criteria applied to form the control and validation regions used to estimate backgrounds, for the $4\ell+2b$, 3ℓ , and $2\ell\text{SC}$ channels relative to those used to define the preselection regions in Table 3. Requirements that are unchanged with respect to the preselection region are not listed (and indicated with a ‘–’ if completely unchanged for a given type of object). The multiplicity of jets, and of b -jets are denoted N_{jet} and $N_{b\text{-jet}}$, respectively. When no p_{T} (or E_{T}) threshold is specified, the default requirements for each object are used, as described in Section 4. Same-charge (opposite-charge) requirements between objects are denoted by ‘SC’ (‘OC’). The notation ‘SF’ is used to indicate where leptons are required to have the same flavour. SFOC (SFSC) stands for same-flavour, opposite-charge (same-flavour, same-charge). The ‘Z-veto’ requires that the invariant mass of two SFOC leptons must satisfy $|m_{\ell\ell} - m_Z| > 10$ GeV, while ‘Z-req.’ inverts this selection. In the $4\ell+2b$ channel, the SFOC lepton pair with an invariant mass closest to the Z boson mass is defined as the lepton pair coming from the on-shell Z boson decay (on-shell- $\ell\ell$) while the remaining SFOC lepton pair is defined as coming from the off-shell Z boson decay (off-shell- $\ell\ell$). The radius of a conversion vertex from the primary vertex is denoted by r_{vtx} , and the invariant mass of the two opposite-charge tracks at the conversion vertex by $m_{\text{trk,trk}}$. Regions that are included in the final fit are indicated with a *.

Channel	Region	Leptons	Jets	b -jets	Additional selections
$4\ell+2b$	$t\bar{t}$ CR*	Off-shell- $\ell\ell$ not SFOC Z-veto	–	–	–
	$t\bar{t}Z$ CR*	Off-shell- $\ell\ell$ not SFOC All ℓ pass loose PLV Z-req.	–	–	–
	VV, H CR* Z+jets CR*	$m_{4\ell}$ req. removed All ℓ pass loose PLV $p_{\text{T}}(\ell_3) < 10$ GeV $p_{\text{T}}(\ell_4) < 10$ GeV Z-req.	–	$N_{b\text{-jet}} = 0$ –	– –
	VR	–	–	–	$ m_{4\ell} - m_H > 10$ GeV
3ℓ	WZ CR* HF- e CR*	Z-req. $\ell_{\text{SC1}}, \ell_{\text{SC2}}$ both e No PLV on any ℓ	– $N_{\text{jet}} \geq 2$	– $N_{b\text{-jet}} \geq 2$	$E_{\text{T}}^{\text{miss}} > 30$ GeV
	HF- μ CR*	$\ell_{\text{SC1}}, \ell_{\text{SC2}}$ both μ No PLV on any ℓ	$N_{\text{jet}} \geq 2$	$N_{b\text{-jet}} \geq 2$	–
	Mat. conv. CR*	$ m_{3\ell} - m_Z < 10$ GeV ℓ_{SC1} or ℓ_{SC2} : $r_{\text{vtx}} > 20$ mm $0 < m_{\text{trk,trk}} < 100$ MeV	–	–	–
	VR	–	–	–	BDT < 0.55
$2\ell\text{SC}$	WZ CR*	$\geq 3\ell(\text{T})$, $p_{\text{T}} > 20$ GeV One SFOC pair Z-req.	–	–	$E_{\text{T}}^{\text{miss}} > 30$ GeV
	$VV\text{jj}$ CR*	$m_{\ell\ell}$ (any pair) > 12 GeV $ m_{3\ell} - m_Z > 10$ GeV Z-veto (SFSC pair)	$m_{\text{jj}} > 300$ GeV	–	BDT < –0.4 BDT $_{\text{Z+jets}}$ > –0.8
	HF- e CR1*	$\ell(\text{T})e(\text{T})$, no PLV	$2 \leq N_{\text{jet}} \leq 3$	$N_{b\text{-jet}} = 1$	–
	HF- e CR2*	$\ell(\text{T})e(\text{T})$, no PLV	$2 \leq N_{\text{jet}} \leq 3$	$N_{b\text{-jet}} \geq 2$	–
	HF- μ CR*	$\ell(\text{T})\mu(\text{T})$, no PLV	$2 \leq N_{\text{jet}} \leq 3$	$N_{b\text{-jet}} \geq 1$	–
	Mat. conv. CR*	$r_{\text{vtx}} > 20$ mm $m_{\text{trk,trk}} < 100$ MeV	–	$N_{b\text{-jet}} \geq 1$	–
	Int. conv. CR*	$r_{\text{vtx}} < 20$ mm $m_{\text{trk,trk}} < 100$ MeV	–	$N_{b\text{-jet}} \geq 1$	–
	Q mis-ID CR VR	$2e(\text{T})$, OC or SC –	$N_{\text{jet}} < 2$ –	– –	– BDT < –0.4

Table 6: Selection criteria applied to form the control and validation regions used to estimate backgrounds, for the $2\ell\text{SC}+\tau_{\text{had}}$, $2\ell+2\tau_{\text{had}}$, and $\ell+2\tau_{\text{had}}$ channels relative to those used to define the preselection regions in Table 3. Requirements that are unchanged with respect to the preselection region are not listed (and indicated with a ‘–’ if completely unchanged for a given type of object). The multiplicity of (anti-ID) $\tau_{\text{had-vis}}$, jets, and b -jets are denoted $N_{(\text{anti-ID})\tau}$, N_{jet} , and $N_{b\text{-jet}}$, respectively. When no p_{T} (or E_{T}) threshold is specified, the default requirements for each object are used, as described in Section 4. Same-charge (opposite-charge) requirements between objects are denoted by ‘SC’ (‘OC’). The notation ‘SFOC’ stands for same-flavour, opposite-charge. The ‘Z-veto’ requires that the invariant mass of two SFOC leptons must satisfy $|m_{\ell\ell} - m_{\text{Z}}| > 10 \text{ GeV}$, while ‘Z-req.’ inverts this selection. Regions that are included in the final fit are indicated with a *. The $2\ell+2\tau_{\text{had}}$ and $\ell+2\tau_{\text{had}}$ channels use the same regions of data to derive fake-factors in the Z+jets-enriched and $t\bar{t}$ -enriched CRs.

Channel	Region	Leptons	(anti-ID) $\tau_{\text{had-vis}}$	Jets	b -jets	Additional selections
$2\ell\text{SC}+\tau_{\text{had}}$	VV CR*	–	–	–	–	BDT < -0.2
	HF- e CR1*	$\ell(\text{T})e(\text{T})$, no PLV	–	$N_{\text{jet}} \geq 2$	$N_{b\text{-jet}} = 1$	–
	HF- e CR2*	$\ell(\text{T})e(\text{T})$, no PLV	–	$N_{\text{jet}} \geq 2$	$N_{b\text{-jet}} \geq 2$	–
	HF- μ CR*	$\ell(\text{T})\mu(\text{T})$, no PLV	–	–	–	–
	Fake- $\tau_{\text{had-vis}}$ CR	OC leptons Z-veto	–	–	–	–
	Z+jets VR	OC leptons Z-req.	–	–	–	–
	$t\bar{t}$ VR	OC leptons Z-veto	–	$N_{\text{jet}} = 2$	$N_{b\text{-jet}} = 1$	–
VR	–	–	$N_{\text{jet}} < 2$	–	–	
$2\ell+2\tau_{\text{had}}$ and $\ell+2\tau_{\text{had}}$	Z+jets CR	$2\ell(\text{T})$, OC Z-req.	$N_{\tau} + N_{\text{anti-ID } \tau} = 2$	$N_{\text{jet}} \geq 1$	$N_{b\text{-jet}} = 0$	–
	$t\bar{t}$ CR	$2\ell(\text{T})$, OC Z-veto	$N_{\tau} + N_{\text{anti-ID } \tau} = 2$	$N_{\text{jet}} \geq 1$	$N_{b\text{-jet}} = 1$	–
$2\ell+2\tau_{\text{had}}$	Fake- $\tau_{\text{had-vis}}$ CR	–	$(N_{\tau} = 1, N_{\text{anti-ID } \tau} = 1)$ or $N_{\text{anti-ID } \tau} = 2$	–	–	–
	Fake- $\tau_{\text{had-vis}}$ VR	–	SC $\tau_{\text{had-vis}}$	–	–	–
$\ell+2\tau_{\text{had}}$	Fake- $\tau_{\text{had-vis}}$ CR	–	$(N_{\tau} = 1, N_{\text{anti-ID } \tau} = 1)$ or $N_{\text{anti-ID } \tau} = 2$	–	–	–
	Fake- $\tau_{\text{had-vis}}$ VR	–	SC $\tau_{\text{had-vis}}$	–	–	–

Normalisation factors of 1.12 ± 0.46 and 1.09 ± 0.42 are obtained. Other CRs, defined in Table 5, are used in the $4\ell+2b$ channel to constrain the $t\bar{t}Z$ ($\mu = 1.27 \pm 0.22$), $t\bar{t}$ ($\mu = 1.50 \pm 0.28$) and Z +jets ($\mu = 1.01 \pm 0.36$) backgrounds. The latter two contain a mix of prompt and non-prompt or misidentified leptons but no attempt is made to separate these and the background shape is determined using MC simulations. The BDT classifier used to discriminate signal from background is applied to the data and simulated samples in the $4\ell+2b$ channel CRs and the resulting BDT output score distributions are included in the final fit.

The normalisation of the $t\bar{t}W$ background in the 2ℓ SC channel is obtained while performing the final fit by allowing the normalisation of the $t\bar{t}W$ process to float in the three CRs used to constrain the non-prompt lepton backgrounds from decays of heavy-flavour hadrons, as described below. The $t\bar{t}W$ process, which can yield a true same-charge lepton pair, provides a significant contribution in these CRs. A μ of 1.17 ± 0.34 is obtained. For all other cases, background processes involving prompt leptons and real hadronic taus are taken directly from MC simulations and normalised to their cross-sections at the highest order available.

7.2 Non-prompt leptons

The non-prompt lepton background category encompasses events where lepton candidates do not originate from the primary interaction point. These non-prompt lepton backgrounds arise from various sources including $t\bar{t}$, Z +jets, W +jets, $V\gamma$, and other processes where a lepton is produced from a heavy-flavour (b , c) hadron decay or from photon conversions. Non-prompt leptons contribute a significant source of background in the 3ℓ , 2ℓ SC, and 2ℓ SC+ τ_{had} channels and are estimated by using a template fit method where a simultaneous fit of the MC simulations to data is performed in several CRs (and the signal regions), each enriched in a different source of non-prompt leptons.

Photon conversions, where high-energy photons transform into electron-positron pairs, occur through two primary mechanisms: internal conversions and material conversions. Internal conversions stem from electron-positron pair creation in a decay that might otherwise have emitted a photon. Material conversions occur when high-energy photons interact with detector materials, generating electron-positron pairs within the detector. In the 3ℓ channel, the contribution of non-prompt leptons coming from internal conversions is very small and the shape and normalisation of this background is estimated using MC simulation. Conversely, the material conversion backgrounds in the 3ℓ channel are constrained using a control region ('Mat. conv. CR' in Table 5) where the same-charge leptons are required to be associated with a conversion vertex with radius $r_{\text{vtx}} > 20$ mm from the primary vertex, and the invariant mass of the two tracks at the conversion vertex, $m_{\text{trk, trk}} < 100$ MeV. An additional requirement that the invariant mass of the three leptons be consistent with the Z boson mass is also applied to preferentially select $Z \rightarrow \ell\ell\gamma^*$ ($\gamma^* \rightarrow \ell'\ell'$) events where one of the leptons is out of acceptance, and further enrich the region with events containing a material conversion. This region is included in the final fit with one bin and a μ of 0.66 ± 0.13 is obtained. For the 2ℓ SC channel, an internal conversion CR ('Int. conv. CR' in Table 5) is defined by requiring that the leptons are associated with a conversion vertex with radius $r_{\text{vtx}} < 20$ mm from the primary vertex, and an invariant mass of the two opposite-charge tracks at the primary vertex, $m_{\text{trk, trk}} < 100$ MeV. Another CR requiring that leptons have a conversion vertex with radius $r_{\text{vtx}} > 20$ mm from the primary vertex and an invariant mass of the two opposite-charge tracks at the conversion vertex, $m_{\text{trk, trk}} < 100$ MeV is used to constrain material conversions ('Mat. conv. CR' in Table 5). These regions are included in the final fit with one bin and μ s of 1.84 ± 0.28 and 1.30 ± 0.39 are obtained for the internal conversion and material conversion processes, respectively. Unlike in the 3ℓ channel where material conversions stem from $V\gamma$ and Z +jets events, in the 2ℓ SC channel this originates mostly from top quark and $V\gamma$ backgrounds, which leads to the

different normalisation factors between the two channels. Photon conversions are a negligible background in the $2\ell\text{SC}+\tau_{\text{had}}$ channel and their shape and normalisation is taken directly from simulations.

Additional dedicated CRs are defined to estimate backgrounds originating from the decay of heavy-flavour hadrons into muons (HF- μ) or electrons (HF- e). For the HF- e (HF- μ) CR in the 3ℓ channel, the same-charge leptons $\ell_{\text{SC}1}$ and $\ell_{\text{SC}2}$ are chosen to be electrons (muons) and the PLV isolation requirements are dropped for all three leptons. Additional selections requiring that there are at least two b -tagged jets are also applied to these CRs to further enrich the heavy-flavour backgrounds. The distribution of the ΔR between ℓ_{OC} and $\ell_{\text{SC}1}$ in the CRs are included in the final fit and μ s of 1.50 ± 0.50 and 1.51 ± 0.23 are obtained from the HF- e CR and HF- μ CR, respectively. Two CRs requiring at least one electron, removing the requirements on the PLV isolation, and requiring that there are two or three jets in the event, are employed in the $2\ell\text{SC}$ channel to estimate the HF- e background. The first CR requires that exactly one of the jets is b -tagged, while the second requires that exactly two jets are b -tagged. The two HF- e CRs contain different relative contributions from electrons with a mis-ID charge (discussed in Section 7.3 below) and including both CRs provides additional information that improves the constraints on the HF- e background. An analogous region is used as a HF- μ CR, where events with at least one μ are selected with the same lepton isolation requirements as in the HF- e CR. In addition, the HF- μ CR is required to have two or three jets, at least one of them b -tagged. The distribution of the ΔR between the two leptons in the first HF- e CR, and the distributions of the scalar sum of the p_{T} of all leptons and $E_{\text{T}}^{\text{miss}}$ in the second HF- e CR and the HF- μ CR, are included in the final fit. Normalisation factors of 1.17 ± 0.30 and 1.63 ± 0.20 are obtained for the HF- e and HF- μ backgrounds, respectively. For the $2\ell\text{SC}+\tau_{\text{had}}$ channel, the same CR definitions as for the $2\ell\text{SC}$ channel are applied relative to the preselection requirements, but loosening the jet multiplicity requirements to allow events to have at least two jets. Normalisation factors of 0.87 ± 0.09 and 0.75 ± 0.06 are obtained for the HF- e and HF- μ backgrounds, respectively.

The systematic uncertainty in this template fit method for the various non-prompt lepton background components is determined by relaxing the isolation and identification criteria applied to the leptons. The templates obtained using MC simulations are compared with the shape of distributions in data after subtracting the expected contributions from processes with prompt leptons using MC simulations. For each source of non-prompt lepton backgrounds, the difference between the simulation-based template and these residual data events obtained with the adjusted criteria are considered as uncertainties in the shape of the estimates obtained under the nominal conditions.

7.3 Charge misassignment

Backgrounds where the charge of the lepton was incorrectly assigned primarily affect the $2\ell\text{SC}$ channel. Such events originate from Z +jets, $t\bar{t}$ and WW processes, where one electron undergoes a hard bremsstrahlung and asymmetric conversion ($e^{\pm} \rightarrow e^{\pm}\gamma^* \rightarrow e^{\pm}e^+e^-$), or the track curvature is mismeasured. The rate of electron charge mismeasurement is measured in data by taking the ratio of same-charge and opposite-charge pairs of electrons in a high purity sample of $Z \rightarrow e^+e^-$ events, following the method described in Ref. [87]. The CR is defined by selecting events satisfying the $2\ell\text{SC}$ preselection criteria, but removing the lepton charge requirements and requiring that there are less than two jets in the event. The charge misidentification rates are measured separately for prompt electrons and electrons that originate from either an internal conversion or a material conversion (following analogous selection requirements as used for the non-prompt lepton CRs described above). Rates are calculated as a function of p_{T} and η of the electrons in each category and range from 10^{-5} for low- p_{T} prompt electrons to 10^{-1} for high- p_{T} electrons with a large-radius conversion, but are more typically around 10^{-3} . The measured charge misassignment rate is applied to

data events satisfying the requirements of the $2\ell\text{SC}$ channel preselection, but requiring that the two leptons have opposite charge. Uncertainties in the method are evaluated by comparing the nominal rates with those computed using simulated $Z \rightarrow e^+e^-$ events, and by varying the requirements on the dielectron invariant mass used to select $Z \rightarrow e^+e^-$ events. The muon charge misassignment rate is negligible in the p_T range considered. Processes with a misassigned charge constitute less than 1% of events in the 3ℓ and $2\ell\text{SC}+\tau_{\text{had}}$ signal regions and for these channels their contribution is taken from the MC simulations.

7.4 Misidentified hadronic taus

Quark- or gluon-initiated jets that are incorrectly reconstructed as a $\tau_{\text{had-vis}}$ (fake- $\tau_{\text{had-vis}}$) are an important background in the $2\ell\text{SC}+\tau_{\text{had}}$, $2\ell+2\tau_{\text{had}}$, and $\ell+2\tau_{\text{had}}$ channels. In the $2\ell\text{SC}+\tau_{\text{had}}$ channel, background processes where a jet fakes the $\tau_{\text{had-vis}}$ are estimated by deriving scale factors to correct the rate of jets to be misidentified as hadronic taus in MC to match the rate in data. The scale factors are derived by comparing the rates of jets satisfying the $\tau_{\text{had-vis}}$ identification requirements in data, to the rate in MC simulations, in a control region defined by applying the same preselection requirements described in Section 5 but requiring that the two light leptons have opposite-sign charge and that their invariant mass is not compatible with m_Z . Contributions from processes containing real $\tau_{\text{had-vis}}$ or prompt leptons are subtracted from data using predictions from MC simulations before computing the ratio. Scale factors are derived separately for one- and three-prong taus, as a function of the $\tau_{\text{had-vis}}$ p_T . The derived scale factors are applied to the relevant simulated events in the signal region and are in the range of 0.68–0.86 (0.48–0.82) for one-prong (three-prong) taus. Two VRs, enriched with fake- $\tau_{\text{had-vis}}$ in Z +jets and $t\bar{t}$ events are respectively defined by modifying the CR to require that the invariant mass of the two light leptons is consistent with the Z boson mass, and by requiring that there are exactly two jets in the event, exactly one of which passes the b -tagging requirements. The largest difference in each region and p_T bin, between the scale factors derived in the nominal CR and those derived in the VRs, is taken as an uncertainty in the method. An additional source of systematic uncertainty is considered by varying the real- $\tau_{\text{had-vis}}$ contribution from simulations up and down by 50%. The total uncertainty in the scale factors ranges from 20% to 34%, depending on the p_T range and number of prongs considered.

Fake- $\tau_{\text{had-vis}}$ backgrounds in the $2\ell+2\tau_{\text{had}}$ and $\ell+2\tau_{\text{had}}$ channels are estimated from data using the fake-factor method described in Ref. [108]. The fake-factors are estimated in a CR enriched in Z +jets events (the ‘ Z +jets CR’ in Table 6) that is common to both channels. The CR requires that there are exactly two tau candidates, each of which is required to satisfy either the $\tau_{\text{had-vis}}$ or anti-ID $\tau_{\text{had-vis}}$ criteria. The events are divided into sub-regions based on whether the leading tau candidate satisfies the $\tau_{\text{had-vis}}$ or anti-ID $\tau_{\text{had-vis}}$ requirements, and the fake-factors are taken as the ratio of the number of events in each sub-region, and are derived as a function of p_T , $|\eta|$ and number of prongs of the (anti-ID) $\tau_{\text{had-vis}}$. The process is repeated, subdividing events based on whether the subleading tau satisfies the $\tau_{\text{had-vis}}$ or anti-ID $\tau_{\text{had-vis}}$ requirements. Finally, the fake-tau backgrounds are estimated in the $2\ell+2\tau_{\text{had}}$ and $\ell+2\tau_{\text{had}}$ signal regions by using the derived fake-factors to reweight templates obtained from data in CRs (the ‘Fake- $\tau_{\text{had-vis}}$ CR’s in Table 6), by applying the respective signal region requirements but requiring that at least one of the two taus instead satisfies the anti-ID $\tau_{\text{had-vis}}$ requirements. The fake-factors are also estimated in a CR enriched in $t\bar{t}$ events in order to check the dependency of the fake-factors to light-flavour quark, heavy-flavour quark, or gluon-initiated jets. The measured fake-factors in the $t\bar{t}$ CR are consistent within statistical uncertainties with the nominal ones, but the difference ($\sim 30\%$) is treated as a systematic uncertainty arising from the different jet compositions in each region. The contribution of real $\tau_{\text{had-vis}}$ satisfying the anti-ID $\tau_{\text{had-vis}}$ requirements is varied up and down by 15% to account for theoretical uncertainties in these processes, and

the impact on the derived fake-factors is considered as an additional source of uncertainty. The fake- $\tau_{\text{had-vis}}$ background estimate is validated in VRs that follow the signal region definition but require that the two $\tau_{\text{had-vis}}$ have the same-sign charge. Good agreement between the data and the background prediction is observed in the $2\ell+2\tau_{\text{had}}$ and $\ell+2\tau_{\text{had}}$ channel fake- $\tau_{\text{had-vis}}$ VRs, within the available statistical precision. A 10% discrepancy is observed in the $\ell+2\tau_{\text{had}}$ fake- $\tau_{\text{had-vis}}$ VR, which is then conservatively considered as an additional uncertainty in the fake- $\tau_{\text{had-vis}}$ background estimate in both the $2\ell+2\tau_{\text{had}}$ and $\ell+2\tau_{\text{had}}$ channels.

7.5 Non-resonant $\gamma\gamma$ production

Non-resonant $\gamma\gamma$ production originates from $\gamma\gamma$ +jets, $V\gamma\gamma$, and $t\bar{t}\gamma\gamma$ processes, as well as from processes where a jet is incorrectly identified as a photon. This $\gamma\gamma$ -continuum background is expected to have a smoothly falling shape. It is modelled using a functional form chosen by fitting the diphoton invariant mass distribution in sidebands around the Higgs boson mass [$105 \text{ GeV} < m_{\gamma\gamma} < 120 \text{ GeV}$, $130 \text{ GeV} < m_{\gamma\gamma} < 160 \text{ GeV}$] in a CR in data, following the methodology described in Refs. [28, 86]. The CR is defined by requiring that events have no P-type leptons (as defined in Table 2) or $\tau_{\text{had-vis}}$, have one ($\gamma\gamma+\ell$ and $\gamma\gamma+\tau_{\text{had}}$ channels) or two ($\gamma\gamma+2(\ell, \tau_{\text{had}})$ channel) jets, and satisfy all other preselection requirements defined in Section 5. A first-order exponential function is observed to provide the best fit to the background model in all regions. This function is used to generate a background histogram, with floating functional form parameters when fitting to the data in sidebands. The fit is performed separately in each region and each channel, but in the $\gamma\gamma+\ell$ and $\gamma\gamma+\tau_{\text{had}}$ channels the BDT Medium and BDT Tight regions are combined to obtain the fit parameters, and the obtained background template is then normalised to the sidebands in each region separately.

The potential bias associated with the choice of functional form to model the continuum background is evaluated in each signal region by fitting the background template using a model with free parameters following the prescriptions described in Refs. [86, 109]. Uncertainties of up to 4% due to this ‘spurious signal’ uncertainty are obtained. An additional source of uncertainty in the shape of the non-resonant background caused by differences in the background composition between the signal region and the CR is estimated using MC simulations of photon pairs produced in association with one or two jets. The background template is derived using these simulated samples in the CR region, requiring exactly zero P-type leptons and $\tau_{\text{had-vis}}$, and comparing this to the background template obtained from the simulated samples when the same lepton and $\tau_{\text{had-vis}}$ requirements of the respective signal regions are applied. The difference between these two estimates is taken as the uncertainty in the nominal background estimate derived from data. Uncertainties in the background normalisation of 13.1% (8.4%) are measured in the Medium (Tight) BDT-score regions of the $\gamma\gamma+\ell$ channel, 12.4% (8.0%) in the Medium (Tight) BDT-score regions of the $\gamma\gamma+\tau_{\text{had}}$ channel, and less than 2% in all other regions.

8 Systematic uncertainties

For every channel, the total uncertainty is dominated by the statistical uncertainty in the number of data events in the signal region. Experimental sources of systematic uncertainty due to the detector response and background modelling are considered, as are theoretical uncertainties in the normalisation and shape of signal and background processes. The finite statistics of MC simulations used in the analysis are also considered as a source of systematic uncertainty. The impact of the different sources of uncertainty in the

expected μ_{HH} upper limit at 95% CL is summarised in Table 7 for the combination of all channels, and for the combinations of the ML channels and $\gamma\gamma$ +ML channels separately.

Table 7: Breakdown of the relative contributions to the uncertainties in the expected μ_{HH} upper limit at 95% CL, as determined in the likelihood fit to data described in Section 9, for combinations of the ML channels, the $\gamma\gamma$ +ML channels, and all channels. The impact of the uncertainties is quantified as the relative variation of the expected upper limit when re-evaluating the profile likelihood ratio after fixing a nuisance parameter to its best-fit value, while all other nuisance parameters are allowed to float. Individual sources of uncertainty that have an impact smaller than 1% in all channels are not listed.

Systematic uncertainty source	Relative impact of systematic uncertainties [%]		
	ML channels	$\gamma\gamma$ +ML channels	Combination
Total	22	14	19
MC statistics	5	<1	3
Experimental	5	<1	3
Detector response	4		3
Jets and E_T^{miss}	3		2
Flavour tagging	1		<1
Background estimate	<1	<1	<1
Theoretical	13	14	13
Signal	10	12	11
Backgrounds	4	2	3
Top quark	1	–	<1
Vector boson	3	–	2
Single Higgs boson	1	2	1
Other	<1	–	<1

8.1 Experimental uncertainties

The uncertainty in the combined 2015–2018 integrated luminosity is 0.83% [45], obtained using the LUCID-2 detector [46] for the primary luminosity measurements, complemented by measurements using the inner detector and calorimeters. An uncertainty arising from the correction of the pile-up distribution in simulation to that in data is also considered.

The impact of uncertainties in the trigger, reconstruction, identification and isolation efficiencies of electrons [87, 103], muons [90, 104], and photons [87, 103] are considered. An additional uncertainty in the track-to-vertexing matching is applied to muons. Reconstruction and identification efficiency uncertainties on $\tau_{\text{had-vis}}$ [97] are also considered, along with the uncertainty associated with measurements of the $\tau_{\text{had-vis}}$ energy scale, and the efficiency of the electron veto used in the $\tau_{\text{had-vis}}$ selection.

Jet energy scale and resolution uncertainties [110] and the uncertainty in the efficiency of matching jets to the primary vertex [98] are considered. These energy scale and resolution uncertainties, in addition to an uncertainty in the tracks matched to the primary vertex but not associated with other reconstructed objects in the event, are propagated to the E_T^{miss} calculation [102]. Uncertainties in the b -jet tagging efficiency and misidentification rates are estimated using $t\bar{t}$ events [100, 111] for b - and c -jets, and Z +jets events for light-flavour jets [112], and considered in the analysis.

Systematic uncertainties associated with the experimental methods used for the background estimates are described in Section 7.

8.2 Theoretical uncertainties

Several sources of theoretical uncertainty impacting the signal models are considered. The uncertainties linked to the modelling of the parton shower and underlying event are assessed by comparing the nominal sample, where the showering process is modelled using PYTHIA 8, with an alternative sample that uses HERWIG 7. Uncertainties in the matrix element calculation are assessed by varying the factorisation and renormalisation scales employed in the generator, either independently or concurrently, by a factor of two. Theoretical uncertainties related to the ggF HH cross-section, stemming from uncertainties in the PDF and α_s ($\pm 3.0\%$), as well as the selection of renormalisation scheme and the top quark mass scheme ($^{+6\%}_{-23\%}$) [16, 17] are also considered. Uncertainties in the VBF HH cross-section are also considered and are dominated by the uncertainty in the PDF and α_s ($\pm 2.1\%$). These cross-section uncertainties are factored into the determination of the upper limits on the HH signal strength, as well as the likelihood-based constraints on the values of the κ_λ modifier. Theoretical uncertainties associated with the branching ratios of the Higgs bosons [113] range from 1.2% to 2.1% and are also considered but their impact is negligible. The variation of the branching ratio uncertainty with κ_λ is not considered.

Background modelling uncertainties due to the choice of generator for the hard scatter and parton shower are considered by comparing them with alternative simulation setups, as detailed in Table 1, where available. Uncertainties due to the choice of renormalisation and factorisation scales are evaluated by varying these by factors of 0.5 and 2, relative to the nominal scales. For background processes where the normalisation is determined from control regions in data, no uncertainty in the cross-section is considered. Uncertainties of 20% [114], and 5% [115] are considered on the normalisations of the $t\bar{t}t$, and tZ/γ^* processes, respectively. Conservatively, a 50% uncertainty in the normalisation of $t\bar{t}t$, tW , tZ/γ^* , $t\bar{t}W^+W^-$, and VVV backgrounds is applied.

Theoretical uncertainties associated with single Higgs boson production cross-sections due to missing higher-order QCD corrections, the effects of PDF and α_s uncertainties, and the uncertainties in the branching fractions, are taken from Ref. [113]. The total theoretical uncertainties in the different single Higgs boson production cross-sections are 9% for ggF, 3% for VBF, 3% for WH , 4% for ZH , and 11% for $t\bar{t}H$. The uncertainty in the single Higgs background processes due to the choice of parton shower model is evaluated for the $t\bar{t}H$ process in the ML channels, and for the ggF, VBF, VH and $t\bar{t}H$ processes in the $\gamma\gamma$ +ML channels by comparing the predictions of the nominal simulation using the PYTHIA 8 model with an alternative simulation in which the same generator-level events are showered with HERWIG 7. The uncertainties are 8% and 10% for the $\gamma\gamma$ +ML and $4\ell+2b$ channels and less than 3% for all other channels. An uncertainty of 10% (40%) is assigned to cover parton shower model uncertainties on VH backgrounds to the 3ℓ and $2\ell SC$ ($4\ell+2b$, $2\ell SC+\tau_{\text{had}}$, $2\ell+2\tau_{\text{had}}$, and $\ell+2\tau_{\text{had}}$) channels, following the observations in Refs. [29, 116]. An additional 100% uncertainty is assigned to the ggF, VBF, and VH processes in the $4\ell+2b$ channel in order to account for difficulties in the modelling of these processes in association with heavy-flavour jets.

9 Statistical treatment and results

Measurements of the HH signal strength and constraints on the self-coupling strength are obtained using a binned likelihood function $L(\alpha, \theta)$, following the method described in Ref. [117]. The variable α represents the parameters of interest (POI) associated with the measurement, while θ represents nuisance parameters corresponding to the systematic uncertainties described in Section 8 and background parameters that are constrained by control regions in data. Theoretical uncertainties in simulated signal and background processes are treated as correlated across all channels, as well as are experimental uncertainties related to the data-taking conditions and physics objects. Uncertainties related to background estimates using data-informed methodologies (derived from template fits, or estimated in CR or side-band data regions) are treated as uncorrelated, except in cases where a common CR is used in which case it is treated as correlated. The global likelihood function $L(\alpha, \theta)$ is the result of multiplying the likelihood functions in each of the nine signal regions and the 19 CRs indicated in Tables 5 and 6. For each channel, the likelihood function is derived from the respective signal and background models of the probability density functions for the variable of interest. These models take into account the expected signal and background yields for given values of α and θ , and the observed distribution of the discriminating variable in each channel – the BDT output score distribution for each of the ML channels, and $m_{\gamma\gamma}$ for the $\gamma\gamma$ +ML channels.

Upper limits are set on the HH signal strength, μ_{HH} at 95% CL, using the profile-likelihood-ratio test statistic and the modified frequentist CL_s technique [118] in the asymptotic approximation [119]. The scenario $\mu_{HH} = 0$ corresponds to the background-only hypothesis and $\mu_{HH} > 0$ corresponds to the presence of an HH signal in addition to the background. Asimov datasets [119] are used to derive the expected limits, with all pre-fit estimates of the nuisance parameters set to values derived from the fit to the data, and the parameters of interest set corresponding to the hypothesis being tested. The 95% CL limits on the signal strength for individual channels, the statistical combinations of the ML and $\gamma\gamma$ +ML signal categories, and the combination of all channels, are shown in Figure 8. The overall combination yields an observed 95% CL upper limit on μ_{HH} of 17, with an expected upper limit of 11 in the absence of HH production, and 12 for the SM case. If systematic uncertainties are neglected then the expected limit is 9.1 when assuming no HH production. The asymptotic results are found to agree within 8% with values obtained using pseudo-experiments.

Constraints on the Higgs self-coupling strength and the $VVHH$ coupling strength, expressed as 68% and 95% confidence intervals (CIs), are determined using the method described in Ref. [27], using a profile-likelihood-ratio test statistic $\Lambda(\alpha, \theta)$ computed from the likelihood function in the asymptotic approximation [119], where the POIs in α are the coupling strength modifier κ_λ and κ_{2V} , respectively. The values of twice the negative-logarithm of the profile likelihood ratio ($-2\ln\Lambda$) as a function of κ_λ and κ_{2V} are shown in Figure 9. The best-fit value of κ_λ is found to be 7.7 from the profile likelihood scan. With the values of all other couplings fixed to their SM value, the observed (expected) 95% CI for κ_λ is found to be $[-6.2, 11.6]$ ($[-4.5, 9.6]$). The observed (expected) 95% CI for κ_{2V} is found to be $[-2.5, 4.6]$ ($[-1.9, 4.1]$) with all other couplings fixed to their SM value. The expected limits are computed assuming the SM. The double-minima structure in the observed limit occurs due to a degeneracy in the best-fit signal yield that arises because of the competing factors of the signal cross-section and effects on the acceptance times efficiency when varying the couplings. As can be seen in Figure 10, the effect is driven by the $\gamma\gamma$ +ML channels, where a mild excess is observed in data compared to the background prediction.

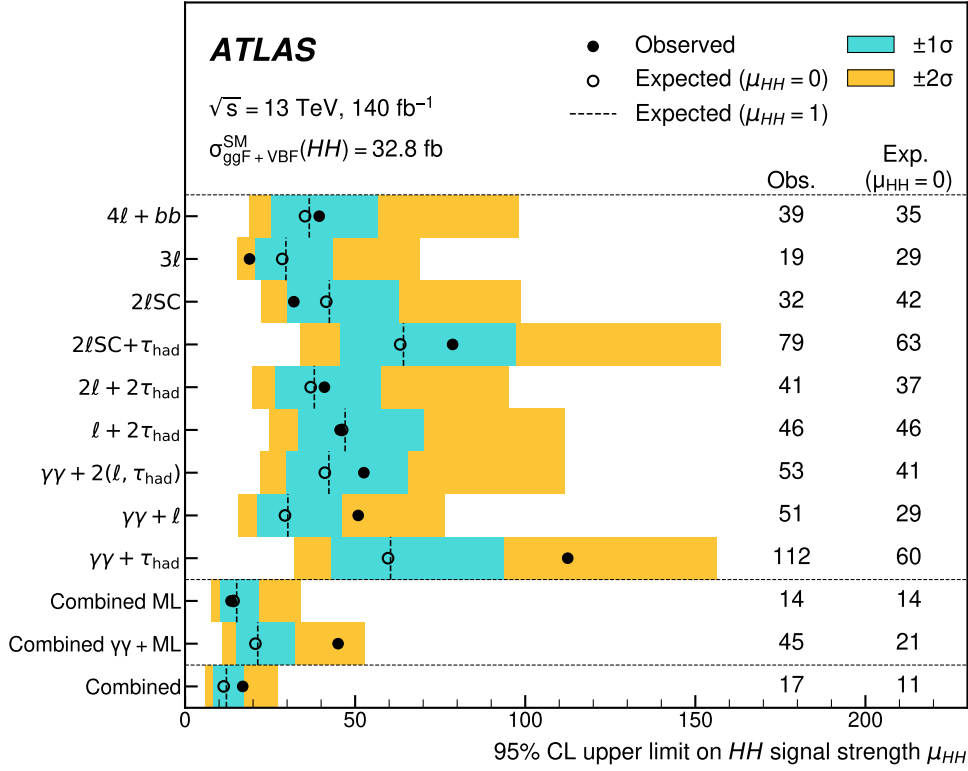


Figure 8: Observed (filled circles) and expected (open circles) 95% CL upper limits on the signal strength for HH production in the background-only ($\mu_{HH} = 0$) hypothesis. The dashed lines indicate the expected 95% CL upper limits on μ_{HH} in the SM hypothesis ($\mu_{HH} = 1$). The inner and outer bands indicate the $\pm 1\sigma$ and $\pm 2\sigma$ variations on the expected limit under the background-only hypothesis due to statistical and systematic uncertainties, respectively. Results are shown individually for the different search channels, the statistical combination of ML and $\gamma\gamma + \text{ML}$ channels separately, and the statistical combination of all channels.

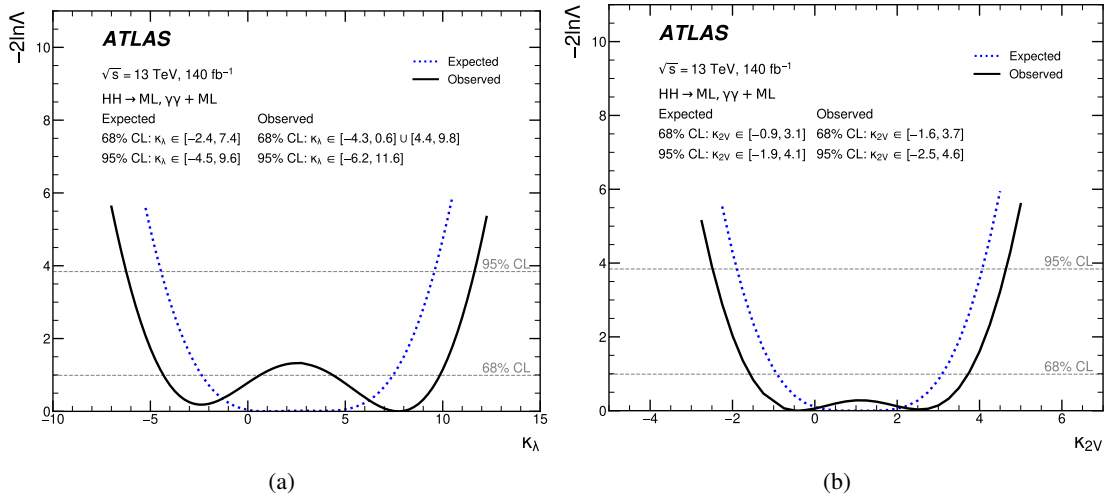


Figure 9: Observed (solid lines) and expected (dashed line) values of $-2\ln\Lambda$ as a function of (a) κ_λ , and (b) κ_{2V} . All other coupling modifiers are fixed to their SM predictions and the expected limits are computed assuming the SM.

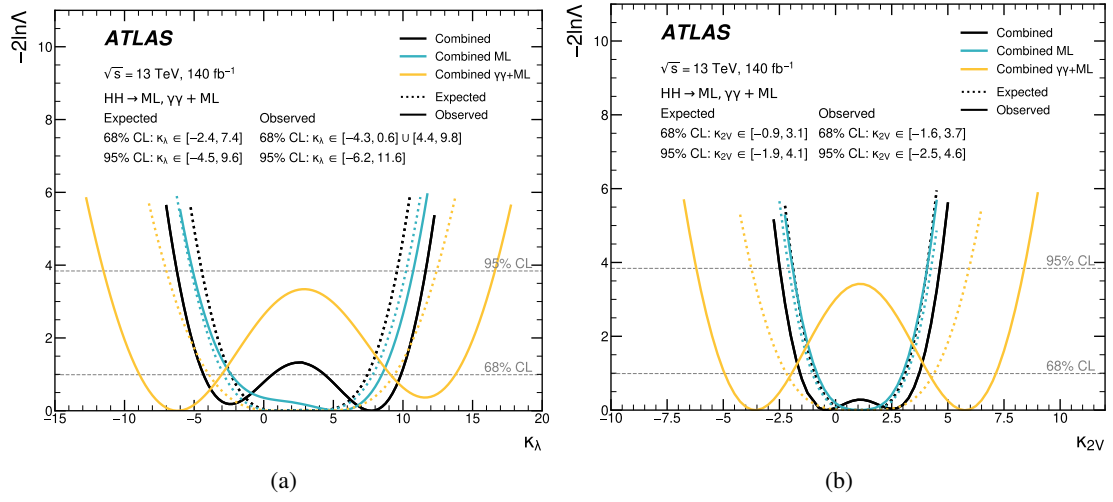


Figure 10: Observed (solid lines) and expected (dashed line) values of $-2\ln\Lambda$ as a function of (a) κ_λ , and (b) κ_{2V} for the ML channels, the $\gamma\gamma$ +ML channels, and their combination. All other coupling modifiers are fixed to their SM predictions and the expected limits are computed assuming the SM.

10 Conclusion

A search for HH production targeting the $bbZZ$, $4V$, $VV\tau\tau$, 4τ , $\gamma\gamma VV$ and $\gamma\gamma\tau\tau$ decay channels is performed for the first time in ATLAS. Final states are categorised based on the multiplicity of light charged leptons (electrons or muons), hadronically decaying tau leptons, and photons. BDTs are used to separate signal from backgrounds in eight of the nine explored channels. The main background processes to the ML channels involving vector bosons and top-quarks are estimated from MC simulation and normalised to data. Background processes involving charge-misidentification of leptons, non-prompt leptons, misidentification of hadronic tau leptons, and non-resonant $\gamma\gamma$ production are estimated by using data-driven methods. The analysis is performed with proton–proton collision data at $\sqrt{s} = 13$ TeV collected from 2015 to 2018 with the ATLAS detector at the LHC, corresponding to an integrated luminosity of 140 fb^{-1} .

Observed (expected) limits of 17 (11) times the SM prediction are set on the HH signal strength, under the background-only hypothesis. The self-coupling strength modifier, κ_λ , is observed (expected) to be constrained to be $-6.2 \leq \kappa_\lambda \leq 11.6$ ($-4.5 \leq \kappa_\lambda \leq 9.6$) and κ_{2V} is observed (expected) to be constrained to be $-2.5 \leq \kappa_{2V} \leq 4.6$ ($-1.9 \leq \kappa_{2V} \leq 4.1$), all at 95% CL with other couplings except for the one being probed fixed to their SM values, and assuming the SM for the expected limits. The sensitivity of the results in all channels is limited by the statistical precision on the available data. The results presented in this study have comparable sensitivity to the other channels already investigated by ATLAS and CMS, and will contribute to improve the global sensitivity to HH production.

Acknowledgements

We thank CERN for the very successful operation of the LHC and its injectors, as well as the support staff at CERN and at our institutions worldwide without whom ATLAS could not be operated efficiently.

The crucial computing support from all WLCG partners is acknowledged gratefully, in particular from CERN, the ATLAS Tier-1 facilities at TRIUMF/SFU (Canada), NDGF (Denmark, Norway, Sweden), CC-IN2P3 (France), KIT/GridKA (Germany), INFN-CNAF (Italy), NL-T1 (Netherlands), PIC (Spain), RAL (UK) and BNL (USA), the Tier-2 facilities worldwide and large non-WLCG resource providers. Major contributors of computing resources are listed in Ref. [120].

We gratefully acknowledge the support of ANPCyT, Argentina; YerPhI, Armenia; ARC, Australia; BMWFW and FWF, Austria; ANAS, Azerbaijan; CNPq and FAPESP, Brazil; NSERC, NRC and CFI, Canada; CERN; ANID, Chile; CAS, MOST and NSFC, China; Minciencias, Colombia; MEYS CR, Czech Republic; DNRF and DNSRC, Denmark; IN2P3-CNRS and CEA-DRF/IRFU, France; SRNSFG, Georgia; BMBF, HGF and MPG, Germany; GSRI, Greece; RGC and Hong Kong SAR, China; ISF and Benozziyo Center, Israel; INFN, Italy; MEXT and JSPS, Japan; CNRST, Morocco; NWO, Netherlands; RCN, Norway; MNiSW, Poland; FCT, Portugal; MNE/IFA, Romania; MESTD, Serbia; MSSR, Slovakia; ARIS and MVZI, Slovenia; DSI/NRF, South Africa; MICIU/AEI, Spain; SRC and Wallenberg Foundation, Sweden; SERI, SNSF and Cantons of Bern and Geneva, Switzerland; NSTC, Taipei; TENMAK, Türkiye; STFC/UKRI, United Kingdom; DOE and NSF, United States of America.

Individual groups and members have received support from BCKDF, CANARIE, CRC and DRAC, Canada; CERN-CZ, FORTE and PRIMUS, Czech Republic; COST, ERC, ERDF, Horizon 2020, ICSC-NextGenerationEU and Marie Skłodowska-Curie Actions, European Union; Investissements d’Avenir Labex, Investissements d’Avenir Idex and ANR, France; DFG and AvH Foundation, Germany; Herakleitos,

Thales and Aristeia programmes co-financed by EU-ESF and the Greek NSRF, Greece; BSF-NSF and MINERVA, Israel; Norwegian Financial Mechanism 2014-2021, Norway; NCN and NAWA, Poland; La Caixa Banking Foundation, CERCA Programme Generalitat de Catalunya and PROMETEO and GenT Programmes Generalitat Valenciana, Spain; Göran Gustafssons Stiftelse, Sweden; The Royal Society and Leverhulme Trust, United Kingdom.

In addition, individual members wish to acknowledge support from CERN: European Organization for Nuclear Research (CERN PJA5); Chile: Agencia Nacional de Investigación y Desarrollo (FONDECYT 1190886, FONDECYT 1230812, FONDECYT 1230987); China: Chinese Ministry of Science and Technology (MOST-2023YFA1605700), National Natural Science Foundation of China (NSFC - 12175119, NSFC 12275265, NSFC-12075060); Czech Republic: Czech Science Foundation (GACR - 24-11373S), Ministry of Education Youth and Sports (FORTE CZ.02.01.01/00/22_008/0004632), PRIMUS Research Programme (PRIMUS/21/SCI/017); EU: H2020 European Research Council (ERC - 101002463); European Union: European Research Council (ERC - 948254, ERC 101089007), Horizon 2020 Framework Programme (MUCCA - CHIST-ERA-19-XAI-00), European Union, Future Artificial Intelligence Research (FAIR-NextGenerationEU PE00000013), Italian Center for High Performance Computing, Big Data and Quantum Computing (ICSC, NextGenerationEU); France: Agence Nationale de la Recherche (ANR-20-CE31-0013, ANR-21-CE31-0013, ANR-21-CE31-0022, ANR-22-EDIR-0002), Investissements d'Avenir Labex (ANR-11-LABX-0012); Germany: Baden-Württemberg Stiftung (BW Stiftung-Postdoc Eliteprogramme), Deutsche Forschungsgemeinschaft (DFG - 469666862, DFG - CR 312/5-2); Italy: Istituto Nazionale di Fisica Nucleare (ICSC, NextGenerationEU), Ministero dell'Università e della Ricerca (PRIN - 20223N7F8K - PNRR M4.C2.1.1); Japan: Japan Society for the Promotion of Science (JSPS KAKENHI JP21H05085, JSPS KAKENHI JP22H01227, JSPS KAKENHI JP22H04944, JSPS KAKENHI JP22KK0227); Netherlands: Netherlands Organisation for Scientific Research (NWO Veni 2020 - VI.Veni.202.179); Norway: Research Council of Norway (RCN-314472); Poland: Ministry of Science and Higher Education (IDUB AGH, POB8, D4 no 9722), Polish National Agency for Academic Exchange (PPN/PPO/2020/1/00002/U/00001), Polish National Science Centre (NCN 2021/42/E/ST2/00350, NCN OPUS nr 2022/47/B/ST2/03059, NCN UMO-2019/34/E/ST2/00393, UMO-2020/37/B/ST2/01043, UMO-2021/40/C/ST2/00187, UMO-2022/47/O/ST2/00148, UMO-2023/49/B/ST2/04085); Slovenia: Slovenian Research Agency (ARIS grant J1-3010); Spain: Generalitat Valenciana (Artemisa, FEDER, IDIFEDER/2018/048), Ministry of Science and Innovation (MCIN & NextGenEU PCI2022-135018-2, MICIN & FEDER PID2021-125273NB, RYC2019-028510-I, RYC2020-030254-I, RYC2021-031273-I, RYC2022-038164-I), PROMETEO and GenT Programmes Generalitat Valenciana (CIDEGENT/2019/023, CIDEGENT/2019/027); Sweden: Swedish Research Council (Swedish Research Council 2023-04654, VR 2018-00482, VR 2022-03845, VR 2022-04683, VR 2023-03403, VR grant 2021-03651), Knut and Alice Wallenberg Foundation (KAW 2018.0157, KAW 2018.0458, KAW 2019.0447, KAW 2022.0358); Switzerland: Swiss National Science Foundation (SNSF - PCEFP2_194658); United Kingdom: Leverhulme Trust (Leverhulme Trust RPG-2020-004), Royal Society (NIF-R1-231091); United States of America: U.S. Department of Energy (ECA DE-AC02-76SF00515), Neubauer Family Foundation.

Appendix

The BDT input variables used in the different ML channels are summarised in Tables 8 and 9 and in the $\gamma\gamma+\ell$ and $\gamma\gamma+\tau_{\text{had}}$ channels in Table 10.

Table 8: Variables used as inputs to the $4\ell+2b$, 3ℓ , and $2\ell\text{SC}$ channel BDTs. The indices i and j refer to the indices of the p_T -ordered objects.

Variable	Description	$4\ell+2b$	3ℓ	$2\ell\text{SC}$
$p_T(\ell_i)$	p_T of the i th lepton	$i = 1, 2, 3, 4$	–	–
$ \eta(\ell_i) $	Absolute η of the i th lepton	$i = 1, 2, 3, 4$	–	$i = 1, 2$
$E_T^{\Delta R < 0.3}/E_T(\ell_i)$	Isolation metric (where $E_T^{\Delta R < 0.3}$ = total transverse energy deposited in a cone of radius $R = 0.3$ around the lepton, and E_T = lepton transverse energy)	$i = 1, 2, 3, 4$	–	–
Dilepton type	$\mu\mu = 1, e\mu/\mu e = 2, ee = 3$	–	–	✓
m_{ℓ_i, ℓ_j}	Invariant mass of the i th and j th leptons	–	$i, j = 1, 2$ $i, j = 1, 3$ $i, j = 2, 3$	$i, j = 1, 2$
$m_{\text{on-shell-}\ell\ell}^{\text{SFOC}}$	Invariant mass of pair of SFOC leptons that minimises the difference with the Z boson mass	✓	✓	–
$m_{\text{off-shell-}\ell\ell}^{\text{SFOC}}$	Invariant mass of the other SFOC lepton pair	✓	–	–
min. $m_{\ell\ell}^{\text{SFOC}}$	Minimum invariant mass out of all SFOC pairs	–	✓	–
$m_{4\ell}$	Invariant mass of four leptons	✓	–	–
$m_{3\ell}$	Invariant mass of three leptons	–	✓	–
$m_{\ell_i, \text{close-jet}}$	Invariant mass of the i th lepton and its closest jet	–	$i = 1, 2, 3$	$i = 1, 2$
$m_{3\ell\text{jj}}$	Invariant mass of the three leptons and the leading (or two leading, for events with $N_{\text{jet}} \geq 2$) jets	–	✓	–
m_{jj}	Invariant mass of the two leading jets	✓	–	–
m_{all}	Invariant mass of all selected objects in the event	–	–	✓
$m_T^W(\ell_i, E_T^{\text{miss}})$	Transverse mass of the i th lepton and the E_T^{miss}	–	–	$i = 1, 2$
$\Delta\eta(\ell_1, \ell_2)$	Separation in η between the first and second leptons	–	–	✓
$\Delta R(\ell_i, \ell_j)$	Separation in R between the i th and j th leptons	–	$i, j = 1, 2$ $i, j = 1, 3$ $i, j = 2, 3$	$i, j = 1, 2$
$\Delta R(\ell_i, \text{close-jet})$	Separation in R between the i th lepton and its closest jet	–	$i = 1, 2, 3$	$i = 1, 2$
min. $\Delta R(\ell, j)$	Minimum separation in R between any lepton and any jet	–	–	✓
L_T	Scalar sum of the p_T of all leptons and the E_T^{miss}	–	✓	✓
H_T	Scalar sum of the p_T of all jets	–	✓	✓
S_T	Scalar sum of the p_T of all objects in the event	✓	✓	–
ΣQ_ℓ	Sum of all lepton charges	–	–	✓
N_{jet}	Number of jets in the event	–	–	✓
$N_{b\text{-jet}}$	Number of b -jets in the event	✓	–	–
$p_T(j_1)$	p_T of the leading jet	✓	–	–
$p_T(\text{jj})$	p_T of the leading dijet system	✓	–	–
E_T^{miss}	Magnitude of the missing transverse momentum	✓	✓	✓
$\Delta\phi(E_T^{\text{miss}}, j_1)$	ϕ angle between the E_T^{miss} and the leading jet	✓	–	–

Table 9: Variables used as inputs to the $2\ell\text{SC}+\tau_{\text{had}}$, $2\ell+2\tau_{\text{had}}$, and $\ell+2\tau_{\text{had}}$ channel BDTs. The indices i and j refer to the indices of the p_{T} -ordered objects.

Variable	Description	$2\ell\text{SC}+\tau_{\text{had}}$	$2\ell+2\tau_{\text{had}}$	$\ell+2\tau_{\text{had}}$
Dilepton type	$\mu\mu = 1, e\mu/\mu e = 2, ee = 3$	–	✓	–
$m_{\ell_1\ell_2}$	Invariant mass of the two leptons	–	✓	–
$m_{\ell_1, \text{close-jet}}$	Invariant mass of the leading lepton and its closest jet	✓	–	✓
$m_{\ell_i j_j}$	Invariant mass of the i th lepton and j th jet	$i, j = 1, 1$ $i, j = 1, 2$ $i, j = 2, 1$	–	–
$\Delta\eta(\ell, \ell)$	Separation in η between the two leptons	✓	–	–
$\Delta R(\ell, \ell)$	Separation in R between the two leptons	✓	✓	–
$\Delta R(\ell_i, j_j)$	Separation in R between the i th lepton and j th jet	$i, j = 1, 1$	–	$i, j = 1, 1$ $i, j = 1, 2$
$\Delta R(\ell_i, \text{close-jet})$	Separation in R between the i th lepton and its closest jet	$i = 1, 2$	–	–
$p_{\text{T}}(j_1)$	p_{T} of the leading jet	–	–	✓
$E_{\text{T}}^{\text{miss}}$	Magnitude of the missing transverse momentum	–	–	✓
$\theta_{\tau_{\text{had}}, j_i}^{\text{boost-}\ell\ell}$	Polar angle between the $\tau_{\text{had-vis}}$ and the i th jet after a Lorentz boost to the dilepton system	$i = 1, 2$	–	–
$\Delta R_{\ell_i, j_j}^{\text{boost-}\ell_i \tau_{\text{had}}}$	Separation in R between the i th lepton and j th jet after a Lorentz boost to the $\tau_{\text{had-vis}}$ and i th lepton system	$i, j = 1, 2$ $i, j = 2, 1$	–	–
$m_{\tau\tau}$	Invariant mass of the two $\tau_{\text{had-vis}}$	–	✓	✓
$\Delta R(\ell_2, \tau_1)$	Separation in R between the second lepton and first $\tau_{\text{had-vis}}$	–	✓	–
$\Delta R(\ell_1, \tau\tau)$	Separation in R between the first lepton and the di- $\tau_{\text{had-vis}}$ system	–	✓	✓
$m_{\ell_2\tau_1}$	Invariant mass of the second lepton and first $\tau_{\text{had-vis}}$	–	✓	–
$m_{\ell\tau\tau}$	Invariant mass of the lepton and two $\tau_{\text{had-vis}}$	–	–	✓
$p_{\text{T}}(\ell + \text{close-jet})$	Vector sum of the p_{T} of the lepton and its closest jet	–	–	✓
$p_{\text{T}}(\tau_1 + \tau_2)$	Vector sum of the p_{T} of the two $\tau_{\text{had-vis}}$	–	✓	✓

Table 10: Variables used as inputs to the $\gamma\gamma+\ell$ and $\gamma\gamma+\tau_{\text{had}}$ channel BDTs. Photons and jets are p_T ordered.

Variable	Description	$\gamma\gamma+\ell$	$\gamma\gamma+\tau_{\text{had}}$
$p_T(\gamma\gamma)$	p_T of the diphoton system	✓	✓
$p_T(\ell)$	p_T of the lepton	✓	–
$p_T(\tau_{\text{had-vis}})$	p_T of the $\tau_{\text{had-vis}}$	–	✓
E_T^{miss}	Magnitude of the missing transverse momentum	✓	✓
$\phi(E_T^{\text{miss}})$	ϕ direction of the E_T^{miss}	–	✓
$\eta(\ell E_T^{\text{miss}})$	η of the lepton- E_T^{miss} system	✓	–
$\eta(\gamma_1)$	η of the leading photon	–	✓
$N_{\text{central-jets}}$	Number of jets with $ \eta < 2.5$	✓	✓
$\Delta R(\ell, E_T^{\text{miss}})$	ΔR between the lepton and the E_T^{miss}	✓	–
$\Delta R(\gamma\gamma, \ell E_T^{\text{miss}})$	ΔR between the diphoton system and the lepton- E_T^{miss} system	✓	–
$\Delta\phi(\ell/\tau_{\text{had-vis}}, \gamma\gamma)$	Separation in ϕ between the lepton or $\tau_{\text{had-vis}}$ and the diphoton system	✓	✓
$\Delta\phi(\gamma_1, \gamma\gamma)$	Separation in ϕ between the leading photon and the diphoton system	✓	✓
$\text{min. } \Delta\phi(E_T^{\text{miss}}, \text{j}, \ell)$	Minimum ϕ angle between any pair of the E_T^{miss} , the lepton, and any jet	✓	–
$\Delta\phi(E_T^{\text{miss}}, \gamma\gamma)$	Separation in ϕ between the E_T^{miss} and the diphoton system	✓	✓

References

- [1] ATLAS Collaboration, *Observation of a new particle in the search for the Standard Model Higgs boson with the ATLAS detector at the LHC*, *Phys. Lett. B* **716** (2012) 1, arXiv: [1207.7214 \[hep-ex\]](#).
- [2] CMS Collaboration, *Observation of a new boson at a mass of 125 GeV with the CMS experiment at the LHC*, *Phys. Lett. B* **716** (2012) 30, arXiv: [1207.7235 \[hep-ex\]](#).
- [3] ATLAS Collaboration, *A detailed map of Higgs boson interactions by the ATLAS experiment ten years after the discovery*, *Nature* **607** (2022) 52, arXiv: [2207.00092 \[hep-ex\]](#), Erratum: *Nature* **612** (2022) E24.
- [4] CMS Collaboration, *A portrait of the Higgs boson by the CMS experiment ten years after the discovery*, *Nature* **607** (2022) 60, arXiv: [2207.00043 \[hep-ex\]](#), Erratum: *Nature* **623** (2023) E4.
- [5] B. Horn, *The Higgs Field and Early Universe Cosmology: A (Brief) Review*, *MDPI Physics* **2** (2020) 503, arXiv: [2007.10377 \[hep-ph\]](#).
- [6] M. Reichert et al., *Probing baryogenesis through the Higgs boson self-coupling*, *Phys. Rev. D* **97** (2018) 075008, arXiv: [1711.00019 \[hep-ph\]](#).
- [7] A. Noble and M. Perelstein, *Higgs self-coupling as a probe of the electroweak phase transition*, *Phys. Rev. D* **78** (2008) 063518, arXiv: [0711.3018 \[hep-ph\]](#).
- [8] F. Bezrukov and M. Shaposhnikov, *The Standard Model Higgs boson as the inflaton*, *Phys. Lett. B* **659** (2008) 703, arXiv: [0710.3755 \[hep-th\]](#).
- [9] T. Markkanen, A. Rajantie and S. Stopyra, *Cosmological Aspects of Higgs Vacuum Metastability*, *Front. Astron. Space Sci.* **5** (2019) 40, arXiv: [1809.06923 \[astro-ph.CO\]](#).
- [10] S. Dawson, S. Dittmaier and M. Spira, *Neutral Higgs-boson pair production at hadron colliders: QCD corrections*, *Phys. Rev. D* **58** (1998) 115012, arXiv: [hep-ph/9805244 \[hep-ph\]](#).
- [11] S. Borowka et al., *Higgs Boson Pair Production in Gluon Fusion at Next-to-Leading Order with Full Top-Quark Mass Dependence*, *Phys. Rev. Lett.* **117** (2016) 012001, arXiv: [1604.06447 \[hep-ph\]](#), Erratum: *Phys. Rev. Lett.* **117** (2016) 079901.
- [12] J. Baglio et al., *Gluon fusion into Higgs pairs at NLO QCD and the top mass scheme*, *Eur. Phys. J. C* **79** (2019) 459, arXiv: [1811.05692 \[hep-ph\]](#).
- [13] D. de Florian and J. Mazzitelli, *Higgs Boson Pair Production at Next-to-Next-to-Leading Order in QCD*, *Phys. Rev. Lett.* **111** (2013) 201801, arXiv: [1309.6594 \[hep-ph\]](#).
- [14] D. Y. Shao, C. S. Li, H. T. Li and J. Wang, *Threshold resummation effects in Higgs boson pair production at the LHC*, *JHEP* **07** (2013) 169, arXiv: [1301.1245 \[hep-ph\]](#).
- [15] D. de Florian and J. Mazzitelli, *Higgs pair production at next-to-next-to-leading logarithmic accuracy at the LHC*, *JHEP* **09** (2015) 53, arXiv: [1505.07122 \[hep-ph\]](#).
- [16] M. Grazzini et al., *Higgs boson pair production at NNLO with top quark mass effects*, *JHEP* **05** (2018) 059, arXiv: [1803.02463 \[hep-ph\]](#).

- [17] J. Baglio et al., $gg \rightarrow HH$: Combined uncertainties, *Phys. Rev. D* **103** (2021) 056002, arXiv: 2008.11626 [hep-ph].
- [18] J. Baglio et al., *The measurement of the Higgs self-coupling at the LHC: theoretical status*, *JHEP* **04** (2013) 151, arXiv: 1212.5581 [hep-ph].
- [19] R. Frederix et al., *Higgs pair production at the LHC with NLO and parton-shower effects*, *Phys. Lett. B* **732** (2014) 142, arXiv: 1401.7340 [hep-ph].
- [20] L.-S. Ling et al., *NNLO QCD corrections to Higgs pair production via vector boson fusion at hadron colliders*, *Phys. Rev. D* **89** (2014) 073001, arXiv: 1401.7754 [hep-ph].
- [21] F. A. Dreyer and A. Karlberg, *Fully differential vector-boson fusion Higgs pair production at next-to-next-to-leading order*, *Phys. Rev. D* **99** (2019) 074028, arXiv: 1811.07918 [hep-ph].
- [22] F. A. Dreyer and A. Karlberg, *Vector-boson fusion Higgs pair production at N^3LO* , *Phys. Rev. D* **98** (2018) 114016, arXiv: 1811.07906 [hep-ph].
- [23] F. A. Dreyer, A. Karlberg, J.-N. Lang and M. Pellen, *Precise predictions for double-Higgs production via vector-boson fusion*, *Eur. Phys. J. C* **80** (2020) 1037, arXiv: 2005.13341 [hep-ph].
- [24] ATLAS Collaboration, *Search for Higgs boson pair production in the two bottom quarks plus two photons final state in pp collisions at $\sqrt{s} = 13$ TeV with the ATLAS detector*, *Phys. Rev. D* **106** (2022) 052001, arXiv: 2112.11876 [hep-ex].
- [25] ATLAS Collaboration, *Search for resonant and non-resonant Higgs boson pair production in the $b\bar{b}\tau^+\tau^-$ decay channel using 13 TeV pp collision data from the ATLAS detector*, *JHEP* **07** (2023) 040, arXiv: 2209.10910 [hep-ex].
- [26] ATLAS Collaboration, *Search for nonresonant pair production of Higgs bosons in the $b\bar{b}b\bar{b}$ final state in pp collisions at $\sqrt{s} = 13$ TeV with the ATLAS detector*, *Phys. Rev. D* **108** (2023) 052003, arXiv: 2301.03212 [hep-ex].
- [27] ATLAS Collaboration, *Constraints on the Higgs boson self-coupling from single- and double-Higgs production with the ATLAS detector using pp collisions at $\sqrt{s} = 13$ TeV*, *Phys. Lett. B* **843** (2023) 137745, arXiv: 2211.01216 [hep-ex].
- [28] ATLAS Collaboration, *Studies of new Higgs boson interactions through nonresonant HH production in the $b\bar{b}\gamma\gamma$ final state in pp collisions at $\sqrt{s} = 13$ TeV with the ATLAS detector*, *JHEP* **01** (2024) 066, arXiv: 2310.12301 [hep-ex].
- [29] ATLAS Collaboration, *Search for the non-resonant production of Higgs boson pairs via gluon fusion and vector-boson fusion in the $b\bar{b}\tau^+\tau^-$ final state in proton–proton collisions at $\sqrt{s} = 13$ TeV with the ATLAS detector*, (2024), arXiv: 2404.12660 [hep-ex].
- [30] ATLAS Collaboration, *Search for non-resonant Higgs boson pair production in the $2b + 2\ell + E_T^{miss}$ final state in pp collisions at $\sqrt{s} = 13$ TeV with the ATLAS detector*, *JHEP* **02** (2024) 037, arXiv: 2310.11286 [hep-ex].
- [31] ATLAS Collaboration, *Search for pair production of boosted Higgs bosons via vector-boson fusion in the $b\bar{b}b\bar{b}$ final state using pp collisions at $\sqrt{s} = 13$ TeV with the ATLAS detector*, (2024), arXiv: 2404.17193 [hep-ex].

- [32] CMS Collaboration, *Search for nonresonant Higgs boson pair production in final states with two bottom quarks and two photons in proton–proton collisions at $\sqrt{s} = 13$ TeV*, *JHEP* **03** (2021) 257, arXiv: [2011.12373](https://arxiv.org/abs/2011.12373) [[hep-ex](#)].
- [33] CMS Collaboration, *Search for nonresonant Higgs boson pair production in final state with two bottom quarks and two tau leptons in proton–proton collisions at $\sqrt{s} = 13$ TeV*, *Phys. Lett. B* **842** (2023) 137531, arXiv: [2206.09401](https://arxiv.org/abs/2206.09401) [[hep-ex](#)].
- [34] CMS Collaboration, *Search for Higgs Boson Pair Production in the Four b Quark Final State in Proton–Proton Collisions at $\sqrt{s} = 13$ TeV*, *Phys. Rev. Lett.* **129** (2022) 081802, arXiv: [2202.09617](https://arxiv.org/abs/2202.09617) [[hep-ex](#)].
- [35] CMS Collaboration, *Search for Nonresonant Pair Production of Highly Energetic Higgs Bosons Decaying to Bottom Quarks*, *Phys. Rev. Lett.* **131** (2023) 041803, arXiv: [2205.06667](https://arxiv.org/abs/2205.06667) [[hep-ex](#)].
- [36] CMS Collaboration, *Search for nonresonant Higgs boson pair production in the four leptons plus two b jets final state in proton–proton collisions at $\sqrt{s} = 13$ TeV*, *JHEP* **06** (2023) 130, arXiv: [2206.10657](https://arxiv.org/abs/2206.10657) [[hep-ex](#)].
- [37] CMS Collaboration, *Search for Higgs boson pairs decaying to WW^*WW^* , $WW^*\tau\tau$, and $\tau\tau\tau\tau$ in proton–proton collisions at $\sqrt{s} = 13$ TeV*, *JHEP* **07** (2023) 095, arXiv: [2206.10268](https://arxiv.org/abs/2206.10268) [[hep-ex](#)].
- [38] ATLAS Collaboration, *The ATLAS Experiment at the CERN Large Hadron Collider*, *JINST* **3** (2008) S08003.
- [39] L. Evans and P. Bryant, *LHC Machine*, *JINST* **3** (2008) S08001.
- [40] ATLAS Collaboration, *ATLAS Insertable B-Layer Technical Design Report*, ATLAS-TDR-19; CERN-LHCC-2010-013, 2010, URL: <https://cds.cern.ch/record/1291633>, Addendum: ATLAS-TDR-19-ADD-1; CERN-LHCC-2012-009, 2012, URL: <https://cds.cern.ch/record/1451888>.
- [41] B. Abbott et al., *Production and integration of the ATLAS Insertable B-Layer*, *JINST* **13** (2018) T05008, arXiv: [1803.00844](https://arxiv.org/abs/1803.00844) [[physics.ins-det](#)].
- [42] ATLAS Collaboration, *Performance of the ATLAS trigger system in 2015*, *Eur. Phys. J. C* **77** (2017) 317, arXiv: [1611.09661](https://arxiv.org/abs/1611.09661) [[hep-ex](#)].
- [43] ATLAS Collaboration, *The ATLAS Collaboration Software and Firmware*, ATL-SOFT-PUB-2021-001, 2021, URL: <https://cds.cern.ch/record/2767187>.
- [44] ATLAS Collaboration, *ATLAS data quality operations and performance for 2015–2018 data-taking*, *JINST* **15** (2020) P04003, arXiv: [1911.04632](https://arxiv.org/abs/1911.04632) [[physics.ins-det](#)].
- [45] ATLAS Collaboration, *Luminosity determination in pp collisions at $\sqrt{s} = 13$ TeV using the ATLAS detector at the LHC*, *Eur. Phys. J. C* **83** (2023) 982, arXiv: [2212.09379](https://arxiv.org/abs/2212.09379) [[hep-ex](#)].
- [46] G. Avoni et al., *The new LUCID-2 detector for luminosity measurement and monitoring in ATLAS*, *JINST* **13** (2018) P07017.
- [47] ATLAS Collaboration, *The ATLAS Simulation Infrastructure*, *Eur. Phys. J. C* **70** (2010) 823, arXiv: [1005.4568](https://arxiv.org/abs/1005.4568) [[physics.ins-det](#)].
- [48] S. Agostinelli et al., *GEANT4 – a simulation toolkit*, *Nucl. Instrum. Meth. A* **506** (2003) 250.
- [49] T. Sjöstrand, S. Mrenna and P. Skands, *A brief introduction to PYTHIA 8.1*, *Comput. Phys. Commun.* **178** (2008) 852, arXiv: [0710.3820](https://arxiv.org/abs/0710.3820) [[hep-ph](#)].

- [50] NNPDF Collaboration, *Parton distributions with LHC data*, *Nucl. Phys. B* **867** (2013) 244, arXiv: [1207.1303 \[hep-ph\]](#).
- [51] ATLAS Collaboration, *The Pythia 8 A3 tune description of ATLAS minimum bias and inelastic measurements incorporating the Donnachie–Landshoff diffractive model*, ATL-PHYS-PUB-2016-017, 2016, URL: <https://cds.cern.ch/record/2206965>.
- [52] ATLAS Collaboration, *Measurement of the Inelastic Proton–Proton Cross Section at $\sqrt{s} = 13$ TeV with the ATLAS Detector at the LHC*, *Phys. Rev. Lett.* **117** (2016) 182002, arXiv: [1606.02625 \[hep-ex\]](#).
- [53] S. Alioli, P. Nason, C. Oleari and E. Re, *A general framework for implementing NLO calculations in shower Monte Carlo programs: the POWHEG BOX*, *JHEP* **06** (2010) 043, arXiv: [1002.2581 \[hep-ph\]](#).
- [54] P. Nason and C. Oleari, *NLO Higgs boson production via vector-boson fusion matched with shower in POWHEG*, *JHEP* **02** (2010) 037, arXiv: [0911.5299 \[hep-ph\]](#).
- [55] J. Butterworth et al., *PDF4LHC recommendations for LHC Run II*, *J. Phys. G* **43** (2016) 023001, arXiv: [1510.03865 \[hep-ph\]](#).
- [56] T. Sjöstrand et al., *An introduction to PYTHIA 8.2*, *Comput. Phys. Commun.* **191** (2015) 159, arXiv: [1410.3012 \[hep-ph\]](#).
- [57] ATLAS Collaboration, *ATLAS Pythia 8 tunes to 7 TeV data*, ATL-PHYS-PUB-2014-021, 2014, URL: <https://cds.cern.ch/record/1966419>.
- [58] ATLAS Collaboration, *Validation of signal Monte Carlo event generation in searches for Higgs boson pairs with the ATLAS detector*, ATL-PHYS-PUB-2019-007, 2019, URL: <https://cds.cern.ch/record/2665057>.
- [59] M. Bähr et al., *Herwig++ physics and manual*, *Eur. Phys. J. C* **58** (2008) 639, arXiv: [0803.0883 \[hep-ph\]](#).
- [60] S. Gieseke, C. Röhr and A. Siódmok, *Colour reconnections in Herwig++*, *Eur. Phys. J. C* **72** (2012) 2225, arXiv: [1206.0041 \[hep-ph\]](#).
- [61] L. A. Harland-Lang, A. D. Martin, P. Motylinski and R. S. Thorne, *Parton distributions in the LHC era: MMHT 2014 PDFs*, *Eur. Phys. J. C* **75** (2015) 204, arXiv: [1412.3989 \[hep-ph\]](#).
- [62] J. Alwall et al., *The automated computation of tree-level and next-to-leading order differential cross sections, and their matching to parton shower simulations*, *JHEP* **07** (2014) 079, arXiv: [1405.0301 \[hep-ph\]](#).
- [63] NNPDF Collaboration, R. D. Ball et al., *Parton distributions for the LHC run II*, *JHEP* **04** (2015) 040, arXiv: [1410.8849 \[hep-ph\]](#).
- [64] P. Golonka and Z. Was, *PHOTOS Monte Carlo: a precision tool for QED corrections in Z and W decays*, *Eur. Phys. J. C* **45** (2006) 97, arXiv: [hep-ph/0506026](#).
- [65] E. Bothmann et al., *Event generation with Sherpa 2.2*, *SciPost Phys.* **7** (2019) 034, arXiv: [1905.09127 \[hep-ph\]](#).
- [66] T. Gleisberg and S. Höche, *Comix, a new matrix element generator*, *JHEP* **12** (2008) 039, arXiv: [0808.3674 \[hep-ph\]](#).

- [67] F. Buccioni et al., *OpenLoops 2*, *Eur. Phys. J. C* **79** (2019) 866, arXiv: [1907.13071 \[hep-ph\]](#).
- [68] F. Cascioli, P. Maierhöfer and S. Pozzorini, *Scattering Amplitudes with Open Loops*, *Phys. Rev. Lett.* **108** (2012) 111601, arXiv: [1111.5206 \[hep-ph\]](#).
- [69] A. Denner, S. Dittmaier and L. Hofer, *COLLIER: A fortran-based complex one-loop library in extended regularizations*, *Comput. Phys. Commun.* **212** (2017) 220, arXiv: [1604.06792 \[hep-ph\]](#).
- [70] S. Schumann and F. Krauss, *A parton shower algorithm based on Catani–Seymour dipole factorisation*, *JHEP* **03** (2008) 038, arXiv: [0709.1027 \[hep-ph\]](#).
- [71] S. Höche, F. Krauss, M. Schönherr and F. Siegert, *A critical appraisal of NLO+PS matching methods*, *JHEP* **09** (2012) 049, arXiv: [1111.1220 \[hep-ph\]](#).
- [72] S. Höche, F. Krauss, M. Schönherr and F. Siegert, *QCD matrix elements + parton showers. The NLO case*, *JHEP* **04** (2013) 027, arXiv: [1207.5030 \[hep-ph\]](#).
- [73] S. Catani, F. Krauss, B. R. Webber and R. Kuhn, *QCD Matrix Elements + Parton Showers*, *JHEP* **11** (2001) 063, arXiv: [hep-ph/0109231](#).
- [74] S. Höche, F. Krauss, S. Schumann and F. Siegert, *QCD matrix elements and truncated showers*, *JHEP* **05** (2009) 053, arXiv: [0903.1219 \[hep-ph\]](#).
- [75] F. Siegert, *A practical guide to event generation for prompt photon production with Sherpa*, *J. Phys. G* **44** (2017) 044007, arXiv: [1611.07226 \[hep-ph\]](#).
- [76] S. Frixione, *Isolated photons in perturbative QCD*, *Phys. Lett. B* **429** (1998) 369, arXiv: [hep-ph/9801442](#).
- [77] D. J. Lange, *The EvtGen particle decay simulation package*, *Nucl. Instrum. Meth. A* **462** (2001) 152.
- [78] S. Frixione, G. Ridolfi and P. Nason, *A positive-weight next-to-leading-order Monte Carlo for heavy flavour hadroproduction*, *JHEP* **09** (2007) 126, arXiv: [0707.3088 \[hep-ph\]](#).
- [79] P. Nason, *A new method for combining NLO QCD with shower Monte Carlo algorithms*, *JHEP* **11** (2004) 040, arXiv: [hep-ph/0409146](#).
- [80] S. Frixione, P. Nason and C. Oleari, *Matching NLO QCD computations with parton shower simulations: the POWHEG method*, *JHEP* **11** (2007) 070, arXiv: [0709.2092 \[hep-ph\]](#).
- [81] E. Re, *Single-top Wt -channel production matched with parton showers using the POWHEG method*, *Eur. Phys. J. C* **71** (2011) 1547, arXiv: [1009.2450 \[hep-ph\]](#).
- [82] S. Alioli, P. Nason, C. Oleari and E. Re, *NLO single-top production matched with shower in POWHEG: s - and t -channel contributions*, *JHEP* **09** (2009) 111, arXiv: [0907.4076 \[hep-ph\]](#), Erratum: *JHEP* **02** (2010) 011.
- [83] ATLAS Collaboration, *Measurement of the Z/γ^* boson transverse momentum distribution in pp collisions at $\sqrt{s} = 7$ TeV with the ATLAS detector*, *JHEP* **09** (2014) 145, arXiv: [1406.3660 \[hep-ex\]](#).

- [84] J. Bellm et al., *Herwig 7.0/Herwig++ 3.0 release note*, *Eur. Phys. J. C* **76** (2016) 196, arXiv: [1512.01178](https://arxiv.org/abs/1512.01178) [[hep-ph](#)].
- [85] ATLAS Collaboration, *Vertex Reconstruction Performance of the ATLAS Detector at $\sqrt{s} = 13$ TeV*, ATL-PHYS-PUB-2015-026, 2015, URL: <https://cds.cern.ch/record/2037717>.
- [86] ATLAS Collaboration, *Measurement of Higgs boson production in the diphoton decay channel in pp collisions at center-of-mass energies of 7 and 8 TeV with the ATLAS detector*, *Phys. Rev. D* **90** (2014) 112015, arXiv: [1408.7084](https://arxiv.org/abs/1408.7084) [[hep-ex](#)].
- [87] ATLAS Collaboration, *Electron and photon performance measurements with the ATLAS detector using the 2015–2017 LHC proton–proton collision data*, *JINST* **14** (2019) P12006, arXiv: [1908.00005](https://arxiv.org/abs/1908.00005) [[hep-ex](#)].
- [88] ATLAS Collaboration, *Electron and photon efficiencies in LHC Run 2 with the ATLAS experiment*, (2023), arXiv: [2308.13362](https://arxiv.org/abs/2308.13362) [[hep-ex](#)].
- [89] ATLAS Collaboration, *Evidence for the associated production of the Higgs boson and a top quark pair with the ATLAS detector*, *Phys. Rev. D* **97** (2018) 072003, arXiv: [1712.08891](https://arxiv.org/abs/1712.08891) [[hep-ex](#)].
- [90] ATLAS Collaboration, *Muon reconstruction and identification efficiency in ATLAS using the full Run 2 pp collision data set at $\sqrt{s} = 13$ TeV*, *Eur. Phys. J. C* **81** (2021) 578, arXiv: [2012.00578](https://arxiv.org/abs/2012.00578) [[hep-ex](#)].
- [91] ATLAS Collaboration, *Jet reconstruction and performance using particle flow with the ATLAS Detector*, *Eur. Phys. J. C* **77** (2017) 466, arXiv: [1703.10485](https://arxiv.org/abs/1703.10485) [[hep-ex](#)].
- [92] ATLAS Collaboration, *Identification and energy calibration of hadronically decaying tau leptons with the ATLAS experiment in pp collisions at $\sqrt{s} = 8$ TeV*, *Eur. Phys. J. C* **75** (2015) 303, arXiv: [1412.7086](https://arxiv.org/abs/1412.7086) [[hep-ex](#)].
- [93] M. Cacciari, G. P. Salam and G. Soyez, *FastJet user manual*, *Eur. Phys. J. C* **72** (2012) 1896, arXiv: [1111.6097](https://arxiv.org/abs/1111.6097) [[hep-ph](#)].
- [94] M. Cacciari, G. P. Salam and G. Soyez, *The anti- k_t jet clustering algorithm*, *JHEP* **04** (2008) 063, arXiv: [0802.1189](https://arxiv.org/abs/0802.1189) [[hep-ph](#)].
- [95] ATLAS Collaboration, *Local Hadronic Calibration*, ATL-PHYS-PUB-2009-001-2, 2009, URL: <https://cds.cern.ch/record/1112035>.
- [96] ATLAS Collaboration, *Identification of hadronic tau lepton decays using neural networks in the ATLAS experiment*, ATL-PHYS-PUB-2019-033, 2019, URL: <https://cds.cern.ch/record/2688062>.
- [97] ATLAS Collaboration, *Measurement of the tau lepton reconstruction and identification performance in the ATLAS experiment using pp collisions at $\sqrt{s} = 13$ TeV*, ATLAS-CONF-2017-029, 2017, URL: <https://cds.cern.ch/record/2261772>.
- [98] ATLAS Collaboration, *Performance of pile-up mitigation techniques for jets in pp collisions at $\sqrt{s} = 8$ TeV using the ATLAS detector*, *Eur. Phys. J. C* **76** (2016) 581, arXiv: [1510.03823](https://arxiv.org/abs/1510.03823) [[hep-ex](#)].
- [99] ATLAS Collaboration, *ATLAS flavour-tagging algorithms for the LHC Run 2 pp collision dataset*, *Eur. Phys. J. C* **83** (2023) 681, arXiv: [2211.16345](https://arxiv.org/abs/2211.16345) [[physics.data-an](#)].

- [100] ATLAS Collaboration, *ATLAS b -jet identification performance and efficiency measurement with $t\bar{t}$ events in pp collisions at $\sqrt{s} = 13$ TeV*, *Eur. Phys. J. C* **79** (2019) 970, arXiv: [1907.05120 \[hep-ex\]](#).
- [101] ATLAS Collaboration, *Evidence for the $H \rightarrow b\bar{b}$ decay with the ATLAS detector*, *JHEP* **12** (2017) 024, arXiv: [1708.03299 \[hep-ex\]](#).
- [102] ATLAS Collaboration, *The performance of missing transverse momentum reconstruction and its significance with the ATLAS detector using 140fb^{-1} of $\sqrt{s} = 13$ TeV pp collisions*, (2024), arXiv: [2402.05858 \[hep-ex\]](#).
- [103] ATLAS Collaboration, *Performance of electron and photon triggers in ATLAS during LHC Run 2*, *Eur. Phys. J. C* **80** (2020) 47, arXiv: [1909.00761 \[hep-ex\]](#).
- [104] ATLAS Collaboration, *Performance of the ATLAS muon triggers in Run 2*, *JINST* **15** (2020) P09015, arXiv: [2004.13447 \[physics.ins-det\]](#).
- [105] J. Friedman, *Greedy function approximation: A gradient boosting machine*, *The Annals of Statistics* **29** (2001) 1189.
- [106] ATLAS Collaboration, *Multi-Boson Simulation for 13 TeV ATLAS Analyses*, ATL-PHYS-PUB-2017-005, 2017, URL: <https://cds.cern.ch/record/2261933>.
- [107] ATLAS Collaboration, *Observation of Electroweak Production of a Same-Sign W Boson Pair in Association with Two Jets in pp Collisions at $\sqrt{s} = 13$ TeV with the ATLAS Detector*, *Phys. Rev. Lett.* **123** (2019) 161801, arXiv: [1906.03203 \[hep-ex\]](#).
- [108] ATLAS Collaboration, *Search for a new heavy scalar particle decaying into a Higgs boson and a new scalar singlet in final states with one or two light leptons and a pair of τ -leptons with the ATLAS detector*, *JHEP* **10** (2023) 009, arXiv: [2307.11120 \[hep-ex\]](#).
- [109] ATLAS Collaboration, *Recommendations for the Modeling of Smooth Backgrounds*, ATL-PHYS-PUB-2020-028, 2020, URL: <https://cds.cern.ch/record/2743717>.
- [110] ATLAS Collaboration, *Jet energy scale and resolution measured in proton–proton collisions at $\sqrt{s} = 13$ TeV with the ATLAS detector*, *Eur. Phys. J. C* **81** (2021) 689, arXiv: [2007.02645 \[hep-ex\]](#).
- [111] ATLAS Collaboration, *Measurement of the c -jet mistagging efficiency in $t\bar{t}$ events using pp collision data at $\sqrt{s} = 13$ TeV collected with the ATLAS detector*, *Eur. Phys. J. C* **82** (2022) 95, arXiv: [2109.10627 \[hep-ex\]](#).
- [112] ATLAS Collaboration, *Calibration of the light-flavour jet mistagging efficiency of the b -tagging algorithms with Z +jets events using 139fb^{-1} of ATLAS proton–proton collision data at $\sqrt{s} = 13$ TeV*, *Eur. Phys. J. C* **83** (2023) 728, arXiv: [2301.06319 \[hep-ex\]](#).
- [113] D. de Florian et al., *Handbook of LHC Higgs Cross Sections: 4. Deciphering the Nature of the Higgs Sector*, (2017), arXiv: [1610.07922 \[hep-ph\]](#).
- [114] R. Frederix, D. Pagani and M. Zaro, *Large NLO corrections in $t\bar{t}W^\pm$ and $t\bar{t}\bar{t}$ hadroproduction from supposedly subleading EW contributions*, *JHEP* **02** (2018) 031, arXiv: [1711.02116 \[hep-ph\]](#).

- [115] ATLAS Collaboration, *Observation of the associated production of a top quark and a Z boson in pp collisions at $\sqrt{s} = 13$ TeV with the ATLAS detector*, *JHEP* **07** (2020) 124, arXiv: [2002.07546 \[hep-ex\]](#).
- [116] ATLAS Collaboration, *Evidence for the $VH, H \rightarrow \tau\tau$ process with the ATLAS detector in Run 2*, (2023), arXiv: [2312.02394 \[hep-ex\]](#).
- [117] ATLAS Collaboration, *Combined search for the Standard Model Higgs boson in pp collisions at $\sqrt{s} = 7$ TeV with the ATLAS detector*, *Phys. Rev. D* **86** (2012) 032003, arXiv: [1207.0319 \[hep-ex\]](#).
- [118] A. L. Read, *Presentation of search results: the CL_S technique*, *J. Phys. G* **28** (2002) 2693.
- [119] G. Cowan, K. Cranmer, E. Gross and O. Vitells, *Asymptotic formulae for likelihood-based tests of new physics*, *Eur. Phys. J. C* **71** (2011) 1554, arXiv: [1007.1727 \[physics.data-an\]](#), Erratum: *Eur. Phys. J. C* **73** (2013) 2501.
- [120] ATLAS Collaboration, *ATLAS Computing Acknowledgements*, ATL-SOFT-PUB-2023-001, 2023, URL: <https://cds.cern.ch/record/2869272>.

The ATLAS Collaboration

G. Aad ¹⁰⁴, E. Aakvaag ¹⁷, B. Abbott ¹²³, S. Abdelhameed ^{119a}, K. Abeling ⁵⁶, N.J. Abicht ⁵⁰, S.H. Abidi ³⁰, M. Aboeela ⁴⁵, A. Aboulhorma ^{36e}, H. Abramowicz ¹⁵⁴, H. Abreu ¹⁵³, Y. Abulaiti ¹²⁰, B.S. Acharya ^{70a,70b,k}, A. Ackermann ^{64a}, C. Adam Bourdarios ⁴, L. Adamczyk ^{87a}, S.V. Addepalli ²⁷, M.J. Addison ¹⁰³, J. Adelman ¹¹⁸, A. Adiguzel ^{22c}, T. Adye ¹³⁷, A.A. Affolder ¹³⁹, Y. Afik ⁴⁰, M.N. Agaras ¹³, J. Agarwala ^{74a,74b}, A. Aggarwal ¹⁰², C. Agheorghiesei ^{28c}, F. Ahmadov ^{39,y}, W.S. Ahmed ¹⁰⁶, S. Ahuja ⁹⁷, X. Ai ^{63e}, G. Aielli ^{77a,77b}, A. Aikot ¹⁶⁶, M. Ait Tamliah ^{36e}, B. Aitbenkikh ^{36a}, M. Akbiyik ¹⁰², T.P.A. Åkesson ¹⁰⁰, A.V. Akimov ³⁸, D. Akiyama ¹⁷¹, N.N. Akolkar ²⁵, S. Aktas ^{22a}, K. Al Houry ⁴², G.L. Alberghi ^{24b}, J. Albert ¹⁶⁸, P. Albicocco ⁵⁴, G.L. Albouy ⁶¹, S. Alderweireldt ⁵³, Z.L. Alegria ¹²⁴, M. Aleksa ³⁷, I.N. Aleksandrov ³⁹, C. Alexa ^{28b}, T. Alexopoulos ¹⁰, F. Alfonsi ^{24b}, M. Algren ⁵⁷, M. Alhroob ¹⁷⁰, B. Ali ¹³⁵, H.M.J. Ali ⁹³, S. Ali ³², S.W. Alibocus ⁹⁴, M. Aliev ^{34c}, G. Alimonti ^{72a}, W. Alkahi ⁵⁶, C. Allaire ⁶⁷, B.M.M. Allbrooke ¹⁴⁹, J.F. Allen ⁵³, C.A. Allendes Flores ^{140f}, P.P. Allport ²¹, A. Aloisio ^{73a,73b}, F. Alonso ⁹², C. Alpigiani ¹⁴¹, Z.M.K. Alsolami ⁹³, M. Alvarez Estevez ¹⁰¹, A. Alvarez Fernandez ¹⁰², M. Alves Cardoso ⁵⁷, M.G. Alvigi ^{73a,73b}, M. Aly ¹⁰³, Y. Amaral Coutinho ^{84b}, A. Ambler ¹⁰⁶, C. Amelung ³⁷, M. Amerl ¹⁰³, C.G. Ames ¹¹¹, D. Amidei ¹⁰⁸, K.J. Amirie ¹⁵⁸, S.P. Amor Dos Santos ^{133a}, K.R. Amos ¹⁶⁶, S. An ⁸⁵, V. Ananiev ¹²⁸, C. Anastopoulos ¹⁴², T. Andeen ¹¹, J.K. Anders ³⁷, A.C. Anderson ⁶⁰, S.Y. Andreev ^{48a,48b}, A. Andreatza ^{72a,72b}, S. Angelidakis ⁹, A. Angerami ⁴², A.V. Anisenkov ³⁸, A. Annovi ^{75a}, C. Antel ⁵⁷, E. Antipov ¹⁴⁸, M. Antonelli ⁵⁴, F. Anulli ^{76a}, M. Aoki ⁸⁵, T. Aoki ¹⁵⁶, M.A. Aparo ¹⁴⁹, L. Aperio Bella ⁴⁹, C. Appelt ¹⁹, A. Apyan ²⁷, S.J. Arbiol Val ⁸⁸, C. Arcangeletti ⁵⁴, A.T.H. Arce ⁵², E. Arena ⁹⁴, J-F. Arguin ¹¹⁰, S. Argyropoulos ⁵⁵, J.-H. Arling ⁴⁹, O. Arnaez ⁴, H. Arnold ¹⁴⁸, G. Artoni ^{76a,76b}, H. Asada ¹¹³, K. Asai ¹²¹, S. Asai ¹⁵⁶, N.A. Asbah ³⁷, R.A. Ashby Pickering ¹⁷⁰, K. Assamagan ³⁰, R. Astalos ^{29a}, K.S.V. Astrand ¹⁰⁰, S. Atashi ¹⁶², R.J. Atkin ^{34a}, M. Atkinson ¹⁶⁵, H. Atmani ^{36f}, P.A. Atmasiddha ¹³¹, K. Augsten ¹³⁵, S. Auricchio ^{73a,73b}, A.D. Auriol ²¹, V.A. Austrup ¹⁰³, G. Avolio ³⁷, K. Axiotis ⁵⁷, G. Azuelos ^{110,ad}, D. Babal ^{29b}, H. Bachacou ¹³⁸, K. Bachas ^{155,o}, A. Bachiu ³⁵, F. Backman ^{48a,48b}, A. Badea ⁴⁰, T.M. Baer ¹⁰⁸, P. Bagnaia ^{76a,76b}, M. Bahmani ¹⁹, D. Bahner ⁵⁵, K. Bai ¹²⁶, J.T. Baines ¹³⁷, L. Baines ⁹⁶, O.K. Baker ¹⁷⁵, E. Bakos ¹⁶, D. Bakshi Gupta ⁸, L.E. Balabram Filho ^{84b}, V. Balakrishnan ¹²³, R. Balasubramanian ¹¹⁷, E.M. Baldin ³⁸, P. Balek ^{87a}, E. Ballabene ^{24b,24a}, F. Balli ¹³⁸, L.M. Baltes ^{64a}, W.K. Balunas ³³, J. Balz ¹⁰², I. Bamwidhi ^{119b}, E. Banas ⁸⁸, M. Bandieramonte ¹³², A. Bandyopadhyay ²⁵, S. Bansal ²⁵, L. Barak ¹⁵⁴, M. Barakat ⁴⁹, E.L. Barberio ¹⁰⁷, D. Barberis ^{58b,58a}, M. Barbero ¹⁰⁴, M.Z. Barel ¹¹⁷, K.N. Barends ^{34a}, T. Barillari ¹¹², M-S. Barisits ³⁷, T. Barklow ¹⁴⁶, P. Baron ¹²⁵, D.A. Baron Moreno ¹⁰³, A. Baroncelli ^{63a}, G. Barone ³⁰, A.J. Barr ¹²⁹, J.D. Barr ⁹⁸, F. Barreiro ¹⁰¹, J. Barreiro Guimarães da Costa ¹⁴, U. Barron ¹⁵⁴, M.G. Barros Teixeira ^{133a}, S. Barsov ³⁸, F. Bartels ^{64a}, R. Bartoldus ¹⁴⁶, A.E. Barton ⁹³, P. Bartos ^{29a}, A. Basan ¹⁰², M. Baselga ⁵⁰, A. Bassalat ^{67,b}, M.J. Basso ^{159a}, S. Bataju ⁴⁵, R. Bate ¹⁶⁷, R.L. Bates ⁶⁰, S. Batlamous ¹⁰¹, B. Batool ¹⁴⁴, M. Battaglia ¹³⁹, D. Battulga ¹⁹, M. Bauce ^{76a,76b}, M. Bauer ⁸⁰, P. Bauer ²⁵, L.T. Bazzano Hurrell ³¹, J.B. Beacham ⁵², T. Beau ¹³⁰, J.Y. Beaucamp ⁹², P.H. Beauchemin ¹⁶¹, P. Bechtel ²⁵, H.P. Beck ^{20,n}, K. Becker ¹⁷⁰, A.J. Beddall ⁸³, V.A. Bednyakov ³⁹, C.P. Bee ¹⁴⁸, L.J. Beemster ¹⁶, T.A. Beermann ³⁷, M. Begalli ^{84d}, M. Begel ³⁰, A. Behera ¹⁴⁸, J.K. Behr ⁴⁹, J.F. Beirer ³⁷, F. Beisiegel ²⁵, M. Belfkir ^{119b}, G. Bella ¹⁵⁴, L. Bellagamba ^{24b}, A. Bellerive ³⁵,

P. Bellos ²¹, K. Beloborodov ³⁸, D. Benchekroun ^{36a}, F. Bendebba ^{36a}, Y. Benhammou ¹⁵⁴,
 K.C. Benkendorfer ⁶², L. Beresford ⁴⁹, M. Beretta ⁵⁴, E. Bergeaas Kuutmann ¹⁶⁴, N. Berger ⁴,
 B. Bergmann ¹³⁵, J. Beringer ^{18a}, G. Bernardi ⁵, C. Bernius ¹⁴⁶, F.U. Bernlochner ²⁵,
 F. Bernon ^{37,104}, A. Berrocal Guardia ¹³, T. Berry ⁹⁷, P. Berta ¹³⁶, A. Berthold ⁵¹, S. Bethke ¹¹²,
 A. Betti ^{76a,76b}, A.J. Bevan ⁹⁶, N.K. Bhalla ⁵⁵, S. Bhatta ¹⁴⁸, D.S. Bhattacharya ¹⁶⁹,
 P. Bhattarai ¹⁴⁶, K.D. Bhide ⁵⁵, V.S. Bhopatkar ¹²⁴, R.M. Bianchi ¹³², G. Bianco ^{24b,24a},
 O. Biebel ¹¹¹, R. Bielski ¹²⁶, M. Biglietti ^{78a}, C.S. Billingsley ⁴⁵, M. Bindi ⁵⁶, A. Bingul ^{22b},
 C. Bini ^{76a,76b}, A. Biondini ⁹⁴, G.A. Bird ³³, M. Birman ¹⁷², M. Biros ¹³⁶, S. Biryukov ¹⁴⁹,
 T. Bisanz ⁵⁰, E. Bisceglie ^{44b,44a}, J.P. Biswal ¹³⁷, D. Biswas ¹⁴⁴, I. Bloch ⁴⁹, A. Blue ⁶⁰,
 U. Blumenschein ⁹⁶, J. Blumenthal ¹⁰², V.S. Bobrovnikov ³⁸, M. Boehler ⁵⁵, B. Boehm ¹⁶⁹,
 D. Bogavac ³⁷, A.G. Bogdanchikov ³⁸, C. Bohm ^{48a}, V. Boisvert ⁹⁷, P. Bokan ³⁷, T. Bold ^{87a},
 M. Bomben ⁵, M. Bona ⁹⁶, M. Boonekamp ¹³⁸, C.D. Booth ⁹⁷, A.G. Borbély ⁶⁰,
 I.S. Bordulev ³⁸, H.M. Borecka-Bielska ¹¹⁰, G. Borissov ⁹³, D. Bortoletto ¹²⁹, D. Boscherini ^{24b},
 M. Bosman ¹³, J.D. Bossio Sola ³⁷, K. Bouaouda ^{36a}, N. Bouchhar ¹⁶⁶, L. Boudet ⁴,
 J. Boudreau ¹³², E.V. Bouhova-Thacker ⁹³, D. Boumediene ⁴¹, R. Bouquet ^{58b,58a}, A. Boveia ¹²²,
 J. Boyd ³⁷, D. Boye ³⁰, I.R. Boyko ³⁹, L. Bozianu ⁵⁷, J. Bracinek ²¹, N. Brahimi ⁴,
 G. Brandt ¹⁷⁴, O. Brandt ³³, F. Braren ⁴⁹, B. Brau ¹⁰⁵, J.E. Brau ¹²⁶, R. Brenner ¹⁷²,
 L. Brenner ¹¹⁷, R. Brenner ¹⁶⁴, S. Bressler ¹⁷², G. Brianti ^{79a,79b}, D. Britton ⁶⁰, D. Britzger ¹¹²,
 I. Brock ²⁵, R. Brock ¹⁰⁹, G. Brooijmans ⁴², E.M. Brooks ^{159b}, E. Brost ³⁰, L.M. Brown ¹⁶⁸,
 L.E. Bruce ⁶², T.L. Bruckler ¹²⁹, P.A. Bruckman de Renstrom ⁸⁸, B. Brüers ⁴⁹, A. Bruni ^{24b},
 G. Bruni ^{24b}, M. Bruschi ^{24b}, N. Bruscano ^{76a,76b}, T. Buanes ¹⁷, Q. Buat ¹⁴¹, D. Buchin ¹¹²,
 A.G. Buckley ⁶⁰, O. Bulekov ³⁸, B.A. Bullard ¹⁴⁶, S. Burdin ⁹⁴, C.D. Burgard ⁵⁰,
 A.M. Burger ³⁷, B. Burghgrave ⁸, O. Burlayenko ⁵⁵, J. Burleson ¹⁶⁵, J.T.P. Burr ³³,
 J.C. Burzynski ¹⁴⁵, E.L. Busch ⁴², V. Büscher ¹⁰², P.J. Bussey ⁶⁰, J.M. Butler ²⁶, C.M. Buttar ⁶⁰,
 J.M. Butterworth ⁹⁸, W. Buttinger ¹³⁷, C.J. Buxo Vazquez ¹⁰⁹, A.R. Buzykaev ³⁸,
 S. Cabrera Urbán ¹⁶⁶, L. Cadamuro ⁶⁷, D. Caforio ⁵⁹, H. Cai ¹³², Y. Cai ^{14,114c}, Y. Cai ^{114a},
 V.M.M. Cairo ³⁷, O. Cakir ^{3a}, N. Calace ³⁷, P. Calafiura ^{18a}, G. Calderini ¹³⁰, P. Calfayan ⁶⁹,
 G. Callea ⁶⁰, L.P. Caloba ^{84b}, D. Calvet ⁴¹, S. Calvet ⁴¹, M. Calvetti ^{75a,75b}, R. Camacho Toro ¹³⁰,
 S. Camarda ³⁷, D. Camarero Munoz ²⁷, P. Camarri ^{77a,77b}, M.T. Camerlingo ^{73a,73b},
 D. Cameron ³⁷, C. Camincher ¹⁶⁸, M. Campanelli ⁹⁸, A. Camplani ⁴³, V. Canale ^{73a,73b},
 A.C. Canbay ^{3a}, E. Canonero ⁹⁷, J. Cantero ¹⁶⁶, Y. Cao ¹⁶⁵, F. Capocasa ²⁷, M. Capua ^{44b,44a},
 A. Carbone ^{72a,72b}, R. Cardarelli ^{77a}, J.C.J. Cardenas ⁸, G. Carducci ^{44b,44a}, T. Carli ³⁷,
 G. Carlino ^{73a}, J.I. Carlotto ¹³, B.T. Carlson ^{132,p}, E.M. Carlson ^{168,159a}, J. Carmignani ⁹⁴,
 L. Carminati ^{72a,72b}, A. Carnelli ¹³⁸, M. Carnesale ^{76a,76b}, S. Caron ¹¹⁶, E. Carquin ^{140f},
 S. Carrá ^{72a}, G. Carratta ^{24b,24a}, A.M. Carroll ¹²⁶, T.M. Carter ⁵³, M.P. Casado ^{13,h},
 M. Caspar ⁴⁹, F.L. Castillo ⁴, L. Castillo Garcia ¹³, V. Castillo Gimenez ¹⁶⁶, N.F. Castro ^{133a,133e},
 A. Catinaccio ³⁷, J.R. Catmore ¹²⁸, T. Cavaliere ⁴, V. Cavaliere ³⁰, N. Cavalli ^{24b,24a},
 L.J. Caviedes Betancourt ^{23b}, Y.C. Cekmecelioglu ⁴⁹, E. Celebi ⁸³, S. Cella ³⁷, F. Celli ¹²⁹,
 M.S. Centonze ^{71a,71b}, V. Cepaitis ⁵⁷, K. Cerny ¹²⁵, A.S. Cerqueira ^{84a}, A. Cerri ¹⁴⁹,
 L. Cerrito ^{77a,77b}, F. Cerutti ^{18a}, B. Cervato ¹⁴⁴, A. Cervelli ^{24b}, G. Cesarini ⁵⁴, S.A. Cetin ⁸³,
 D. Chakraborty ¹¹⁸, J. Chan ^{18a}, W.Y. Chan ¹⁵⁶, J.D. Chapman ³³, E. Chapon ¹³⁸,
 B. Chargeishvili ^{152b}, D.G. Charlton ²¹, M. Chatterjee ²⁰, C. Chauhan ¹³⁶, Y. Che ^{114a},
 S. Chekanov ⁶, S.V. Chekulaev ^{159a}, G.A. Chelkov ^{39,a}, A. Chen ¹⁰⁸, B. Chen ¹⁵⁴, B. Chen ¹⁶⁸,
 H. Chen ^{114a}, H. Chen ³⁰, J. Chen ^{63c}, J. Chen ¹⁴⁵, M. Chen ¹²⁹, S. Chen ¹⁵⁶, S.J. Chen ^{114a},
 X. Chen ^{63c,138}, X. Chen ^{15,ac}, Y. Chen ^{63a}, C.L. Cheng ¹⁷³, H.C. Cheng ^{65a}, S. Cheong ¹⁴⁶,
 A. Cheplakov ³⁹, E. Cheremushkina ⁴⁹, E. Cherepanova ¹¹⁷, R. Cherkaoui El Moursli ^{36e},
 E. Cheu ⁷, K. Cheung ⁶⁶, L. Chevalier ¹³⁸, V. Chiarella ⁵⁴, G. Chiarelli ^{75a}, N. Chiedde ¹⁰⁴,

G. Chiodini ^{71a}, A.S. Chisholm ²¹, A. Chitan ^{28b}, M. Chitishvili ¹⁶⁶, M.V. Chizhov ^{39,q}, K. Choi ¹¹, Y. Chou ¹⁴¹, E.Y.S. Chow ¹¹⁶, K.L. Chu ¹⁷², M.C. Chu ^{65a}, X. Chu ^{14,114c}, Z. Chubinidze ⁵⁴, J. Chudoba ¹³⁴, J.J. Chwastowski ⁸⁸, D. Cieri ¹¹², K.M. Ciesla ^{87a}, V. Cindro ⁹⁵, A. Ciocio ^{18a}, F. Cirotto ^{73a,73b}, Z.H. Citron ¹⁷², M. Citterio ^{72a}, D.A. Ciubotaru ^{28b}, A. Clark ⁵⁷, P.J. Clark ⁵³, N. Clarke Hall ⁹⁸, C. Clarry ¹⁵⁸, J.M. Clavijo Columbie ⁴⁹, S.E. Clawson ⁴⁹, C. Clement ^{48a,48b}, Y. Coadou ¹⁰⁴, M. Cobal ^{70a,70c}, A. Coccaro ^{58b}, R.F. Coelho Barrue ^{133a}, R. Coelho Lopes De Sa ¹⁰⁵, S. Coelli ^{72a}, B. Cole ⁴², J. Collot ⁶¹, P. Conde Muiño ^{133a,133g}, M.P. Connell ^{34c}, S.H. Connell ^{34c}, E.I. Conroy ¹²⁹, F. Conventi ^{73a,ae}, H.G. Cooke ²¹, A.M. Cooper-Sarkar ¹²⁹, F.A. Corchia ^{24b,24a}, A. Cordeiro Oudot Choi ¹³⁰, L.D. Corpe ⁴¹, M. Corradi ^{76a,76b}, F. Corriveau ^{106,w}, A. Cortes-Gonzalez ¹⁹, M.J. Costa ¹⁶⁶, F. Costanza ⁴, D. Costanzo ¹⁴², B.M. Cote ¹²², J. Couthures ⁴, G. Cowan ⁹⁷, K. Cranmer ¹⁷³, D. Cremonini ^{24b,24a}, S. Crépe-Renaudin ⁶¹, F. Crescioli ¹³⁰, M. Cristinziani ¹⁴⁴, M. Cristoforetti ^{79a,79b}, V. Croft ¹¹⁷, J.E. Crosby ¹²⁴, G. Crosetti ^{44b,44a}, A. Cueto ¹⁰¹, H. Cui ⁹⁸, Z. Cui ⁷, W.R. Cunningham ⁶⁰, F. Curcio ¹⁶⁶, J.R. Curran ⁵³, P. Czodrowski ³⁷, M.M. Czurylo ³⁷, M.J. Da Cunha Sargedas De Sousa ^{58b,58a}, J.V. Da Fonseca Pinto ^{84b}, C. Da Via ¹⁰³, W. Dabrowski ^{87a}, T. Dado ⁵⁰, S. Dahbi ¹⁵¹, T. Dai ¹⁰⁸, D. Dal Santo ²⁰, C. Dallapiccola ¹⁰⁵, M. Dam ⁴³, G. D'amen ³⁰, V. D'Amico ¹¹¹, J. Damp ¹⁰², J.R. Dandoy ³⁵, D. Dannheim ³⁷, M. Danninger ¹⁴⁵, V. Dao ¹⁴⁸, G. Darbo ^{58b}, S.J. Das ^{30,af}, F. Dattola ⁴⁹, S. D'Auria ^{72a,72b}, A. D'Avanzo ^{73a,73b}, C. David ^{34a}, T. Davidek ¹³⁶, I. Dawson ⁹⁶, H.A. Day-hall ¹³⁵, K. De ⁸, R. De Asmundis ^{73a}, N. De Biase ⁴⁹, S. De Castro ^{24b,24a}, N. De Groot ¹¹⁶, P. de Jong ¹¹⁷, H. De la Torre ¹¹⁸, A. De Maria ^{114a}, A. De Salvo ^{76a}, U. De Sanctis ^{77a,77b}, F. De Santis ^{71a,71b}, A. De Santo ¹⁴⁹, J.B. De Vivie De Regie ⁶¹, D.V. Dedovich ³⁹, J. Degens ⁹⁴, A.M. Deiana ⁴⁵, F. Del Corso ^{24b,24a}, J. Del Peso ¹⁰¹, F. Del Rio ^{64a}, L. Delagrangé ¹³⁰, F. Deliot ¹³⁸, C.M. Delitzsch ⁵⁰, M. Della Pietra ^{73a,73b}, D. Della Volpe ⁵⁷, A. Dell'Acqua ³⁷, L. Dell'Asta ^{72a,72b}, M. Delmastro ⁴, P.A. Delsart ⁶¹, S. Demers ¹⁷⁵, M. Demichev ³⁹, S.P. Denisov ³⁸, L. D'Eramo ⁴¹, D. Derendarz ⁸⁸, F. Derue ¹³⁰, P. Dervan ⁹⁴, K. Desch ²⁵, C. Deutsch ²⁵, F.A. Di Bello ^{58b,58a}, A. Di Ciaccio ^{77a,77b}, L. Di Ciaccio ⁴, A. Di Domenico ^{76a,76b}, C. Di Donato ^{73a,73b}, A. Di Girolamo ³⁷, G. Di Gregorio ³⁷, A. Di Luca ^{79a,79b}, B. Di Micco ^{78a,78b}, R. Di Nardo ^{78a,78b}, K.F. Di Petrillo ⁴⁰, M. Diamantopoulou ³⁵, F.A. Dias ¹¹⁷, T. Dias Do Vale ¹⁴⁵, M.A. Diaz ^{140a,140b}, F.G. Diaz Capriles ²⁵, A.R. Didenko ³⁹, M. Didenko ¹⁶⁶, E.B. Diehl ¹⁰⁸, S. Díez Cornell ⁴⁹, C. Diez Pardos ¹⁴⁴, C. Dimitriadi ¹⁶⁴, A. Dimitrievska ²¹, J. Dingfelder ²⁵, T. Dingley ¹²⁹, I-M. Dinu ^{28b}, S.J. Dittmeier ^{64b}, F. Dittus ³⁷, M. Divisek ¹³⁶, F. Djama ¹⁰⁴, T. Djobava ^{152b}, C. Doglioni ^{103,100}, A. Dohnalova ^{29a}, J. Dolejsi ¹³⁶, Z. Dolezal ¹³⁶, K. Domijan ^{87a}, K.M. Dona ⁴⁰, M. Donadelli ^{84d}, B. Dong ¹⁰⁹, J. Donini ⁴¹, A. D'Onofrio ^{73a,73b}, M. D'Onofrio ⁹⁴, J. Dopke ¹³⁷, A. Doria ^{73a}, N. Dos Santos Fernandes ^{133a}, P. Dougan ¹⁰³, M.T. Dova ⁹², A.T. Doyle ⁶⁰, M.A. Draguet ¹²⁹, E. Dreyer ¹⁷², I. Drivas-koulouris ¹⁰, M. Drnevich ¹²⁰, M. Drozdova ⁵⁷, D. Du ^{63a}, T.A. du Pree ¹¹⁷, F. Dubinin ³⁸, M. Dubovsky ^{29a}, E. Duchovni ¹⁷², G. Duckeck ¹¹¹, O.A. Ducu ^{28b}, D. Duda ⁵³, A. Dudarev ³⁷, E.R. Duden ²⁷, M. D'uffizi ¹⁰³, L. Duflost ⁶⁷, M. Dührssen ³⁷, I. Duminica ^{28g}, A.E. Dumitriu ^{28b}, M. Dunford ^{64a}, S. Dungs ⁵⁰, K. Dunne ^{48a,48b}, A. Duperrin ¹⁰⁴, H. Duran Yildiz ^{3a}, M. Düren ⁵⁹, A. Durglishvili ^{152b}, B.L. Dwyer ¹¹⁸, G.I. Dyckes ^{18a}, M. Dyndal ^{87a}, B.S. Dziedzic ³⁷, Z.O. Earnshaw ¹⁴⁹, G.H. Eberwein ¹²⁹, B. Eckerova ^{29a}, S. Eggebrecht ⁵⁶, E. Egidio Purcino De Souza ¹³⁰, L.F. Ehrke ⁵⁷, G. Eigen ¹⁷, K. Einsweiler ^{18a}, T. Ekelof ¹⁶⁴, P.A. Ekman ¹⁰⁰, S. El Farkh ^{36b}, Y. El Ghazali ^{36b}, H. El Jarrari ³⁷, A. El Moussaouy ^{36a}, V. Ellajosyula ¹⁶⁴, M. Ellert ¹⁶⁴, F. Ellinghaus ¹⁷⁴, N. Ellis ³⁷, J. Elmsheuser ³⁰, M. Elsayy ^{119a}, M. Elsing ³⁷, D. Emelianov ¹³⁷, Y. Enari ¹⁵⁶, I. Ene ^{18a}, S. Epari ¹³, P.A. Erland ⁸⁸,

D. Ernani Martins Neto [ID88](#), M. Errenst [ID174](#), M. Escalier [ID67](#), C. Escobar [ID166](#), E. Etzion [ID154](#),
 G. Evans [ID133a](#), H. Evans [ID69](#), L.S. Evans [ID97](#), A. Ezhilov [ID38](#), S. Ezzarqtouni [ID36a](#), F. Fabbri [ID24b,24a](#),
 L. Fabbri [ID24b,24a](#), G. Facini [ID98](#), V. Fadeyev [ID139](#), R.M. Fakhruddinov [ID38](#), D. Fakoudis [ID102](#),
 S. Falciano [ID76a](#), L.F. Falda Ulhoa Coelho [ID37](#), F. Fallavollita [ID112](#), G. Falsetti [ID44b,44a](#), J. Faltova [ID136](#),
 C. Fan [ID165](#), Y. Fan [ID14](#), Y. Fang [ID14,114c](#), M. Fanti [ID72a,72b](#), M. Faraj [ID70a,70b](#), Z. Farazpay [ID99](#),
 A. Farbin [ID8](#), A. Farilla [ID78a](#), T. Farooque [ID109](#), S.M. Farrington [ID53](#), F. Fassi [ID36e](#), D. Fassouliotis [ID9](#),
 M. Faucci Giannelli [ID77a,77b](#), W.J. Fawcett [ID33](#), L. Fayard [ID67](#), P. Federic [ID136](#), P. Federicova [ID134](#),
 O.L. Fedin [ID38,a](#), M. Feickert [ID173](#), L. Feligioni [ID104](#), D.E. Fellers [ID126](#), C. Feng [ID63b](#), M. Feng [ID15](#),
 Z. Feng [ID117](#), M.J. Fenton [ID162](#), L. Ferencz [ID49](#), R.A.M. Ferguson [ID93](#), S.I. Fernandez Luengo [ID140f](#),
 P. Fernandez Martinez [ID13](#), M.J.V. Fernoux [ID104](#), J. Ferrando [ID93](#), A. Ferrari [ID164](#), P. Ferrari [ID117,116](#),
 R. Ferrari [ID74a](#), D. Ferrere [ID57](#), C. Ferretti [ID108](#), D. Fiacco [ID76a,76b](#), F. Fiedler [ID102](#), P. Fiedler [ID135](#),
 A. Filipčič [ID95](#), E.K. Filmer [ID1](#), F. Filthaut [ID116](#), M.C.N. Fiolhais [ID133a,133c,c](#), L. Fiorini [ID166](#),
 W.C. Fisher [ID109](#), T. Fitschen [ID103](#), P.M. Fitzhugh [ID138](#), I. Fleck [ID144](#), P. Fleischmann [ID108](#), T. Flick [ID174](#),
 M. Flores [ID34d,aa](#), L.R. Flores Castillo [ID65a](#), L. Flores Sanz De Acedo [ID37](#), F.M. Follega [ID79a,79b](#),
 N. Fomin [ID33](#), J.H. Foo [ID158](#), A. Formica [ID138](#), A.C. Forti [ID103](#), E. Fortin [ID37](#), A.W. Fortman [ID18a](#),
 M.G. Foti [ID18a](#), L. Fountas [ID9,i](#), D. Fournier [ID67](#), H. Fox [ID93](#), P. Francavilla [ID75a,75b](#), S. Francescato [ID62](#),
 S. Franchellucci [ID57](#), M. Franchini [ID24b,24a](#), S. Franchino [ID64a](#), D. Francis [ID37](#), L. Franco [ID116](#),
 V. Franco Lima [ID37](#), L. Franconi [ID49](#), M. Franklin [ID62](#), G. Frattari [ID27](#), Y.Y. Frid [ID154](#), J. Friend [ID60](#),
 N. Fritzsche [ID51](#), A. Froch [ID55](#), D. Froidevaux [ID37](#), J.A. Frost [ID129](#), Y. Fu [ID63a](#),
 S. Fuenzalida Garrido [ID140f](#), M. Fujimoto [ID104](#), K.Y. Fung [ID65a](#), E. Furtado De Simas Filho [ID84e](#),
 M. Furukawa [ID156](#), J. Fuster [ID166](#), A. Gaa [ID56](#), A. Gabrielli [ID24b,24a](#), A. Gabrielli [ID158](#), P. Gadow [ID37](#),
 G. Gagliardi [ID58b,58a](#), L.G. Gagnon [ID18a](#), S. Gaid [ID163](#), S. Galantzan [ID154](#), E.J. Gallas [ID129](#),
 B.J. Gallop [ID137](#), K.K. Gan [ID122](#), S. Ganguly [ID156](#), Y. Gao [ID53](#), F.M. Garay Walls [ID140a,140b](#), B. Garcia [ID30](#),
 C. García [ID166](#), A. Garcia Alonso [ID117](#), A.G. Garcia Caffaro [ID175](#), J.E. García Navarro [ID166](#),
 M. Garcia-Sciveres [ID18a](#), G.L. Gardner [ID131](#), R.W. Gardner [ID40](#), N. Garelli [ID161](#), D. Garg [ID81](#),
 R.B. Garg [ID146](#), J.M. Gargan [ID53](#), C.A. Garner [ID158](#), C.M. Garvey [ID34a](#), V.K. Gassmann [ID161](#), G. Gaudio [ID74a](#),
 V. Gautam [ID13](#), P. Gauzzi [ID76a,76b](#), J. Gavranovic [ID95](#), I.L. Gavrilenko [ID38](#), A. Gavriluk [ID38](#), C. Gay [ID167](#),
 G. Gaycken [ID126](#), E.N. Gazis [ID10](#), A.A. Geanta [ID28b](#), C.M. Gee [ID139](#), A. Gekow [ID122](#), C. Gemme [ID58b](#),
 M.H. Genest [ID61](#), A.D. Gentry [ID115](#), S. George [ID97](#), W.F. George [ID21](#), T. Geralis [ID47](#),
 P. Gessinger-Befurt [ID37](#), M.E. Geyik [ID174](#), M. Ghani [ID170](#), K. Ghorbanian [ID96](#), A. Ghosal [ID144](#),
 A. Ghosh [ID162](#), A. Ghosh [ID7](#), B. Giacobbe [ID24b](#), S. Giagu [ID76a,76b](#), T. Giani [ID117](#), A. Giannini [ID63a](#),
 S.M. Gibson [ID97](#), M. Gignac [ID139](#), D.T. Gil [ID87b](#), A.K. Gilbert [ID87a](#), B.J. Gilbert [ID42](#), D. Gillberg [ID35](#),
 G. Gilles [ID117](#), L. Ginabat [ID130](#), D.M. Gingrich [ID2,ad](#), M.P. Giordani [ID70a,70c](#), P.F. Giraud [ID138](#),
 G. Giugliarelli [ID70a,70c](#), D. Giugni [ID72a](#), F. Giuli [ID37](#), I. Gkialas [ID9,i](#), L.K. Gladilin [ID38](#), C. Glasman [ID101](#),
 G.R. Gledhill [ID126](#), G. Glemža [ID49](#), M. Glisic [ID126](#), I. Gnesi [ID44b,e](#), Y. Go [ID30](#), M. Goblirsch-Kolb [ID37](#),
 B. Gocke [ID50](#), D. Godin [ID110](#), B. Gokturk [ID22a](#), S. Goldfarb [ID107](#), T. Golling [ID57](#), M.G.D. Gololo [ID34g](#),
 D. Golubkov [ID38](#), J.P. Gombas [ID109](#), A. Gomes [ID133a,133b](#), G. Gomes Da Silva [ID144](#),
 A.J. Gomez Delegido [ID166](#), R. Gonçalo [ID133a](#), L. Gonella [ID21](#), A. Gongadze [ID152c](#), F. Gonnella [ID21](#),
 J.L. Gonski [ID146](#), R.Y. González Andana [ID53](#), S. González de la Hoz [ID166](#), R. Gonzalez Lopez [ID94](#),
 C. Gonzalez Renteria [ID18a](#), M.V. Gonzalez Rodrigues [ID49](#), R. Gonzalez Suarez [ID164](#),
 S. Gonzalez-Sevilla [ID57](#), L. Goossens [ID37](#), B. Gorini [ID37](#), E. Gorini [ID71a,71b](#), A. Gorišek [ID95](#),
 T.C. Gosart [ID131](#), A.T. Goshaw [ID52](#), M.I. Gostkin [ID39](#), S. Goswami [ID124](#), C.A. Gottardo [ID37](#),
 S.A. Gotz [ID111](#), M. Goughri [ID36b](#), V. Goumarre [ID49](#), A.G. Goussiou [ID141](#), N. Govender [ID34c](#),
 I. Grabowska-Bold [ID87a](#), K. Graham [ID35](#), E. Gramstad [ID128](#), S. Grancagnolo [ID71a,71b](#), C.M. Grant [ID1,138](#),
 P.M. Gravila [ID28f](#), F.G. Gravili [ID71a,71b](#), H.M. Gray [ID18a](#), M. Greco [ID71a,71b](#), M.J. Green [ID1](#), C. Grefe [ID25](#),
 A.S. Grefsrud [ID17](#), I.M. Gregor [ID49](#), K.T. Greif [ID162](#), P. Grenier [ID146](#), S.G. Grewe [ID112](#), A.A. Grillo [ID139](#),
 K. Grimm [ID32](#), S. Grinstein [ID13,s](#), J.-F. Grivaz [ID67](#), E. Gross [ID172](#), J. Grosse-Knetter [ID56](#),

J.C. Grundy ¹²⁹, L. Guan ¹⁰⁸, J.G.R. Guerrero Rojas ¹⁶⁶, G. Guerrieri ^{70a,70c}, R. Gugel ¹⁰², J.A.M. Guhit ¹⁰⁸, A. Guida ¹⁹, E. Guilloton ¹⁷⁰, S. Guindon ³⁷, F. Guo ^{14,114c}, J. Guo ^{63c}, L. Guo ⁴⁹, Y. Guo ¹⁰⁸, R. Gupta ¹³², S. Gurbuz ²⁵, S.S. Gurdasani ⁵⁵, G. Gustavino ^{76a,76b}, P. Gutierrez ¹²³, L.F. Gutierrez Zagazeta ¹³¹, M. Gutsche ⁵¹, C. Gutschow ⁹⁸, C. Gwenlan ¹²⁹, C.B. Gwilliam ⁹⁴, E.S. Haaland ¹²⁸, A. Haas ¹²⁰, M. Habedank ⁴⁹, C. Haber ^{18a}, H.K. Hadavand ⁸, A. Hadeef ⁵¹, S. Hadzic ¹¹², A.I. Hagan ⁹³, J.J. Hahn ¹⁴⁴, E.H. Haines ⁹⁸, M. Haleem ¹⁶⁹, J. Haley ¹²⁴, J.J. Hall ¹⁴², G.D. Hallewell ¹⁰⁴, L. Halser ²⁰, K. Hamano ¹⁶⁸, M. Hamer ²⁵, G.N. Hamity ⁵³, E.J. Hampshire ⁹⁷, J. Han ^{63b}, K. Han ^{63a}, L. Han ^{114a}, L. Han ^{63a}, S. Han ^{18a}, Y.F. Han ¹⁵⁸, K. Hanagaki ⁸⁵, M. Hance ¹³⁹, D.A. Hangal ⁴², H. Hanif ¹⁴⁵, M.D. Hank ¹³¹, J.B. Hansen ⁴³, P.H. Hansen ⁴³, K. Hara ¹⁶⁰, D. Harada ⁵⁷, T. Harenberg ¹⁷⁴, S. Harkusha ³⁸, M.L. Harris ¹⁰⁵, Y.T. Harris ¹²⁹, J. Harrison ¹³, N.M. Harrison ¹²², P.F. Harrison ¹⁷⁰, N.M. Hartman ¹¹², N.M. Hartmann ¹¹¹, R.Z. Hasan ^{97,137}, Y. Hasegawa ¹⁴³, S. Hassan ¹⁷, R. Hauser ¹⁰⁹, C.M. Hawkes ²¹, R.J. Hawkings ³⁷, Y. Hayashi ¹⁵⁶, S. Hayashida ¹¹³, D. Hayden ¹⁰⁹, C. Hayes ¹⁰⁸, R.L. Hayes ¹¹⁷, C.P. Hays ¹²⁹, J.M. Hays ⁹⁶, H.S. Hayward ⁹⁴, F. He ^{63a}, M. He ^{14,114c}, Y. He ¹⁵⁷, Y. He ⁴⁹, Y. He ⁹⁸, N.B. Heatley ⁹⁶, V. Hedberg ¹⁰⁰, A.L. Heggelund ¹²⁸, N.D. Hehir ^{96,*}, C. Heidegger ⁵⁵, K.K. Heidegger ⁵⁵, J. Heilman ³⁵, S. Heim ⁴⁹, T. Heim ^{18a}, J.G. Heinlein ¹³¹, J.J. Heinrich ¹²⁶, L. Heinrich ^{112,ab}, J. Hejbal ¹³⁴, A. Held ¹⁷³, S. Hellesund ¹⁷, C.M. Helling ¹⁶⁷, S. Hellman ^{48a,48b}, R.C.W. Henderson ⁹³, L. Henkelmann ³³, A.M. Henriques Correia ³⁷, H. Herde ¹⁰⁰, Y. Hernández Jiménez ¹⁴⁸, L.M. Herrmann ²⁵, T. Herrmann ⁵¹, G. Herten ⁵⁵, R. Hertenberger ¹¹¹, L. Hervas ³⁷, M.E. Hespings ¹⁰², N.P. Hessey ^{159a}, M. Hidaoui ^{36b}, N. Hidic ¹³⁶, E. Hill ¹⁵⁸, S.J. Hillier ²¹, J.R. Hinds ¹⁰⁹, F. Hinterkeuser ²⁵, M. Hirose ¹²⁷, S. Hirose ¹⁶⁰, D. Hirschbuehl ¹⁷⁴, T.G. Hitchings ¹⁰³, B. Hiti ⁹⁵, J. Hobbs ¹⁴⁸, R. Hobincu ^{28e}, N. Hod ¹⁷², M.C. Hodgkinson ¹⁴², B.H. Hodgkinson ¹²⁹, A. Hoecker ³⁷, D.D. Hofer ¹⁰⁸, J. Hofer ⁴⁹, T. Holm ²⁵, M. Holzbock ¹¹², L.B.A.H. Hommels ³³, B.P. Honan ¹⁰³, J.J. Hong ⁶⁹, J. Hong ^{63c}, T.M. Hong ¹³², B.H. Hooberman ¹⁶⁵, W.H. Hopkins ⁶, M.C. Hoppesch ¹⁶⁵, Y. Horii ¹¹³, S. Hou ¹⁵¹, A.S. Howard ⁹⁵, J. Howarth ⁶⁰, J. Hoya ⁶, M. Hrabovsky ¹²⁵, A. Hrynevich ⁴⁹, T. Hryn'ova ⁴, P.J. Hsu ⁶⁶, S.-C. Hsu ¹⁴¹, T. Hsu ⁶⁷, M. Hu ^{18a}, Q. Hu ^{63a}, S. Huang ^{65b}, X. Huang ^{14,114c}, Y. Huang ¹⁴², Y. Huang ¹⁰², Y. Huang ¹⁴, Z. Huang ¹⁰³, Z. Hubacek ¹³⁵, M. Huebner ²⁵, F. Huegging ²⁵, T.B. Huffman ¹²⁹, C.A. Hugli ⁴⁹, M. Huhtinen ³⁷, S.K. Huiberts ¹⁷, R. Hulsken ¹⁰⁶, N. Huseynov ¹², J. Huston ¹⁰⁹, J. Huth ⁶², R. Hyneman ¹⁴⁶, G. Iacobucci ⁵⁷, G. Iakovidis ³⁰, L. Iconomidou-Fayard ⁶⁷, J.P. Iddon ³⁷, P. Iengo ^{73a,73b}, R. Iguchi ¹⁵⁶, Y. Iiyama ¹⁵⁶, T. Iizawa ¹²⁹, Y. Ikegami ⁸⁵, N. Ilic ¹⁵⁸, H. Imam ^{36a}, M. Ince Lezki ⁵⁷, T. Ingebretsen Carlson ^{48a,48b}, J.M. Inglis ⁹⁶, G. Introzzi ^{74a,74b}, M. Iodice ^{78a}, V. Ippolito ^{76a,76b}, R.K. Irwin ⁹⁴, M. Ishino ¹⁵⁶, W. Islam ¹⁷³, C. Issever ^{19,49}, S. Istin ^{22a,ah}, H. Ito ¹⁷¹, R. Iuppa ^{79a,79b}, A. Ivina ¹⁷², J.M. Izen ⁴⁶, V. Izzo ^{73a}, P. Jacka ¹³⁴, P. Jackson ¹, C.S. Jagfeld ¹¹¹, G. Jain ^{159a}, P. Jain ⁴⁹, K. Jakobs ⁵⁵, T. Jakoubek ¹⁷², J. Jamieson ⁶⁰, W. Jang ¹⁵⁶, M. Javurkova ¹⁰⁵, P. Jawahar ¹⁰³, L. Jeanty ¹²⁶, J. Jejelava ^{152a,z}, P. Jenni ^{55,f}, C.E. Jessiman ³⁵, C. Jia ^{63b}, J. Jia ¹⁴⁸, X. Jia ⁶², X. Jia ^{14,114c}, Z. Jia ^{114a}, C. Jiang ⁵³, S. Jiggins ⁴⁹, J. Jimenez Pena ¹³, S. Jin ^{114a}, A. Jinaru ^{28b}, O. Jinnouchi ¹⁵⁷, P. Johansson ¹⁴², K.A. Johns ⁷, J.W. Johnson ¹³⁹, D.M. Jones ¹⁴⁹, E. Jones ⁴⁹, P. Jones ³³, R.W.L. Jones ⁹³, T.J. Jones ⁹⁴, H.L. Joos ^{56,37}, R. Joshi ¹²², J. Jovicevic ¹⁶, X. Ju ^{18a}, J.J. Junggeburth ¹⁰⁵, T. Junkermann ^{64a}, A. Juste Rozas ^{13,s}, M.K. Juzek ⁸⁸, S. Kabana ^{140e}, A. Kaczmarska ⁸⁸, M. Kado ¹¹², H. Kagan ¹²², M. Kagan ¹⁴⁶, A. Kahn ¹³¹, C. Kahra ¹⁰², T. Kaji ¹⁵⁶, E. Kajomovitz ¹⁵³, N. Kakati ¹⁷², I. Kalaitzidou ⁵⁵, C.W. Kalderon ³⁰, N.J. Kang ¹³⁹, D. Kar ^{34g}, K. Karava ¹²⁹, M.J. Kareem ^{159b}, E. Karentzos ⁵⁵, O. Karkout ¹¹⁷, S.N. Karpov ³⁹, Z.M. Karpova ³⁹, V. Kartvelishvili ⁹³, A.N. Karyukhin ³⁸, E. Kasimi ¹⁵⁵, J. Katzy ⁴⁹, S. Kaur ³⁵,

K. Kawade ¹⁴³, M.P. Kawale ¹²³, C. Kawamoto ⁸⁹, T. Kawamoto ^{63a}, E.F. Kay ³⁷, F.I. Kaya ¹⁶¹,
 S. Kazakos ¹⁰⁹, V.F. Kazanin ³⁸, Y. Ke ¹⁴⁸, J.M. Keaveney ^{34a}, R. Keeler ¹⁶⁸, G.V. Kehris ⁶²,
 J.S. Keller ³⁵, A.S. Kelly ⁹⁸, J.J. Kempster ¹⁴⁹, P.D. Kennedy ¹⁰², O. Kepka ¹³⁴, B.P. Kerridge ¹³⁷,
 S. Kersten ¹⁷⁴, B.P. Kerševan ⁹⁵, L. Keszezhova ^{29a}, S. Ketabchi Haghighat ¹⁵⁸, R.A. Khan ¹³²,
 A. Khanov ¹²⁴, A.G. Kharlamov ³⁸, T. Kharlamova ³⁸, E.E. Khoda ¹⁴¹, M. Kholodenko ³⁸,
 T.J. Khoo ¹⁹, G. Khoraiuli ¹⁶⁹, J. Khubua ^{152b,*}, Y.A.R. Khwaira ¹³⁰, B. Kibirige ^{34g}, D. Kim ⁶,
 D.W. Kim ^{48a,48b}, Y.K. Kim ⁴⁰, N. Kimura ⁹⁸, M.K. Kingston ⁵⁶, A. Kirchhoff ⁵⁶, C. Kirfel ²⁵,
 F. Kirfel ²⁵, J. Kirk ¹³⁷, A.E. Kiryunin ¹¹², C. Kitsaki ¹⁰, O. Kivernyk ²⁵, M. Klassen ¹⁶¹,
 C. Klein ³⁵, L. Klein ¹⁶⁹, M.H. Klein ⁴⁵, S.B. Klein ⁵⁷, U. Klein ⁹⁴, P. Klimek ³⁷,
 A. Klimentov ³⁰, T. Klioutchnikova ³⁷, P. Kluit ¹¹⁷, S. Kluth ¹¹², E. Kneringer ⁸⁰,
 T.M. Knight ¹⁵⁸, A. Knue ⁵⁰, R. Kobayashi ⁸⁹, D. Kobylanskii ¹⁷², S.F. Koch ¹²⁹,
 M. Kocian ¹⁴⁶, P. Kodyš ¹³⁶, D.M. Koeck ¹²⁶, P.T. Koenig ²⁵, T. Koffas ³⁵, O. Kolay ⁵¹,
 I. Koletsou ⁴, T. Komarek ⁸⁸, K. Köneke ⁵⁵, A.X.Y. Kong ¹, T. Kono ¹²¹, N. Konstantinidis ⁹⁸,
 P. Kontaxakis ⁵⁷, B. Konya ¹⁰⁰, R. Kopeliansky ⁴², S. Koperny ^{87a}, K. Korcyl ⁸⁸,
 K. Kordas ^{155,d}, A. Korn ⁹⁸, S. Korn ⁵⁶, I. Korolkov ¹³, N. Korotkova ³⁸, B. Kortman ¹¹⁷,
 O. Kortner ¹¹², S. Kortner ¹¹², W.H. Kostecka ¹¹⁸, V.V. Kostyukhin ¹⁴⁴, A. Kotsokechagia ¹³⁸,
 A. Kotwal ⁵², A. Koulouris ³⁷, A. Kourkoumeli-Charalampidi ^{74a,74b}, C. Kourkoumelis ⁹,
 E. Kourlitis ^{112,ab}, O. Kovanda ¹²⁶, R. Kowalewski ¹⁶⁸, W. Kozanecki ¹³⁸, A.S. Kozhin ³⁸,
 V.A. Kramarenko ³⁸, G. Kramberger ⁹⁵, P. Kramer ¹⁰², M.W. Krasny ¹³⁰, A. Krasznahorkay ³⁷,
 A.C. Kraus ¹¹⁸, J.W. Kraus ¹⁷⁴, J.A. Kremer ⁴⁹, T. Kresse ⁵¹, L. Kretschmann ¹⁷⁴,
 J. Kretschmar ⁹⁴, K. Kreul ¹⁹, P. Krieger ¹⁵⁸, S. Krishnamurthy ¹⁰⁵, M. Krivos ¹³⁶,
 K. Krizka ²¹, K. Kroeninger ⁵⁰, H. Kroha ¹¹², J. Kroll ¹³⁴, J. Kroll ¹³¹, K.S. Krowpman ¹⁰⁹,
 U. Kruchonak ³⁹, H. Krüger ²⁵, N. Krumnack ⁸², M.C. Kruse ⁵², O. Kuchinskaja ³⁸, S. Kuday ^{3a},
 S. Kuehn ³⁷, R. Kuesters ⁵⁵, T. Kuhl ⁴⁹, V. Kukhtin ³⁹, Y. Kulchitsky ^{38,a}, S. Kuleshov ^{140d,140b},
 M. Kumar ^{34g}, N. Kumari ⁴⁹, P. Kumari ^{159b}, A. Kupco ¹³⁴, T. Kupfer ⁵⁰, A. Kupich ³⁸,
 O. Kuprash ⁵⁵, H. Kurashige ⁸⁶, L.L. Kurchaninov ^{159a}, O. Kurdysh ⁶⁷, Y.A. Kurochkin ³⁸,
 A. Kurova ³⁸, M. Kuze ¹⁵⁷, A.K. Kvam ¹⁰⁵, J. Kvita ¹²⁵, T. Kwan ¹⁰⁶, N.G. Kyriacou ¹⁰⁸,
 L.A.O. Laatu ¹⁰⁴, C. Lacasta ¹⁶⁶, F. Lacava ^{76a,76b}, H. Lacker ¹⁹, D. Lacour ¹³⁰, N.N. Lad ⁹⁸,
 E. Ladygin ³⁹, A. Lafarge ⁴¹, B. Laforge ¹³⁰, T. Lagouri ¹⁷⁵, F.Z. Lahbabi ^{36a}, S. Lai ⁵⁶,
 J.E. Lambert ¹⁶⁸, S. Lammers ⁶⁹, W. Lampl ⁷, C. Lampoudis ^{155,d}, G. Lamprinoudis ¹⁰²,
 A.N. Lancaster ¹¹⁸, E. Lançon ³⁰, U. Landgraf ⁵⁵, M.P.J. Landon ⁹⁶, V.S. Lang ⁵⁵,
 O.K.B. Langrekken ¹²⁸, A.J. Lankford ¹⁶², F. Lanni ³⁷, K. Lantzsch ²⁵, A. Lanza ^{74a},
 J.F. Laporte ¹³⁸, T. Lari ^{72a}, F. Lasagni Manghi ^{24b}, M. Lassnig ³⁷, V. Latonova ¹³⁴,
 A. Laurier ¹⁵³, S.D. Lawlor ¹⁴², Z. Lawrence ¹⁰³, R. Lazaridou ¹⁷⁰, M. Lazzaroni ^{72a,72b}, B. Le ¹⁰³,
 E.M. Le Boulicaut ⁵², L.T. Le Pottier ^{18a}, B. Leban ^{24b,24a}, A. Lebedev ⁸², M. LeBlanc ¹⁰³,
 F. Ledroit-Guillon ⁶¹, S.C. Lee ¹⁵¹, S. Lee ^{48a,48b}, T.F. Lee ⁹⁴, L.L. Leeuw ^{34c}, H.P. Lefebvre ⁹⁷,
 M. Lefebvre ¹⁶⁸, C. Leggett ^{18a}, G. Lehmann Miotto ³⁷, M. Leigh ⁵⁷, W.A. Leight ¹⁰⁵,
 W. Leinonen ¹¹⁶, A. Leisos ^{155,r}, M.A.L. Leite ^{84c}, C.E. Leitgeb ¹⁹, R. Leitner ¹³⁶,
 K.J.C. Leney ⁴⁵, T. Lenz ²⁵, S. Leone ^{75a}, C. Leonidopoulos ⁵³, A. Leopold ¹⁴⁷, R. Les ¹⁰⁹,
 C.G. Lester ³³, M. Levchenko ³⁸, J. Levêque ⁴, L.J. Levinson ¹⁷², G. Levrini ^{24b,24a},
 M.P. Lewicki ⁸⁸, C. Lewis ¹⁴¹, D.J. Lewis ⁴, A. Li ⁵, B. Li ^{63b}, C. Li ^{63a}, C-Q. Li ¹¹², H. Li ^{63a},
 H. Li ^{63b}, H. Li ^{114a}, H. Li ¹⁵, H. Li ^{63b}, J. Li ^{63c}, K. Li ¹⁴¹, L. Li ^{63c}, M. Li ^{14,114c},
 S. Li ^{14,114c}, S. Li ^{63d,63c}, T. Li ⁵, X. Li ¹⁰⁶, Z. Li ¹²⁹, Z. Li ¹⁵⁶, Z. Li ^{14,114c}, S. Liang ^{14,114c},
 Z. Liang ¹⁴, M. Liberatore ¹³⁸, B. Liberti ^{77a}, K. Lie ^{65c}, J. Lieber Marin ^{84e}, H. Lien ⁶⁹,
 H. Lin ¹⁰⁸, K. Lin ¹⁰⁹, R.E. Lindley ⁷, J.H. Lindon ², J. Ling ⁶², E. Lipeles ¹³¹,
 A. Lipniacka ¹⁷, A. Lister ¹⁶⁷, J.D. Little ⁶⁹, B. Liu ¹⁴, B.X. Liu ^{114b}, D. Liu ^{63d,63c},
 E.H.L. Liu ²¹, J.B. Liu ^{63a}, J.K.K. Liu ³³, K. Liu ^{63d}, K. Liu ^{63d,63c}, M. Liu ^{63a}, M.Y. Liu ^{63a},







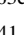

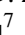




P. Liu ¹⁴, Q. Liu ^{63d,141,63c}, X. Liu ^{63a}, X. Liu ^{63b}, Y. Liu ^{114b,114c}, Y.L. Liu ^{63b}, Y.W. Liu ^{63a},
 J. Llorente Merino ¹⁴⁵, S.L. Lloyd ⁹⁶, E.M. Lobodzinska ⁴⁹, P. Loch ⁷, T. Lohse ¹⁹,
 K. Lohwasser ¹⁴², E. Loiacono ⁴⁹, M. Lokajicek ^{134,*}, J.D. Lomas ²¹, J.D. Long ¹⁶⁵,
 I. Longarini ¹⁶², R. Longo ¹⁶⁵, I. Lopez Paz ⁶⁸, A. Lopez Solis ⁴⁹, N. Lorenzo Martinez ⁴,
 A.M. Lory ¹¹¹, M. Losada ^{119a}, G. Löschke Centeno ¹⁴⁹, O. Loseva ³⁸, X. Lou ^{48a,48b},
 X. Lou ^{14,114c}, A. Lounis ⁶⁷, P.A. Love ⁹³, G. Lu ^{14,114c}, M. Lu ⁶⁷, S. Lu ¹³¹, Y.J. Lu ⁶⁶,
 H.J. Lubatti ¹⁴¹, C. Luci ^{76a,76b}, F.L. Lucio Alves ^{114a}, F. Luehring ⁶⁹, I. Luise ¹⁴⁸,
 O. Lukianchuk ⁶⁷, O. Lundberg ¹⁴⁷, B. Lund-Jensen ^{147,*}, N.A. Luongo ⁶, M.S. Lutz ³⁷,
 A.B. Lux ²⁶, D. Lynn ³⁰, R. Lysak ¹³⁴, E. Lytken ¹⁰⁰, V. Lyubushkin ³⁹, T. Lyubushkina ³⁹,
 M.M. Lyukova ¹⁴⁸, M.Firdaus M. Soberi ⁵³, H. Ma ³⁰, K. Ma ^{63a}, L.L. Ma ^{63b}, W. Ma ^{63a},
 Y. Ma ¹²⁴, J.C. MacDonald ¹⁰², P.C. Machado De Abreu Farias ^{84e}, R. Madar ⁴¹, T. Madula ⁹⁸,
 J. Maeda ⁸⁶, T. Maeno ³⁰, H. Maguire ¹⁴², V. Maiboroda ¹³⁸, A. Maio ^{133a,133b,133d}, K. Maj ^{87a},
 O. Majersky ⁴⁹, S. Majewski ¹²⁶, N. Makovec ⁶⁷, V. Maksimovic ¹⁶, B. Malaescu ¹³⁰,
 Pa. Malecki ⁸⁸, V.P. Maleev ³⁸, F. Malek ^{61,m}, M. Mali ⁹⁵, D. Malito ⁹⁷, U. Mallik ^{81,*},
 S. Maltezos ¹⁰, S. Malyukov ³⁹, J. Mamuzic ¹³, G. Mancini ⁵⁴, M.N. Mancini ²⁷, G. Manco ^{74a,74b},
 J.P. Mandalia ⁹⁶, S.S. Mandarry ¹⁴⁹, I. Mandić ⁹⁵, L. Manhaes de Andrade Filho ^{84a},
 I.M. Maniatis ¹⁷², J. Manjarres Ramos ⁹¹, D.C. Mankad ¹⁷², A. Mann ¹¹¹, S. Manzoni ³⁷,
 L. Mao ^{63c}, X. Mapekula ^{34c}, A. Marantis ^{155,r}, G. Marchiori ⁵, M. Marcisovsky ¹³⁴,
 C. Marcon ^{72a}, M. Marinescu ²¹, S. Marium ⁴⁹, M. Marjanovic ¹²³, A. Markhoos ⁵⁵,
 M. Markovitch ⁶⁷, E.J. Marshall ⁹³, Z. Marshall ^{18a}, S. Marti-Garcia ¹⁶⁶, J. Martin ⁹⁸,
 T.A. Martin ¹³⁷, V.J. Martin ⁵³, B. Martin dit Latour ¹⁷, L. Martinelli ^{76a,76b}, M. Martinez ^{13,s},
 P. Martinez Agullo ¹⁶⁶, V.I. Martinez Outschoorn ¹⁰⁵, P. Martinez Suarez ¹³, S. Martin-Haugh ¹³⁷,
 G. Martinovicova ¹³⁶, V.S. Martoiu ^{28b}, A.C. Martyniuk ⁹⁸, A. Marzin ³⁷, D. Mascione ^{79a,79b},
 L. Masetti ¹⁰², T. Mashimo ¹⁵⁶, J. Masik ¹⁰³, A.L. Maslennikov ³⁸, P. Massarotti ^{73a,73b},
 P. Mastrandrea ^{75a,75b}, A. Mastroberardino ^{44b,44a}, T. Masubuchi ¹⁵⁶, T. Mathisen ¹⁶⁴,
 J. Matousek ¹³⁶, N. Matsuzawa ¹⁵⁶, J. Maurer ^{28b}, A.J. Maury ⁶⁷, B. Maček ⁹⁵, D.A. Maximov ³⁸,
 A.E. May ¹⁰³, R. Mazini ¹⁵¹, I. Maznas ¹¹⁸, M. Mazza ¹⁰⁹, S.M. Mazza ¹³⁹, E. Mazzeo ^{72a,72b},
 C. Mc Ginn ³⁰, J.P. Mc Gowan ¹⁶⁸, S.P. Mc Kee ¹⁰⁸, C.C. McCracken ¹⁶⁷, E.F. McDonald ¹⁰⁷,
 A.E. McDougall ¹¹⁷, J.A. Mcfayden ¹⁴⁹, R.P. McGovern ¹³¹, R.P. Mckenzie ^{34g},
 T.C. McLachlan ⁴⁹, D.J. McLaughlin ⁹⁸, S.J. McMahon ¹³⁷, C.M. Mcpartland ⁹⁴,
 R.A. McPherson ^{168,w}, S. Mehlhase ¹¹¹, A. Mehta ⁹⁴, D. Melini ¹⁶⁶, B.R. Mellado Garcia ^{34g},
 A.H. Melo ⁵⁶, F. Meloni ⁴⁹, A.M. Mendes Jacques Da Costa ¹⁰³, H.Y. Meng ¹⁵⁸, L. Meng ⁹³,
 S. Menke ¹¹², M. Mentink ³⁷, E. Meoni ^{44b,44a}, G. Mercado ¹¹⁸, S. Merianos ¹⁵⁵,
 C. Merlassino ^{70a,70c}, L. Merola ^{73a,73b}, C. Meroni ^{72a,72b}, J. Metcalfe ⁶, A.S. Mete ⁶,
 E. Meuser ¹⁰², C. Meyer ⁶⁹, J-P. Meyer ¹³⁸, R.P. Middleton ¹³⁷, L. Mijović ⁵³,
 G. Mikenberg ¹⁷², M. Mikesikova ¹³⁴, M. Mikuž ⁹⁵, H. Mildner ¹⁰², A. Milic ³⁷,
 D.W. Miller ⁴⁰, E.H. Miller ¹⁴⁶, L.S. Miller ³⁵, A. Milov ¹⁷², D.A. Milstead ^{48a,48b}, T. Min ^{114a},
 A.A. Minaenko ³⁸, I.A. Minashvili ^{152b}, L. Mince ⁶⁰, A.I. Mincer ¹²⁰, B. Mindur ^{87a},
 M. Mineev ³⁹, Y. Mino ⁸⁹, L.M. Mir ¹³, M. Miralles Lopez ⁶⁰, M. Mironova ^{18a}, A. Mishima ¹⁵⁶,
 M.C. Missio ¹¹⁶, A. Mitra ¹⁷⁰, V.A. Mitsou ¹⁶⁶, Y. Mitsumori ¹¹³, O. Miu ¹⁵⁸,
 P.S. Miyagawa ⁹⁶, T. Mkrtchyan ^{64a}, M. Mlinarevic ⁹⁸, T. Mlinarevic ⁹⁸, M. Mlynarikova ³⁷,
 S. Mobius ²⁰, P. Mogg ¹¹¹, M.H. Mohamed Farook ¹¹⁵, A.F. Mohammed ^{14,114c}, S. Mohapatra ⁴²,
 G. Mokgatitwane ^{34g}, L. Moleri ¹⁷², B. Mondal ¹⁴⁴, S. Mondal ¹³⁵, K. Mönig ⁴⁹,
 E. Monnier ¹⁰⁴, L. Monsonis Romero ¹⁶⁶, J. Montejo Berlingen ¹³, M. Montella ¹²²,
 F. Montekali ^{78a,78b}, F. Monticelli ⁹², S. Monzani ^{70a,70c}, N. Morange ⁶⁷,
 A.L. Moreira De Carvalho ⁴⁹, M. Moreno Llácer ¹⁶⁶, C. Moreno Martinez ⁵⁷, P. Morettini ^{58b},
 S. Morgenstern ³⁷, M. Morii ⁶², M. Morinaga ¹⁵⁶, F. Morodei ^{76a,76b}, L. Morvaj ³⁷,

P. Moschovakos [ID³⁷](#), B. Moser [ID³⁷](#), M. Mosidze [ID^{152b}](#), T. Moskalets [ID⁴⁵](#), P. Moskvitina [ID¹¹⁶](#),
 J. Moss [ID^{32j}](#), P. Moszkowicz [ID^{87a}](#), A. Moussa [ID^{36d}](#), E.J.W. Moyse [ID¹⁰⁵](#), O. Mtintsilana [ID^{34g}](#),
 S. Muanza [ID¹⁰⁴](#), J. Mueller [ID¹³²](#), D. Muenstermann [ID⁹³](#), R. Müller [ID³⁷](#), G.A. Mullier [ID¹⁶⁴](#),
 A.J. Mullin [ID³³](#), J.J. Mullin [ID¹³¹](#), D.P. Mungo [ID¹⁵⁸](#), D. Munoz Perez [ID¹⁶⁶](#), F.J. Munoz Sanchez [ID¹⁰³](#),
 M. Murin [ID¹⁰³](#), W.J. Murray [ID^{170,137}](#), M. Muškinja [ID⁹⁵](#), C. Mwewa [ID³⁰](#), A.G. Myagkov [ID^{38,a}](#),
 A.J. Myers [ID⁸](#), G. Myers [ID¹⁰⁸](#), M. Myska [ID¹³⁵](#), B.P. Nachman [ID^{18a}](#), O. Nackenhorst [ID⁵⁰](#), K. Nagai [ID¹²⁹](#),
 K. Nagano [ID⁸⁵](#), J.L. Nagle [ID^{30,af}](#), E. Nagy [ID¹⁰⁴](#), A.M. Nairz [ID³⁷](#), Y. Nakahama [ID⁸⁵](#), K. Nakamura [ID⁸⁵](#),
 K. Nakkalil [ID⁵](#), H. Nanjo [ID¹²⁷](#), E.A. Narayanan [ID¹¹⁵](#), I. Naryshkin [ID³⁸](#), L. Nasella [ID^{72a,72b}](#),
 M. Naseri [ID³⁵](#), S. Nasri [ID^{119b}](#), C. Nass [ID²⁵](#), G. Navarro [ID^{23a}](#), J. Navarro-Gonzalez [ID¹⁶⁶](#), R. Nayak [ID¹⁵⁴](#),
 A. Nayaz [ID¹⁹](#), P.Y. Nechaeva [ID³⁸](#), S. Nechaeva [ID^{24b,24a}](#), F. Nechansky [ID⁴⁹](#), L. Nedic [ID¹²⁹](#), T.J. Neep [ID²¹](#),
 A. Negri [ID^{74a,74b}](#), M. Negrini [ID^{24b}](#), C. Nellist [ID¹¹⁷](#), C. Nelson [ID¹⁰⁶](#), K. Nelson [ID¹⁰⁸](#), S. Nemecek [ID¹³⁴](#),
 M. Nessi [ID^{37,g}](#), M.S. Neubauer [ID¹⁶⁵](#), F. Neuhaus [ID¹⁰²](#), J. Neundorf [ID⁴⁹](#), P.R. Newman [ID²¹](#),
 C.W. Ng [ID¹³²](#), Y.W.Y. Ng [ID⁴⁹](#), B. Ngair [ID^{119a}](#), H.D.N. Nguyen [ID¹¹⁰](#), R.B. Nickerson [ID¹²⁹](#),
 R. Nicolaidou [ID¹³⁸](#), J. Nielsen [ID¹³⁹](#), M. Niemeyer [ID⁵⁶](#), J. Niermann [ID⁵⁶](#), N. Nikiforou [ID³⁷](#),
 V. Nikolaenko [ID^{38,a}](#), I. Nikolic-Audit [ID¹³⁰](#), K. Nikolopoulos [ID²¹](#), P. Nilsson [ID³⁰](#), I. Ninca [ID⁴⁹](#),
 G. Ninio [ID¹⁵⁴](#), A. Nisati [ID^{76a}](#), N. Nishu [ID²](#), R. Nisius [ID¹¹²](#), J-E. Nitschke [ID⁵¹](#), E.K. Nkadimeng [ID^{34g}](#),
 T. Nobe [ID¹⁵⁶](#), T. Nommensen [ID¹⁵⁰](#), M.B. Norfolk [ID¹⁴²](#), B.J. Norman [ID³⁵](#), M. Noury [ID^{36a}](#), J. Novak [ID⁹⁵](#),
 T. Novak [ID⁹⁵](#), L. Novotny [ID¹³⁵](#), R. Novotny [ID¹¹⁵](#), L. Nozka [ID¹²⁵](#), K. Ntekas [ID¹⁶²](#),
 N.M.J. Nunes De Moura Junior [ID^{84b}](#), J. Ocariz [ID¹³⁰](#), A. Ochi [ID⁸⁶](#), I. Ochoa [ID^{133a}](#), S. Oerdek [ID^{49,t}](#),
 J.T. Offermann [ID⁴⁰](#), A. Ogrodnik [ID¹³⁶](#), A. Oh [ID¹⁰³](#), C.C. Ohm [ID¹⁴⁷](#), H. Oide [ID⁸⁵](#), R. Oishi [ID¹⁵⁶](#),
 M.L. Ojeda [ID⁴⁹](#), Y. Okumura [ID¹⁵⁶](#), L.F. Oleiro Seabra [ID^{133a}](#), I. Oleksiyuk [ID⁵⁷](#), S.A. Olivares Pino [ID^{140d}](#),
 G. Oliveira Correa [ID¹³](#), D. Oliveira Damazio [ID³⁰](#), D. Oliveira Goncalves [ID^{84a}](#), J.L. Oliver [ID¹⁶²](#),
 Ö.O. Öncel [ID⁵⁵](#), A.P. O'Neill [ID²⁰](#), A. Onofre [ID^{133a,133e}](#), P.U.E. Onyisi [ID¹¹](#), M.J. Oreglia [ID⁴⁰](#),
 G.E. Orellana [ID⁹²](#), D. Orestano [ID^{78a,78b}](#), N. Orlando [ID¹³](#), R.S. Orr [ID¹⁵⁸](#), L.M. Osojnak [ID¹³¹](#),
 R. Ospanov [ID^{63a}](#), G. Otero y Garzon [ID³¹](#), H. Otono [ID⁹⁰](#), P.S. Ott [ID^{64a}](#), G.J. Ottino [ID^{18a}](#), M. Ouchrif [ID^{36d}](#),
 F. Ould-Saada [ID¹²⁸](#), T. Ovsiannikova [ID¹⁴¹](#), M. Owen [ID⁶⁰](#), R.E. Owen [ID¹³⁷](#), V.E. Ozcan [ID^{22a}](#),
 F. Ozturk [ID⁸⁸](#), N. Ozturk [ID⁸](#), S. Ozturk [ID⁸³](#), H.A. Pacey [ID¹²⁹](#), A. Pacheco Pages [ID¹³](#),
 C. Padilla Aranda [ID¹³](#), G. Padovano [ID^{76a,76b}](#), S. Pagan Griso [ID^{18a}](#), G. Palacino [ID⁶⁹](#), A. Palazzo [ID^{71a,71b}](#),
 J. Pampel [ID²⁵](#), J. Pan [ID¹⁷⁵](#), T. Pan [ID^{65a}](#), D.K. Panchal [ID¹¹](#), C.E. Pandini [ID¹¹⁷](#), J.G. Panduro Vazquez [ID¹³⁷](#),
 H.D. Pandya [ID¹](#), H. Pang [ID¹⁵](#), P. Pani [ID⁴⁹](#), G. Panizzo [ID^{70a,70c}](#), L. Panwar [ID¹³⁰](#), L. Paolozzi [ID⁵⁷](#),
 S. Parajuli [ID¹⁶⁵](#), A. Paramonov [ID⁶](#), C. Paraskevopoulos [ID⁵⁴](#), D. Paredes Hernandez [ID^{65b}](#),
 A. Pareti [ID^{74a,74b}](#), K.R. Park [ID⁴²](#), T.H. Park [ID¹⁵⁸](#), M.A. Parker [ID³³](#), F. Parodi [ID^{58b,58a}](#), E.W. Parrish [ID¹¹⁸](#),
 V.A. Parrish [ID⁵³](#), J.A. Parsons [ID⁴²](#), U. Parzefall [ID⁵⁵](#), B. Pascual Dias [ID¹¹⁰](#), L. Pascual Dominguez [ID¹⁰¹](#),
 E. Pasqualucci [ID^{76a}](#), S. Passaggio [ID^{58b}](#), F. Pastore [ID⁹⁷](#), P. Patel [ID⁸⁸](#), U.M. Patel [ID⁵²](#), J.R. Pater [ID¹⁰³](#),
 T. Pauly [ID³⁷](#), C.I. Pazos [ID¹⁶¹](#), J. Pearkes [ID¹⁴⁶](#), M. Pedersen [ID¹²⁸](#), R. Pedro [ID^{133a}](#), S.V. Peleganchuk [ID³⁸](#),
 O. Penc [ID³⁷](#), E.A. Pender [ID⁵³](#), G.D. Penn [ID¹⁷⁵](#), K.E. Penski [ID¹¹¹](#), M. Penzin [ID³⁸](#), B.S. Peralva [ID^{84d}](#),
 A.P. Pereira Peixoto [ID¹⁴¹](#), L. Pereira Sanchez [ID¹⁴⁶](#), D.V. Perepelitsa [ID^{30,af}](#), G. Perera [ID¹⁰⁵](#),
 E. Perez Codina [ID^{159a}](#), M. Perganti [ID¹⁰](#), H. Pernegger [ID³⁷](#), S. Perrella [ID^{76a,76b}](#), O. Perrin [ID⁴¹](#),
 K. Peters [ID⁴⁹](#), R.F.Y. Peters [ID¹⁰³](#), B.A. Petersen [ID³⁷](#), T.C. Petersen [ID⁴³](#), E. Petit [ID¹⁰⁴](#), V. Petousis [ID¹³⁵](#),
 C. Petridou [ID^{155,d}](#), T. Petru [ID¹³⁶](#), A. Petrukhin [ID¹⁴⁴](#), M. Pettee [ID^{18a}](#), A. Petukhov [ID³⁸](#), K. Petukhova [ID³⁷](#),
 R. Pezoa [ID^{140f}](#), L. Pezzotti [ID³⁷](#), G. Pezzullo [ID¹⁷⁵](#), T.M. Pham [ID¹⁷³](#), T. Pham [ID¹⁰⁷](#), P.W. Phillips [ID¹³⁷](#),
 G. Piacquadio [ID¹⁴⁸](#), E. Pianori [ID^{18a}](#), F. Piazza [ID¹²⁶](#), R. Piegai [ID³¹](#), D. Pietreanu [ID^{28b}](#),
 A.D. Pilkington [ID¹⁰³](#), M. Pinamonti [ID^{70a,70c}](#), J.L. Pinfeld [ID²](#), B.C. Pinheiro Pereira [ID^{133a}](#),
 A.E. Pinto Pinoargote [ID^{138,138}](#), L. Pintucci [ID^{70a,70c}](#), K.M. Piper [ID¹⁴⁹](#), A. Pirttikoski [ID⁵⁷](#), D.A. Pizzi [ID³⁵](#),
 L. Pizzimento [ID^{65b}](#), A. Pizzini [ID¹¹⁷](#), M.-A. Pleier [ID³⁰](#), V. Pleskot [ID¹³⁶](#), E. Plotnikova [ID³⁹](#), G. Poddar [ID⁹⁶](#),
 R. Poettgen [ID¹⁰⁰](#), L. Poggioli [ID¹³⁰](#), I. Pokharel [ID⁵⁶](#), S. Polacek [ID¹³⁶](#), G. Polesello [ID^{74a}](#),
 A. Poley [ID^{145,159a}](#), A. Polini [ID^{24b}](#), C.S. Pollard [ID¹⁷⁰](#), Z.B. Pollock [ID¹²²](#), E. Pompa Pacchi [ID^{76a,76b}](#),

N.I. Pond ⁹⁸, D. Ponomarenko ¹¹⁶, L. Pontecorvo ³⁷, S. Popa ^{28a}, G.A. Popeneciu ^{28d},
 A. Poreba ³⁷, D.M. Portillo Quintero ^{159a}, S. Pospisil ¹³⁵, M.A. Postill ¹⁴², P. Postolache ^{28c},
 K. Potamianos ¹⁷⁰, P.A. Potepa ^{87a}, I.N. Potrap ³⁹, C.J. Potter ³³, H. Potti ¹⁵⁰, J. Poveda ¹⁶⁶,
 M.E. Pozo Astigarraga ³⁷, A. Prades Ibanez ¹⁶⁶, J. Pretel ⁵⁵, D. Price ¹⁰³, M. Primavera ^{71a},
 M.A. Principe Martin ¹⁰¹, R. Privara ¹²⁵, T. Procter ⁶⁰, M.L. Proffitt ¹⁴¹, N. Proklova ¹³¹,
 K. Prokofiev ^{65c}, G. Proto ¹¹², J. Proudfoot ⁶, M. Przybycien ^{87a}, W.W. Przygoda ^{87b},
 A. Psallidas ⁴⁷, J.E. Puddefoot ¹⁴², D. Pudzha ⁵⁵, D. Pyatiizbyantseva ³⁸, J. Qian ¹⁰⁸,
 D. Qichen ¹⁰³, Y. Qin ¹³, T. Qiu ⁵³, A. Quadt ⁵⁶, M. Queitsch-Maitland ¹⁰³, G. Quetant ⁵⁷,
 R.P. Quinn ¹⁶⁷, G. Rabanal Bolanos ⁶², D. Rafanoharana ⁵⁵, F. Raffaelli ^{77a,77b}, F. Ragusa ^{72a,72b},
 J.L. Rainbolt ⁴⁰, J.A. Raine ⁵⁷, S. Rajagopalan ³⁰, E. Ramakoti ³⁸, I.A. Ramirez-Berend ³⁵,
 K. Ran ^{49,114c}, N.P. Rapheeha ^{34g}, H. Rasheed ^{28b}, V. Raskina ¹³⁰, D.F. Rassloff ^{64a},
 A. Rastogi ^{18a}, S. Rave ¹⁰², S. Ravera ^{58b,58a}, B. Ravina ⁵⁶, I. Ravinovich ¹⁷², M. Raymond ³⁷,
 A.L. Read ¹²⁸, N.P. Readioff ¹⁴², D.M. Rebuzzi ^{74a,74b}, G. Redlinger ³⁰, A.S. Reed ¹¹²,
 K. Reeves ²⁷, J.A. Reidelsturz ¹⁷⁴, D. Reikher ¹⁵⁴, A. Rej ⁵⁰, C. Rembser ³⁷, M. Renda ^{28b},
 F. Renner ⁴⁹, A.G. Rennie ¹⁶², A.L. Rescia ⁴⁹, S. Resconi ^{72a}, M. Ressegotti ^{58b,58a}, S. Rettie ³⁷,
 J.G. Reyes Rivera ¹⁰⁹, E. Reynolds ^{18a}, O.L. Rezanova ³⁸, P. Reznicek ¹³⁶, H. Riani ^{36d},
 N. Ribaric ⁹³, E. Ricci ^{79a,79b}, R. Richter ¹¹², S. Richter ^{48a,48b}, E. Richter-Was ^{87b},
 M. Ridel ¹³⁰, S. Ridouani ^{36d}, P. Rieck ¹²⁰, P. Riedler ³⁷, E.M. Riefel ^{48a,48b}, J.O. Rieger ¹¹⁷,
 M. Rijssenbeek ¹⁴⁸, M. Rimoldi ³⁷, L. Rinaldi ^{24b,24a}, P. Rincke ^{56,164}, T.T. Rinn ³⁰,
 M.P. Rinnagel ¹¹¹, G. Ripellino ¹⁶⁴, I. Riu ¹³, J.C. Rivera Vergara ¹⁶⁸, F. Rizatdinova ¹²⁴,
 E. Rizvi ⁹⁶, B.R. Roberts ^{18a}, S.H. Robertson ^{106,w}, D. Robinson ³³, C.M. Robles Gajardo ^{140f},
 M. Robles Manzano ¹⁰², A. Robson ⁶⁰, A. Rocchi ^{77a,77b}, C. Roda ^{75a,75b}, S. Rodriguez Bosca ³⁷,
 Y. Rodriguez Garcia ^{23a}, A. Rodriguez Rodriguez ⁵⁵, A.M. Rodríguez Vera ¹¹⁸, S. Roe ³⁷,
 J.T. Roemer ³⁷, A.R. Roepe-Gier ¹³⁹, O. Røhne ¹²⁸, R.A. Rojas ¹⁰⁵, C.P.A. Roland ¹³⁰,
 J. Roloff ³⁰, A. Romaniouk ³⁸, E. Romano ^{74a,74b}, M. Romano ^{24b}, A.C. Romero Hernandez ¹⁶⁵,
 N. Rompotis ⁹⁴, L. Roos ¹³⁰, S. Rosati ^{76a}, B.J. Rosser ⁴⁰, E. Rossi ¹²⁹, E. Rossi ^{73a,73b},
 L.P. Rossi ⁶², L. Rossini ⁵⁵, R. Rosten ¹²², M. Rotaru ^{28b}, B. Rottler ⁵⁵, C. Rougier ⁹¹,
 D. Rousseau ⁶⁷, D. Rousso ⁴⁹, A. Roy ¹⁶⁵, S. Roy-Garand ¹⁵⁸, A. Rozanov ¹⁰⁴,
 Z.M.A. Rozario ⁶⁰, Y. Rozen ¹⁵³, A. Rubio Jimenez ¹⁶⁶, A.J. Ruby ⁹⁴, V.H. Ruelas Rivera ¹⁹,
 T.A. Ruggeri ¹, A. Ruggiero ¹²⁹, A. Ruiz-Martinez ¹⁶⁶, A. Rummler ³⁷, Z. Rurikova ⁵⁵,
 N.A. Rusakovich ³⁹, H.L. Russell ¹⁶⁸, G. Russo ^{76a,76b}, J.P. Rutherford ⁷,
 S. Rutherford Colmenares ³³, M. Rybar ¹³⁶, E.B. Rye ¹²⁸, A. Ryzhov ⁴⁵, J.A. Sabater Iglesias ⁵⁷,
 P. Sabatini ¹⁶⁶, H.F-W. Sadrozinski ¹³⁹, F. Safai Tehrani ^{76a}, B. Safarzadeh Samani ¹³⁷, S. Saha ¹,
 M. Sahinsoy ¹¹², A. Saibel ¹⁶⁶, M. Saimpert ¹³⁸, M. Saito ¹⁵⁶, T. Saito ¹⁵⁶, A. Sala ^{72a,72b},
 D. Salamani ³⁷, A. Salnikov ¹⁴⁶, J. Salt ¹⁶⁶, A. Salvador Salas ¹⁵⁴, D. Salvatore ^{44b,44a},
 F. Salvatore ¹⁴⁹, A. Salzburger ³⁷, D. Sammel ⁵⁵, E. Sampson ⁹³, D. Sampsonidis ^{155,d},
 D. Sampsonidou ¹²⁶, J. Sánchez ¹⁶⁶, V. Sanchez Sebastian ¹⁶⁶, H. Sandaker ¹²⁸, C.O. Sander ⁴⁹,
 J.A. Sandesara ¹⁰⁵, M. Sandhoff ¹⁷⁴, C. Sandoval ^{23b}, L. Sanfilippo ^{64a}, D.P.C. Sankey ¹³⁷,
 T. Sano ⁸⁹, A. Sansoni ⁵⁴, L. Santi ^{37,76b}, C. Santoni ⁴¹, H. Santos ^{133a,133b}, A. Santra ¹⁷²,
 E. Sanzani ^{24b,24a}, K.A. Saoucha ¹⁶³, J.G. Saraiva ^{133a,133d}, J. Sardain ⁷, O. Sasaki ⁸⁵,
 K. Sato ¹⁶⁰, C. Sauer ^{64b}, E. Sauvan ⁴, P. Savard ^{158,ad}, R. Sawada ¹⁵⁶, C. Sawyer ¹³⁷,
 L. Sawyer ⁹⁹, C. Sbarra ^{24b}, A. Sbrizzi ^{24b,24a}, T. Scanlon ⁹⁸, J. Schaarschmidt ¹⁴¹,
 U. Schäfer ¹⁰², A.C. Schaffer ^{67,45}, D. Schaile ¹¹¹, R.D. Schamberger ¹⁴⁸, C. Scharf ¹⁹,
 M.M. Schefer ²⁰, V.A. Schegelsky ³⁸, D. Scheirich ¹³⁶, M. Schernau ¹⁶², C. Scheulen ⁵⁶,
 C. Schiavi ^{58b,58a}, M. Schioppa ^{44b,44a}, B. Schlag ^{146,1}, K.E. Schleicher ⁵⁵, S. Schlenker ³⁷,
 J. Schmeing ¹⁷⁴, M.A. Schmidt ¹⁷⁴, K. Schmieden ¹⁰², C. Schmitt ¹⁰², N. Schmitt ¹⁰²,
 S. Schmitt ⁴⁹, L. Schoeffel ¹³⁸, A. Schoening ^{64b}, P.G. Scholer ³⁵, E. Schopf ¹²⁹, M. Schott ²⁵,

J. Schovancova ³⁷, S. Schramm ⁵⁷, T. Schroer ⁵⁷, H-C. Schultz-Coulon ^{64a}, M. Schumacher ⁵⁵, B.A. Schumm ¹³⁹, Ph. Schune ¹³⁸, A.J. Schuy ¹⁴¹, H.R. Schwartz ¹³⁹, A. Schwartzman ¹⁴⁶, T.A. Schwarz ¹⁰⁸, Ph. Schwemling ¹³⁸, R. Schwienhorst ¹⁰⁹, F.G. Sciacca ²⁰, A. Sciandra ³⁰, G. Sciolla ²⁷, F. Scuri ^{75a}, C.D. Sebastiani ⁹⁴, K. Sedlaczek ¹¹⁸, S.C. Seidel ¹¹⁵, A. Seiden ¹³⁹, B.D. Seidlitz ⁴², C. Seitz ⁴⁹, J.M. Seixas ^{84b}, G. Sekhniaidze ^{73a}, L. Selem ⁶¹, N. Semprini-Cesari ^{24b,24a}, D. Sengupta ⁵⁷, V. Senthilkumar ¹⁶⁶, L. Serin ⁶⁷, M. Sessa ^{77a,77b}, H. Severini ¹²³, F. Sforza ^{58b,58a}, A. Sfyrta ⁵⁷, Q. Sha ¹⁴, E. Shabalina ⁵⁶, A.H. Shah ³³, R. Shaheen ¹⁴⁷, J.D. Shahinian ¹³¹, D. Shaked Renous ¹⁷², L.Y. Shan ¹⁴, M. Shapiro ^{18a}, A. Sharma ³⁷, A.S. Sharma ¹⁶⁷, P. Sharma ⁸¹, P.B. Shatalov ³⁸, K. Shaw ¹⁴⁹, S.M. Shaw ¹⁰³, Q. Shen ^{63c}, D.J. Sheppard ¹⁴⁵, P. Sherwood ⁹⁸, L. Shi ⁹⁸, X. Shi ¹⁴, C.O. Shimmin ¹⁷⁵, J.D. Shinner ⁹⁷, I.P.J. Shipsey ¹²⁹, S. Shirabe ⁹⁰, M. Shiyakova ^{39,u}, M.J. Shochet ⁴⁰, J. Shojaii ¹⁰⁷, D.R. Shope ¹²⁸, B. Shrestha ¹²³, S. Shrestha ^{122,ag}, M.J. Shroff ¹⁶⁸, P. Sicho ¹³⁴, A.M. Sickles ¹⁶⁵, E. Sideras Haddad ^{34g}, A.C. Sidley ¹¹⁷, A. Sidoti ^{24b}, F. Siegert ⁵¹, Dj. Sijacki ¹⁶, F. Sili ⁹², J.M. Silva ⁵³, I. Silva Ferreira ^{84b}, M.V. Silva Oliveira ³⁰, S.B. Silverstein ^{48a}, S. Simion ⁶⁷, R. Simoniello ³⁷, E.L. Simpson ¹⁰³, H. Simpson ¹⁴⁹, L.R. Simpson ¹⁰⁸, N.D. Simpson ¹⁰⁰, S. Simsek ⁸³, S. Sindhu ⁵⁶, P. Sinervo ¹⁵⁸, S. Singh ¹⁵⁸, S. Sinha ⁴⁹, S. Sinha ¹⁰³, M. Sioli ^{24b,24a}, I. Siral ³⁷, E. Sitnikova ⁴⁹, J. Sjölin ^{48a,48b}, A. Skaf ⁵⁶, E. Skorda ²¹, P. Skubic ¹²³, M. Slawinska ⁸⁸, V. Smakhtin ¹⁷², B.H. Smart ¹³⁷, S.Yu. Smirnov ³⁸, Y. Smirnov ³⁸, L.N. Smirnova ^{38,a}, O. Smirnova ¹⁰⁰, A.C. Smith ⁴², D.R. Smith ¹⁶², E.A. Smith ⁴⁰, H.A. Smith ¹²⁹, J.L. Smith ¹⁰³, R. Smith ¹⁴⁶, M. Smizanska ⁹³, K. Smolek ¹³⁵, A.A. Snesarev ³⁸, S.R. Snider ¹⁵⁸, H.L. Snoek ¹¹⁷, S. Snyder ³⁰, R. Sobie ^{168,w}, A. Soffer ¹⁵⁴, C.A. Solans Sanchez ³⁷, E.Yu. Soldatov ³⁸, U. Soldevila ¹⁶⁶, A.A. Solodkov ³⁸, S. Solomon ²⁷, A. Soloshenko ³⁹, K. Solovieva ⁵⁵, O.V. Solovyanov ⁴¹, P. Sommer ³⁷, A. Sonay ¹³, W.Y. Song ^{159b}, A. Sopczak ¹³⁵, A.L. Soppio ⁹⁸, F. Sopkova ^{29b}, J.D. Sorenson ¹¹⁵, I.R. Sotarriva Alvarez ¹⁵⁷, V. Sothilingam ^{64a}, O.J. Soto Sandoval ^{140c,140b}, S. Sottocornola ⁶⁹, R. Soualah ¹⁶³, Z. Soumami ^{36e}, D. South ⁴⁹, N. Soybelman ¹⁷², S. Spagnolo ^{71a,71b}, M. Spalla ¹¹², D. Sperlich ⁵⁵, G. Spigo ³⁷, S. Spinali ⁹³, B. Spisso ^{73a,73b}, D.P. Spiteri ⁶⁰, M. Spousta ¹³⁶, E.J. Staats ³⁵, R. Stamen ^{64a}, A. Stampekis ²¹, M. Standke ²⁵, E. Stanecka ⁸⁸, W. Stanek-Maslouska ⁴⁹, M.V. Stange ⁵¹, B. Stanislaus ^{18a}, M.M. Stanitzki ⁴⁹, B. Stapf ⁴⁹, E.A. Starchenko ³⁸, G.H. Stark ¹³⁹, J. Stark ⁹¹, P. Staroba ¹³⁴, P. Starovoitov ^{64a}, S. Stärz ¹⁰⁶, R. Staszewski ⁸⁸, G. Stavropoulos ⁴⁷, A. Steff ³⁷, P. Steinberg ³⁰, B. Stelzer ^{145,159a}, H.J. Stelzer ¹³², O. Stelzer-Chilton ^{159a}, H. Stenzel ⁵⁹, T.J. Stevenson ¹⁴⁹, G.A. Stewart ³⁷, J.R. Stewart ¹²⁴, M.C. Stockton ³⁷, G. Stoicea ^{28b}, M. Stolarski ^{133a}, S. Stonjek ¹¹², A. Straessner ⁵¹, J. Strandberg ¹⁴⁷, S. Strandberg ^{48a,48b}, M. Stratmann ¹⁷⁴, M. Strauss ¹²³, T. Streblner ¹⁰⁴, P. Strizenec ^{29b}, R. Ströhmer ¹⁶⁹, D.M. Strom ¹²⁶, R. Stroynowski ⁴⁵, A. Strubig ^{48a,48b}, S.A. Stucci ³⁰, B. Stugu ¹⁷, J. Stupak ¹²³, N.A. Styles ⁴⁹, D. Su ¹⁴⁶, S. Su ^{63a}, W. Su ^{63d}, X. Su ^{63a}, D. Suchy ^{29a}, K. Sugizaki ¹⁵⁶, V.V. Sulim ³⁸, M.J. Sullivan ⁹⁴, D.M.S. Sultan ¹²⁹, L. Sultanaliev ³⁸, S. Sultansoy ^{3b}, T. Sumida ⁸⁹, S. Sun ¹⁷³, O. Sunneborn Gudnadottir ¹⁶⁴, N. Sur ¹⁰⁴, M.R. Sutton ¹⁴⁹, H. Suzuki ¹⁶⁰, M. Svatos ¹³⁴, M. Swiatlowski ^{159a}, T. Swirski ¹⁶⁹, I. Sykora ^{29a}, M. Sykora ¹³⁶, T. Sykora ¹³⁶, D. Ta ¹⁰², K. Tackmann ^{49,t}, A. Taffard ¹⁶², R. Tafirout ^{159a}, J.S. Tafoya Vargas ⁶⁷, Y. Takubo ⁸⁵, M. Talby ¹⁰⁴, A.A. Talyshv ³⁸, K.C. Tam ^{65b}, N.M. Tamir ¹⁵⁴, A. Tanaka ¹⁵⁶, J. Tanaka ¹⁵⁶, R. Tanaka ⁶⁷, M. Tanasini ¹⁴⁸, Z. Tao ¹⁶⁷, S. Tapia Araya ^{140f}, S. Tapprogge ¹⁰², A. Tarek Abouelfadl Mohamed ¹⁰⁹, S. Tarem ¹⁵³, K. Tariq ¹⁴, G. Tarna ^{28b}, G.F. Tartarelli ^{72a}, M.J. Tartarin ⁹¹, P. Tas ¹³⁶, M. Tasevsky ¹³⁴, E. Tassi ^{44b,44a}, A.C. Tate ¹⁶⁵, G. Tateno ¹⁵⁶, Y. Tayalati ^{36e,v}, G.N. Taylor ¹⁰⁷, W. Taylor ^{159b}, R. Teixeira De Lima ¹⁴⁶, P. Teixeira-Dias ⁹⁷, J.J. Teoh ¹⁵⁸, K. Terashi ¹⁵⁶, J. Terron ¹⁰¹, S. Terzo ¹³, M. Testa ⁵⁴, R.J. Teuscher ^{158,w}

A. Thaler ⁸⁰, O. Theiner ⁵⁷, N. Themistokleous ⁵³, T. Thevenaux-Pelzer ¹⁰⁴, O. Thielmann ¹⁷⁴,
 D.W. Thomas ⁹⁷, J.P. Thomas ²¹, E.A. Thompson ^{18a}, P.D. Thompson ²¹, E. Thomson ¹³¹,
 R.E. Thornberry ⁴⁵, C. Tian ^{63a}, Y. Tian ⁵⁶, V. Tikhomirov ^{38,a}, Yu.A. Tikhonov ³⁸,
 S. Timoshenko ³⁸, D. Timoshyn ¹³⁶, E.X.L. Ting ¹, P. Tipton ¹⁷⁵, A. Tishelman-Charny ³⁰,
 S.H. Tlou ^{34g}, K. Todome ¹⁵⁷, S. Todorova-Nova ¹³⁶, S. Todt ⁵¹, L. Toffolin ^{70a,70c}, M. Togawa ⁸⁵,
 J. Tojo ⁹⁰, S. Tokár ^{29a}, K. Tokushuku ⁸⁵, O. Toldaiev ⁶⁹, R. Tombs ³³, M. Tomoto ^{85,113},
 L. Tompkins ^{146,1}, K.W. Topolnicki ^{87b}, E. Torrence ¹²⁶, H. Torres ⁹¹, E. Torró Pastor ¹⁶⁶,
 M. Toscani ³¹, C. Tosciri ⁴⁰, M. Tost ¹¹, D.R. Tovey ¹⁴², I.S. Trandafir ^{28b}, T. Trefzger ¹⁶⁹,
 A. Tricoli ³⁰, I.M. Trigger ^{159a}, S. Trincaz-Duvoid ¹³⁰, D.A. Trischuk ²⁷, B. Trocmé ⁶¹,
 A. Tropina ³⁹, L. Truong ^{34c}, M. Trzebinski ⁸⁸, A. Trzupiek ⁸⁸, F. Tsai ¹⁴⁸, M. Tsai ¹⁰⁸,
 A. Tsiamis ^{155,d}, P.V. Tsiarehka ³⁸, S. Tsigaridas ^{159a}, A. Tsirigotis ^{155,r}, V. Tsiskaridze ¹⁵⁸,
 E.G. Tskhadadze ^{152a}, M. Tsopoulou ¹⁵⁵, Y. Tsujikawa ⁸⁹, I.I. Tsukerman ³⁸, V. Tsulaia ^{18a},
 S. Tsuno ⁸⁵, K. Tsuru ¹²¹, D. Tsybychev ¹⁴⁸, Y. Tu ^{65b}, A. Tudorache ^{28b}, V. Tudorache ^{28b},
 A.N. Tuna ⁶², S. Turchikhin ^{58b,58a}, I. Turk Cakir ^{3a}, R. Turra ^{72a}, T. Turtuvshin ^{39,x},
 P.M. Tuts ⁴², S. Tzamarias ^{155,d}, E. Tzovara ¹⁰², F. Ukegawa ¹⁶⁰, P.A. Ulloa Poblete ^{140c,140b},
 E.N. Umaka ³⁰, G. Unal ³⁷, A. Undrus ³⁰, G. Unel ¹⁶², J. Urban ^{29b}, P. Urrejola ^{140a},
 G. Usai ⁸, R. Ushioda ¹⁵⁷, M. Usman ¹¹⁰, Z. Uysal ⁸³, V. Vacek ¹³⁵, B. Vachon ¹⁰⁶,
 T. Vafeiadis ³⁷, A. Vaitkus ⁹⁸, C. Valderanis ¹¹¹, E. Valdes Santurio ^{48a,48b}, M. Valente ^{159a},
 S. Valentinetti ^{24b,24a}, A. Valero ¹⁶⁶, E. Valiente Moreno ¹⁶⁶, A. Vallier ⁹¹, J.A. Valls Ferrer ¹⁶⁶,
 D.R. Van Arneeman ¹¹⁷, T.R. Van Daalen ¹⁴¹, A. Van Der Graaf ⁵⁰, P. Van Gemmeren ⁶,
 M. Van Rijnbach ³⁷, S. Van Stroud ⁹⁸, I. Van Vulpen ¹¹⁷, P. Vana ¹³⁶, M. Vanadia ^{77a,77b},
 W. Vandelli ³⁷, E.R. Vandewall ¹²⁴, D. Vannicola ¹⁵⁴, L. Vannoli ⁵⁴, R. Vari ^{76a}, E.W. Varnes ⁷,
 C. Varni ^{18b}, T. Varol ¹⁵¹, D. Varouchas ⁶⁷, L. Varriale ¹⁶⁶, K.E. Varvell ¹⁵⁰, M.E. Vasile ^{28b},
 L. Vaslin ⁸⁵, G.A. Vasquez ¹⁶⁸, A. Vasyukov ³⁹, L.M. Vaughan ¹²⁴, R. Vavricka ¹⁰²,
 T. Vazquez Schroeder ³⁷, J. Veatch ³², V. Vecchio ¹⁰³, M.J. Veen ¹⁰⁵, I. Veliscek ³⁰,
 L.M. Veloce ¹⁵⁸, F. Veloso ^{133a,133c}, S. Veneziano ^{76a}, A. Ventura ^{71a,71b}, S. Ventura Gonzalez ¹³⁸,
 A. Verbytskyi ¹¹², M. Verducci ^{75a,75b}, C. Vergis ⁹⁶, M. Verissimo De Araujo ^{84b},
 W. Verkerke ¹¹⁷, J.C. Vermeulen ¹¹⁷, C. Vernieri ¹⁴⁶, M. Vessella ¹⁰⁵, M.C. Vetterli ^{145,ad},
 A. Vgenopoulos ¹⁰², N. Viaux Maira ^{140f}, T. Vickey ¹⁴², O.E. Vickey Boeriu ¹⁴²,
 G.H.A. Viehhauser ¹²⁹, L. Vigani ^{64b}, M. Villa ^{24b,24a}, M. Villaplana Perez ¹⁶⁶, E.M. Villhauer ⁵³,
 E. Vilucchi ⁵⁴, M.G. Vincter ³⁵, A. Visible ¹¹⁷, C. Vittori ³⁷, I. Vivarelli ^{24b,24a}, E. Voevodina ¹¹²,
 F. Vogel ¹¹¹, J.C. Voigt ⁵¹, P. Vokac ¹³⁵, Yu. Volkotrub ^{87b}, J. Von Ahnen ⁴⁹, E. Von Toerne ²⁵,
 B. Vormwald ³⁷, V. Vorobel ¹³⁶, K. Vorobev ³⁸, M. Vos ¹⁶⁶, K. Voss ¹⁴⁴, M. Vozak ¹¹⁷,
 L. Vozdecky ¹²³, N. Vranjes ¹⁶, M. Vranjes Milosavljevic ¹⁶, M. Vreeswijk ¹¹⁷, N.K. Vu ^{63d,63c},
 R. Vuillermet ³⁷, O. Vujinovic ¹⁰², I. Vukotic ⁴⁰, S. Wada ¹⁶⁰, C. Wagner ¹⁰⁵, J.M. Wagner ^{18a},
 W. Wagner ¹⁷⁴, S. Wahdan ¹⁷⁴, H. Wahlberg ⁹², M. Wakida ¹¹³, J. Walder ¹³⁷, R. Walker ¹¹¹,
 W. Walkowiak ¹⁴⁴, A. Wall ¹³¹, E.J. Wallin ¹⁰⁰, T. Wamorkar ⁶, A.Z. Wang ¹³⁹, C. Wang ¹⁰²,
 C. Wang ¹¹, H. Wang ^{18a}, J. Wang ^{65c}, P. Wang ⁹⁸, R. Wang ⁶², R. Wang ⁶, S.M. Wang ¹⁵¹,
 S. Wang ^{63b}, S. Wang ¹⁴, T. Wang ^{63a}, W.T. Wang ⁸¹, W. Wang ¹⁴, X. Wang ^{114a}, X. Wang ¹⁶⁵,
 X. Wang ^{63c}, Y. Wang ^{63d}, Y. Wang ^{114a}, Y. Wang ^{63a}, Z. Wang ¹⁰⁸, Z. Wang ^{63d,52,63c},
 Z. Wang ¹⁰⁸, A. Warburton ¹⁰⁶, R.J. Ward ²¹, N. Warrack ⁶⁰, S. Waterhouse ⁹⁷, A.T. Watson ²¹,
 H. Watson ⁶⁰, M.F. Watson ²¹, E. Watton ^{60,137}, G. Watts ¹⁴¹, B.M. Waugh ⁹⁸, J.M. Webb ⁵⁵,
 C. Weber ³⁰, H.A. Weber ¹⁹, M.S. Weber ²⁰, S.M. Weber ^{64a}, C. Wei ^{63a}, Y. Wei ⁵⁵,
 A.R. Weidberg ¹²⁹, E.J. Weik ¹²⁰, J. Weingarten ⁵⁰, C. Weiser ⁵⁵, C.J. Wells ⁴⁹, T. Wenaus ³⁰,
 B. Wendland ⁵⁰, T. Wengler ³⁷, N.S. Wenke ¹¹², N. Wermes ²⁵, M. Wessels ^{64a}, A.M. Wharton ⁹³,
 A.S. White ⁶², A. White ⁸, M.J. White ¹, D. Whiteson ¹⁶², L. Wickremasinghe ¹²⁷,
 W. Wiedenmann ¹⁷³, M. Wielers ¹³⁷, C. Wiglesworth ⁴³, D.J. Wilbern ¹²³, H.G. Wilkens ³⁷,

J.J.H. Wilkinson ³³, D.M. Williams ⁴², H.H. Williams¹³¹, S. Williams ³³, S. Willocq ¹⁰⁵, B.J. Wilson ¹⁰³, P.J. Windischhofer ⁴⁰, F.I. Winkel ³¹, F. Winklmeier ¹²⁶, B.T. Winter ⁵⁵, J.K. Winter ¹⁰³, M. Wittgen¹⁴⁶, M. Wobisch ⁹⁹, T. Wojtkowski⁶¹, Z. Wolffs ¹¹⁷, J. Wollrath¹⁶², M.W. Wolter ⁸⁸, H. Wolters ^{133a,133c}, M.C. Wong¹³⁹, E.L. Woodward ⁴², S.D. Worm ⁴⁹, B.K. Wosiek ⁸⁸, K.W. Woźniak ⁸⁸, S. Wozniowski ⁵⁶, K. Wraight ⁶⁰, C. Wu ²¹, M. Wu ^{114b}, M. Wu ¹¹⁶, S.L. Wu ¹⁷³, X. Wu ⁵⁷, Y. Wu ^{63a}, Z. Wu ⁴, J. Wuerzinger ^{112,ab}, T.R. Wyatt ¹⁰³, B.M. Wynne ⁵³, S. Xella ⁴³, L. Xia ^{114a}, M. Xia ¹⁵, M. Xie ^{63a}, S. Xin ^{14,114c}, A. Xiong ¹²⁶, J. Xiong ^{18a}, D. Xu ¹⁴, H. Xu ^{63a}, L. Xu ^{63a}, R. Xu ¹³¹, T. Xu ¹⁰⁸, Y. Xu ¹⁵, Z. Xu ⁵³, Z. Xu^{114a}, B. Yabsley ¹⁵⁰, S. Yacoob ^{34a}, Y. Yamaguchi ¹⁵⁷, E. Yamashita ¹⁵⁶, H. Yamauchi ¹⁶⁰, T. Yamazaki ^{18a}, Y. Yamazaki ⁸⁶, J. Yan^{63c}, S. Yan ⁶⁰, Z. Yan ¹⁰⁵, H.J. Yang ^{63c,63d}, H.T. Yang ^{63a}, S. Yang ^{63a}, T. Yang ^{65c}, X. Yang ³⁷, X. Yang ¹⁴, Y. Yang ⁴⁵, Y. Yang^{63a}, Z. Yang ^{63a}, W.-M. Yao ^{18a}, H. Ye ^{114a}, H. Ye ⁵⁶, J. Ye ¹⁴, S. Ye ³⁰, X. Ye ^{63a}, Y. Yeh ⁹⁸, I. Yeletsikh ³⁹, B. Yeo ^{18b}, M.R. Yexley ⁹⁸, T.P. Yildirim ¹²⁹, P. Yin ⁴², K. Yorita ¹⁷¹, S. Younas ^{28b}, C.J.S. Young ³⁷, C. Young ¹⁴⁶, C. Yu ^{14,114c}, Y. Yu ^{63a}, J. Yuan ^{14,114c}, M. Yuan ¹⁰⁸, R. Yuan ^{63d,63c}, L. Yue ⁹⁸, M. Zaazoua ^{63a}, B. Zabinski ⁸⁸, E. Zaid⁵³, Z.K. Zak ⁸⁸, T. Zakareishvili ¹⁶⁶, S. Zambito ⁵⁷, J.A. Zamora Saa ^{140d,140b}, J. Zang ¹⁵⁶, D. Zanzi ⁵⁵, O. Zaplatilek ¹³⁵, C. Zeitnitz ¹⁷⁴, H. Zeng ¹⁴, J.C. Zeng ¹⁶⁵, D.T. Zenger Jr ²⁷, O. Zenin ³⁸, T. Ženiš ^{29a}, S. Zenz ⁹⁶, S. Zerradi ^{36a}, D. Zerwas ⁶⁷, M. Zhai ^{14,114c}, D.F. Zhang ¹⁴², J. Zhang ^{63b}, J. Zhang ⁶, K. Zhang ^{14,114c}, L. Zhang ^{63a}, L. Zhang ^{114a}, P. Zhang ^{14,114c}, R. Zhang ¹⁷³, S. Zhang ¹⁰⁸, S. Zhang ⁹¹, T. Zhang ¹⁵⁶, X. Zhang ^{63c}, X. Zhang ^{63b}, Y. Zhang ^{63c}, Y. Zhang ⁹⁸, Y. Zhang ^{114a}, Z. Zhang ^{18a}, Z. Zhang ^{63b}, Z. Zhang ⁶⁷, H. Zhao ¹⁴¹, T. Zhao ^{63b}, Y. Zhao ¹³⁹, Z. Zhao ^{63a}, Z. Zhao ^{63a}, A. Zhemchugov ³⁹, J. Zheng ^{114a}, K. Zheng ¹⁶⁵, X. Zheng ^{63a}, Z. Zheng ¹⁴⁶, D. Zhong ¹⁶⁵, B. Zhou ¹⁰⁸, H. Zhou ⁷, N. Zhou ^{63c}, Y. Zhou ¹⁵, Y. Zhou ^{114a}, Y. Zhou⁷, C.G. Zhu ^{63b}, J. Zhu ¹⁰⁸, X. Zhu^{63d}, Y. Zhu ^{63c}, Y. Zhu ^{63a}, X. Zhuang ¹⁴, K. Zhukov ³⁸, N.I. Zimine ³⁹, J. Zinsser ^{64b}, M. Ziolkowski ¹⁴⁴, L. Živković ¹⁶, A. Zoccoli ^{24b,24a}, K. Zoch ⁶², T.G. Zorbas ¹⁴², O. Zormpa ⁴⁷, W. Zou ⁴², L. Zwalinski ³⁷.

¹Department of Physics, University of Adelaide, Adelaide; Australia.

²Department of Physics, University of Alberta, Edmonton AB; Canada.

^{3(a)}Department of Physics, Ankara University, Ankara; ^(b)Division of Physics, TOBB University of Economics and Technology, Ankara; Türkiye.

⁴LAPP, Université Savoie Mont Blanc, CNRS/IN2P3, Annecy; France.

⁵APC, Université Paris Cité, CNRS/IN2P3, Paris; France.

⁶High Energy Physics Division, Argonne National Laboratory, Argonne IL; United States of America.

⁷Department of Physics, University of Arizona, Tucson AZ; United States of America.

⁸Department of Physics, University of Texas at Arlington, Arlington TX; United States of America.

⁹Physics Department, National and Kapodistrian University of Athens, Athens; Greece.

¹⁰Physics Department, National Technical University of Athens, Zografou; Greece.

¹¹Department of Physics, University of Texas at Austin, Austin TX; United States of America.

¹²Institute of Physics, Azerbaijan Academy of Sciences, Baku; Azerbaijan.

¹³Institut de Física d'Altes Energies (IFAE), Barcelona Institute of Science and Technology, Barcelona; Spain.

¹⁴Institute of High Energy Physics, Chinese Academy of Sciences, Beijing; China.

¹⁵Physics Department, Tsinghua University, Beijing; China.

¹⁶Institute of Physics, University of Belgrade, Belgrade; Serbia.

¹⁷Department for Physics and Technology, University of Bergen, Bergen; Norway.

- ^{18(a)}Physics Division, Lawrence Berkeley National Laboratory, Berkeley CA;^(b)University of California, Berkeley CA; United States of America.
- ¹⁹Institut für Physik, Humboldt Universität zu Berlin, Berlin; Germany.
- ²⁰Albert Einstein Center for Fundamental Physics and Laboratory for High Energy Physics, University of Bern, Bern; Switzerland.
- ²¹School of Physics and Astronomy, University of Birmingham, Birmingham; United Kingdom.
- ^{22(a)}Department of Physics, Bogazici University, Istanbul;^(b)Department of Physics Engineering, Gaziantep University, Gaziantep;^(c)Department of Physics, Istanbul University, Istanbul; Türkiye.
- ^{23(a)}Facultad de Ciencias y Centro de Investigaciones, Universidad Antonio Nariño, Bogotá;^(b)Departamento de Física, Universidad Nacional de Colombia, Bogotá; Colombia.
- ^{24(a)}Dipartimento di Fisica e Astronomia A. Righi, Università di Bologna, Bologna;^(b)INFN Sezione di Bologna; Italy.
- ²⁵Physikalisches Institut, Universität Bonn, Bonn; Germany.
- ²⁶Department of Physics, Boston University, Boston MA; United States of America.
- ²⁷Department of Physics, Brandeis University, Waltham MA; United States of America.
- ^{28(a)}Transilvania University of Brasov, Brasov;^(b)Horia Hulubei National Institute of Physics and Nuclear Engineering, Bucharest;^(c)Department of Physics, Alexandru Ioan Cuza University of Iasi, Iasi;^(d)National Institute for Research and Development of Isotopic and Molecular Technologies, Physics Department, Cluj-Napoca;^(e)National University of Science and Technology Politehnica, Bucharest;^(f)West University in Timisoara, Timisoara;^(g)Faculty of Physics, University of Bucharest, Bucharest; Romania.
- ^{29(a)}Faculty of Mathematics, Physics and Informatics, Comenius University, Bratislava;^(b)Department of Subnuclear Physics, Institute of Experimental Physics of the Slovak Academy of Sciences, Kosice; Slovak Republic.
- ³⁰Physics Department, Brookhaven National Laboratory, Upton NY; United States of America.
- ³¹Universidad de Buenos Aires, Facultad de Ciencias Exactas y Naturales, Departamento de Física, y CONICET, Instituto de Física de Buenos Aires (IFIBA), Buenos Aires; Argentina.
- ³²California State University, CA; United States of America.
- ³³Cavendish Laboratory, University of Cambridge, Cambridge; United Kingdom.
- ^{34(a)}Department of Physics, University of Cape Town, Cape Town;^(b)iThemba Labs, Western Cape;^(c)Department of Mechanical Engineering Science, University of Johannesburg, Johannesburg;^(d)National Institute of Physics, University of the Philippines Diliman (Philippines);^(e)University of South Africa, Department of Physics, Pretoria;^(f)University of Zululand, KwaDlangezwa;^(g)School of Physics, University of the Witwatersrand, Johannesburg; South Africa.
- ³⁵Department of Physics, Carleton University, Ottawa ON; Canada.
- ^{36(a)}Faculté des Sciences Ain Chock, Université Hassan II de Casablanca;^(b)Faculté des Sciences, Université Ibn-Tofail, Kénitra;^(c)Faculté des Sciences Semlalia, Université Cadi Ayyad, LPHEA-Marrakech;^(d)LPMR, Faculté des Sciences, Université Mohamed Premier, Oujda;^(e)Faculté des sciences, Université Mohammed V, Rabat;^(f)Institute of Applied Physics, Mohammed VI Polytechnic University, Ben Guerir; Morocco.
- ³⁷CERN, Geneva; Switzerland.
- ³⁸Affiliated with an institute covered by a cooperation agreement with CERN.
- ³⁹Affiliated with an international laboratory covered by a cooperation agreement with CERN.
- ⁴⁰Enrico Fermi Institute, University of Chicago, Chicago IL; United States of America.
- ⁴¹LPC, Université Clermont Auvergne, CNRS/IN2P3, Clermont-Ferrand; France.
- ⁴²Nevis Laboratory, Columbia University, Irvington NY; United States of America.
- ⁴³Niels Bohr Institute, University of Copenhagen, Copenhagen; Denmark.
- ^{44(a)}Dipartimento di Fisica, Università della Calabria, Rende;^(b)INFN Gruppo Collegato di Cosenza,

Laboratori Nazionali di Frascati; Italy.

⁴⁵Physics Department, Southern Methodist University, Dallas TX; United States of America.

⁴⁶Physics Department, University of Texas at Dallas, Richardson TX; United States of America.

⁴⁷National Centre for Scientific Research "Demokritos", Agia Paraskevi; Greece.

^{48(a)}Department of Physics, Stockholm University;^(b)Oskar Klein Centre, Stockholm; Sweden.

⁴⁹Deutsches Elektronen-Synchrotron DESY, Hamburg and Zeuthen; Germany.

⁵⁰Fakultät Physik, Technische Universität Dortmund, Dortmund; Germany.

⁵¹Institut für Kern- und Teilchenphysik, Technische Universität Dresden, Dresden; Germany.

⁵²Department of Physics, Duke University, Durham NC; United States of America.

⁵³SUPA - School of Physics and Astronomy, University of Edinburgh, Edinburgh; United Kingdom.

⁵⁴INFN e Laboratori Nazionali di Frascati, Frascati; Italy.

⁵⁵Physikalisches Institut, Albert-Ludwigs-Universität Freiburg, Freiburg; Germany.

⁵⁶II. Physikalisches Institut, Georg-August-Universität Göttingen, Göttingen; Germany.

⁵⁷Département de Physique Nucléaire et Corpusculaire, Université de Genève, Genève; Switzerland.

^{58(a)}Dipartimento di Fisica, Università di Genova, Genova;^(b)INFN Sezione di Genova; Italy.

⁵⁹II. Physikalisches Institut, Justus-Liebig-Universität Giessen, Giessen; Germany.

⁶⁰SUPA - School of Physics and Astronomy, University of Glasgow, Glasgow; United Kingdom.

⁶¹LPSC, Université Grenoble Alpes, CNRS/IN2P3, Grenoble INP, Grenoble; France.

⁶²Laboratory for Particle Physics and Cosmology, Harvard University, Cambridge MA; United States of America.

^{63(a)}Department of Modern Physics and State Key Laboratory of Particle Detection and Electronics, University of Science and Technology of China, Hefei;^(b)Institute of Frontier and Interdisciplinary Science and Key Laboratory of Particle Physics and Particle Irradiation (MOE), Shandong University, Qingdao;^(c)School of Physics and Astronomy, Shanghai Jiao Tong University, Key Laboratory for Particle Astrophysics and Cosmology (MOE), SKLPPC, Shanghai;^(d)Tsung-Dao Lee Institute, Shanghai;^(e)School of Physics and Microelectronics, Zhengzhou University; China.

^{64(a)}Kirchhoff-Institut für Physik, Ruprecht-Karls-Universität Heidelberg, Heidelberg;^(b)Physikalisches Institut, Ruprecht-Karls-Universität Heidelberg, Heidelberg; Germany.

^{65(a)}Department of Physics, Chinese University of Hong Kong, Shatin, N.T., Hong Kong;^(b)Department of Physics, University of Hong Kong, Hong Kong;^(c)Department of Physics and Institute for Advanced Study, Hong Kong University of Science and Technology, Clear Water Bay, Kowloon, Hong Kong; China.

⁶⁶Department of Physics, National Tsing Hua University, Hsinchu; Taiwan.

⁶⁷IJCLab, Université Paris-Saclay, CNRS/IN2P3, 91405, Orsay; France.

⁶⁸Centro Nacional de Microelectrónica (IMB-CNM-CSIC), Barcelona; Spain.

⁶⁹Department of Physics, Indiana University, Bloomington IN; United States of America.

^{70(a)}INFN Gruppo Collegato di Udine, Sezione di Trieste, Udine;^(b)ICTP, Trieste;^(c)Dipartimento Politecnico di Ingegneria e Architettura, Università di Udine, Udine; Italy.

^{71(a)}INFN Sezione di Lecce;^(b)Dipartimento di Matematica e Fisica, Università del Salento, Lecce; Italy.

^{72(a)}INFN Sezione di Milano;^(b)Dipartimento di Fisica, Università di Milano, Milano; Italy.

^{73(a)}INFN Sezione di Napoli;^(b)Dipartimento di Fisica, Università di Napoli, Napoli; Italy.

^{74(a)}INFN Sezione di Pavia;^(b)Dipartimento di Fisica, Università di Pavia, Pavia; Italy.

^{75(a)}INFN Sezione di Pisa;^(b)Dipartimento di Fisica E. Fermi, Università di Pisa, Pisa; Italy.

^{76(a)}INFN Sezione di Roma;^(b)Dipartimento di Fisica, Sapienza Università di Roma, Roma; Italy.

^{77(a)}INFN Sezione di Roma Tor Vergata;^(b)Dipartimento di Fisica, Università di Roma Tor Vergata, Roma; Italy.

^{78(a)}INFN Sezione di Roma Tre;^(b)Dipartimento di Matematica e Fisica, Università Roma Tre, Roma; Italy.

- ^{79(a)}INFN-TIFPA;^(b)Università degli Studi di Trento, Trento; Italy.
- ⁸⁰Universität Innsbruck, Department of Astro and Particle Physics, Innsbruck; Austria.
- ⁸¹University of Iowa, Iowa City IA; United States of America.
- ⁸²Department of Physics and Astronomy, Iowa State University, Ames IA; United States of America.
- ⁸³Istinye University, Sariyer, Istanbul; Türkiye.
- ^{84(a)}Departamento de Engenharia Elétrica, Universidade Federal de Juiz de Fora (UFJF), Juiz de Fora;^(b)Universidade Federal do Rio De Janeiro COPPE/EE/IF, Rio de Janeiro;^(c)Instituto de Física, Universidade de São Paulo, São Paulo;^(d)Rio de Janeiro State University, Rio de Janeiro;^(e)Federal University of Bahia, Bahia; Brazil.
- ⁸⁵KEK, High Energy Accelerator Research Organization, Tsukuba; Japan.
- ⁸⁶Graduate School of Science, Kobe University, Kobe; Japan.
- ^{87(a)}AGH University of Krakow, Faculty of Physics and Applied Computer Science, Krakow;^(b)Marian Smoluchowski Institute of Physics, Jagiellonian University, Krakow; Poland.
- ⁸⁸Institute of Nuclear Physics Polish Academy of Sciences, Krakow; Poland.
- ⁸⁹Faculty of Science, Kyoto University, Kyoto; Japan.
- ⁹⁰Research Center for Advanced Particle Physics and Department of Physics, Kyushu University, Fukuoka ; Japan.
- ⁹¹L2IT, Université de Toulouse, CNRS/IN2P3, UPS, Toulouse; France.
- ⁹²Instituto de Física La Plata, Universidad Nacional de La Plata and CONICET, La Plata; Argentina.
- ⁹³Physics Department, Lancaster University, Lancaster; United Kingdom.
- ⁹⁴Oliver Lodge Laboratory, University of Liverpool, Liverpool; United Kingdom.
- ⁹⁵Department of Experimental Particle Physics, Jožef Stefan Institute and Department of Physics, University of Ljubljana, Ljubljana; Slovenia.
- ⁹⁶School of Physics and Astronomy, Queen Mary University of London, London; United Kingdom.
- ⁹⁷Department of Physics, Royal Holloway University of London, Egham; United Kingdom.
- ⁹⁸Department of Physics and Astronomy, University College London, London; United Kingdom.
- ⁹⁹Louisiana Tech University, Ruston LA; United States of America.
- ¹⁰⁰Fysiska institutionen, Lunds universitet, Lund; Sweden.
- ¹⁰¹Departamento de Física Teórica C-15 and CIAFF, Universidad Autónoma de Madrid, Madrid; Spain.
- ¹⁰²Institut für Physik, Universität Mainz, Mainz; Germany.
- ¹⁰³School of Physics and Astronomy, University of Manchester, Manchester; United Kingdom.
- ¹⁰⁴CPPM, Aix-Marseille Université, CNRS/IN2P3, Marseille; France.
- ¹⁰⁵Department of Physics, University of Massachusetts, Amherst MA; United States of America.
- ¹⁰⁶Department of Physics, McGill University, Montreal QC; Canada.
- ¹⁰⁷School of Physics, University of Melbourne, Victoria; Australia.
- ¹⁰⁸Department of Physics, University of Michigan, Ann Arbor MI; United States of America.
- ¹⁰⁹Department of Physics and Astronomy, Michigan State University, East Lansing MI; United States of America.
- ¹¹⁰Group of Particle Physics, University of Montreal, Montreal QC; Canada.
- ¹¹¹Fakultät für Physik, Ludwig-Maximilians-Universität München, München; Germany.
- ¹¹²Max-Planck-Institut für Physik (Werner-Heisenberg-Institut), München; Germany.
- ¹¹³Graduate School of Science and Kobayashi-Maskawa Institute, Nagoya University, Nagoya; Japan.
- ^{114(a)}Department of Physics, Nanjing University, Nanjing;^(b)School of Science, Shenzhen Campus of Sun Yat-sen University;^(c)University of Chinese Academy of Science (UCAS), Beijing; China.
- ¹¹⁵Department of Physics and Astronomy, University of New Mexico, Albuquerque NM; United States of America.
- ¹¹⁶Institute for Mathematics, Astrophysics and Particle Physics, Radboud University/Nikhef, Nijmegen;

Netherlands.

¹¹⁷Nikhef National Institute for Subatomic Physics and University of Amsterdam, Amsterdam; Netherlands.

¹¹⁸Department of Physics, Northern Illinois University, DeKalb IL; United States of America.

¹¹⁹^(a)New York University Abu Dhabi, Abu Dhabi;^(b)United Arab Emirates University, Al Ain; United Arab Emirates.

¹²⁰Department of Physics, New York University, New York NY; United States of America.

¹²¹Ochanomizu University, Otsuka, Bunkyo-ku, Tokyo; Japan.

¹²²Ohio State University, Columbus OH; United States of America.

¹²³Homer L. Dodge Department of Physics and Astronomy, University of Oklahoma, Norman OK; United States of America.

¹²⁴Department of Physics, Oklahoma State University, Stillwater OK; United States of America.

¹²⁵Palacký University, Joint Laboratory of Optics, Olomouc; Czech Republic.

¹²⁶Institute for Fundamental Science, University of Oregon, Eugene, OR; United States of America.

¹²⁷Graduate School of Science, Osaka University, Osaka; Japan.

¹²⁸Department of Physics, University of Oslo, Oslo; Norway.

¹²⁹Department of Physics, Oxford University, Oxford; United Kingdom.

¹³⁰LPNHE, Sorbonne Université, Université Paris Cité, CNRS/IN2P3, Paris; France.

¹³¹Department of Physics, University of Pennsylvania, Philadelphia PA; United States of America.

¹³²Department of Physics and Astronomy, University of Pittsburgh, Pittsburgh PA; United States of America.

¹³³^(a)Laboratório de Instrumentação e Física Experimental de Partículas - LIP, Lisboa;^(b)Departamento de Física, Faculdade de Ciências, Universidade de Lisboa, Lisboa;^(c)Departamento de Física, Universidade de Coimbra, Coimbra;^(d)Centro de Física Nuclear da Universidade de Lisboa, Lisboa;^(e)Departamento de Física, Universidade do Minho, Braga;^(f)Departamento de Física Teórica y del Cosmos, Universidad de Granada, Granada (Spain);^(g)Departamento de Física, Instituto Superior Técnico, Universidade de Lisboa, Lisboa; Portugal.

¹³⁴Institute of Physics of the Czech Academy of Sciences, Prague; Czech Republic.

¹³⁵Czech Technical University in Prague, Prague; Czech Republic.

¹³⁶Charles University, Faculty of Mathematics and Physics, Prague; Czech Republic.

¹³⁷Particle Physics Department, Rutherford Appleton Laboratory, Didcot; United Kingdom.

¹³⁸IRFU, CEA, Université Paris-Saclay, Gif-sur-Yvette; France.

¹³⁹Santa Cruz Institute for Particle Physics, University of California Santa Cruz, Santa Cruz CA; United States of America.

¹⁴⁰^(a)Departamento de Física, Pontificia Universidad Católica de Chile, Santiago;^(b)Millennium Institute for Subatomic physics at high energy frontier (SAPHIR), Santiago;^(c)Instituto de Investigación Multidisciplinario en Ciencia y Tecnología, y Departamento de Física, Universidad de La Serena;^(d)Universidad Andres Bello, Department of Physics, Santiago;^(e)Instituto de Alta Investigación, Universidad de Tarapacá, Arica;^(f)Departamento de Física, Universidad Técnica Federico Santa María, Valparaíso; Chile.

¹⁴¹Department of Physics, University of Washington, Seattle WA; United States of America.

¹⁴²Department of Physics and Astronomy, University of Sheffield, Sheffield; United Kingdom.

¹⁴³Department of Physics, Shinshu University, Nagano; Japan.

¹⁴⁴Department Physik, Universität Siegen, Siegen; Germany.

¹⁴⁵Department of Physics, Simon Fraser University, Burnaby BC; Canada.

¹⁴⁶SLAC National Accelerator Laboratory, Stanford CA; United States of America.

¹⁴⁷Department of Physics, Royal Institute of Technology, Stockholm; Sweden.

- ¹⁴⁸Departments of Physics and Astronomy, Stony Brook University, Stony Brook NY; United States of America.
- ¹⁴⁹Department of Physics and Astronomy, University of Sussex, Brighton; United Kingdom.
- ¹⁵⁰School of Physics, University of Sydney, Sydney; Australia.
- ¹⁵¹Institute of Physics, Academia Sinica, Taipei; Taiwan.
- ¹⁵²(^a)E. Andronikashvili Institute of Physics, Iv. Javakhishvili Tbilisi State University, Tbilisi; (^b)High Energy Physics Institute, Tbilisi State University, Tbilisi; (^c)University of Georgia, Tbilisi; Georgia.
- ¹⁵³Department of Physics, Technion, Israel Institute of Technology, Haifa; Israel.
- ¹⁵⁴Raymond and Beverly Sackler School of Physics and Astronomy, Tel Aviv University, Tel Aviv; Israel.
- ¹⁵⁵Department of Physics, Aristotle University of Thessaloniki, Thessaloniki; Greece.
- ¹⁵⁶International Center for Elementary Particle Physics and Department of Physics, University of Tokyo, Tokyo; Japan.
- ¹⁵⁷Department of Physics, Tokyo Institute of Technology, Tokyo; Japan.
- ¹⁵⁸Department of Physics, University of Toronto, Toronto ON; Canada.
- ¹⁵⁹(^a)TRIUMF, Vancouver BC; (^b)Department of Physics and Astronomy, York University, Toronto ON; Canada.
- ¹⁶⁰Division of Physics and Tomonaga Center for the History of the Universe, Faculty of Pure and Applied Sciences, University of Tsukuba, Tsukuba; Japan.
- ¹⁶¹Department of Physics and Astronomy, Tufts University, Medford MA; United States of America.
- ¹⁶²Department of Physics and Astronomy, University of California Irvine, Irvine CA; United States of America.
- ¹⁶³University of Sharjah, Sharjah; United Arab Emirates.
- ¹⁶⁴Department of Physics and Astronomy, University of Uppsala, Uppsala; Sweden.
- ¹⁶⁵Department of Physics, University of Illinois, Urbana IL; United States of America.
- ¹⁶⁶Instituto de Física Corpuscular (IFIC), Centro Mixto Universidad de Valencia - CSIC, Valencia; Spain.
- ¹⁶⁷Department of Physics, University of British Columbia, Vancouver BC; Canada.
- ¹⁶⁸Department of Physics and Astronomy, University of Victoria, Victoria BC; Canada.
- ¹⁶⁹Fakultät für Physik und Astronomie, Julius-Maximilians-Universität Würzburg, Würzburg; Germany.
- ¹⁷⁰Department of Physics, University of Warwick, Coventry; United Kingdom.
- ¹⁷¹Waseda University, Tokyo; Japan.
- ¹⁷²Department of Particle Physics and Astrophysics, Weizmann Institute of Science, Rehovot; Israel.
- ¹⁷³Department of Physics, University of Wisconsin, Madison WI; United States of America.
- ¹⁷⁴Fakultät für Mathematik und Naturwissenschaften, Fachgruppe Physik, Bergische Universität Wuppertal, Wuppertal; Germany.
- ¹⁷⁵Department of Physics, Yale University, New Haven CT; United States of America.
- ^a Also Affiliated with an institute covered by a cooperation agreement with CERN.
- ^b Also at An-Najah National University, Nablus; Palestine.
- ^c Also at Borough of Manhattan Community College, City University of New York, New York NY; United States of America.
- ^d Also at Center for Interdisciplinary Research and Innovation (CIRI-AUTH), Thessaloniki; Greece.
- ^e Also at Centro Studi e Ricerche Enrico Fermi; Italy.
- ^f Also at CERN, Geneva; Switzerland.
- ^g Also at Département de Physique Nucléaire et Corpusculaire, Université de Genève, Genève; Switzerland.
- ^h Also at Departament de Física de la Universitat Autònoma de Barcelona, Barcelona; Spain.
- ⁱ Also at Department of Financial and Management Engineering, University of the Aegean, Chios; Greece.
- ^j Also at Department of Physics, California State University, Sacramento; United States of America.

- ^k Also at Department of Physics, King's College London, London; United Kingdom.
- ^l Also at Department of Physics, Stanford University, Stanford CA; United States of America.
- ^m Also at Department of Physics, Stellenbosch University; South Africa.
- ⁿ Also at Department of Physics, University of Fribourg, Fribourg; Switzerland.
- ^o Also at Department of Physics, University of Thessaly; Greece.
- ^p Also at Department of Physics, Westmont College, Santa Barbara; United States of America.
- ^q Also at Faculty of Physics, Sofia University, 'St. Kliment Ohridski', Sofia; Bulgaria.
- ^r Also at Hellenic Open University, Patras; Greece.
- ^s Also at Institutio Catalana de Recerca i Estudis Avancats, ICREA, Barcelona; Spain.
- ^t Also at Institut für Experimentalphysik, Universität Hamburg, Hamburg; Germany.
- ^u Also at Institute for Nuclear Research and Nuclear Energy (INRNE) of the Bulgarian Academy of Sciences, Sofia; Bulgaria.
- ^v Also at Institute of Applied Physics, Mohammed VI Polytechnic University, Ben Guerir; Morocco.
- ^w Also at Institute of Particle Physics (IPP); Canada.
- ^x Also at Institute of Physics and Technology, Mongolian Academy of Sciences, Ulaanbaatar; Mongolia.
- ^y Also at Institute of Physics, Azerbaijan Academy of Sciences, Baku; Azerbaijan.
- ^z Also at Institute of Theoretical Physics, Ilia State University, Tbilisi; Georgia.
- ^{aa} Also at National Institute of Physics, University of the Philippines Diliman (Philippines); Philippines.
- ^{ab} Also at Technical University of Munich, Munich; Germany.
- ^{ac} Also at The Collaborative Innovation Center of Quantum Matter (CICQM), Beijing; China.
- ^{ad} Also at TRIUMF, Vancouver BC; Canada.
- ^{ae} Also at Università di Napoli Parthenope, Napoli; Italy.
- ^{af} Also at University of Colorado Boulder, Department of Physics, Colorado; United States of America.
- ^{ag} Also at Washington College, Chestertown, MD; United States of America.
- ^{ah} Also at Yeditepe University, Physics Department, Istanbul; Türkiye.
- * Deceased